The authors appreciate the reviewers very much for reviewing our manuscript and providing constructive comments. As suggested, we carefully revised the manuscript thoroughly according to the valuable advices, as well as proof-read the manuscript to minimize typographical, grammatical, and bibliographical errors. Our replies to the comments and our actions taken to revise the paper (in blue) are given below (the original comments are copied here). The revised parts in the manuscript are marked up in red.

Note: The figures added in the comments reply is represented by 'Figure', which is distinguished from 'Fig.' in the manuscript.

Anonymous Referee #3

General comments:

This paper presents the atmospheric chemistry component of CAS-ESM, IAP-AACM, and compares the offline model results (driven by WRF) with various observational data worldwide. This is an important step towards improving the Earth system simulations by CAS/IAP, a key participant of IPCC assessments. Below are a few suggestions to improve the paper.

The model evaluation focuses on comparisons with measurements of surface concentrations of pollutants, particularly aerosol pollutants. Because this model is developed primarily for climate studies, evaluation of the tropospheric chemistry (in addition to surface air quality) will be very important. Specifically, It would be very useful to include/expand the evaluation of vertical profiles and tropospheric burdens against observations. There are many satellite data for ozone, NO2, SO2 and HCHO, and many vertical profile data (e.g., ATOM) for gaseous/aerosol species. Other important measures of tropospheric chemistry that can be discussed include the mean OH concentration and budgets, ozone budgets, methane lifetime, and MCF lifetime.

Reply: It is a good suggestion to include vertical comparison to improve the model evaluation work. We evaluated the tropospheric column concentration of NO2 and O3 with satellite data (GOME2A and OMI) and discussed the profile concentration of OH with other models. The budget of ozone and CO are also evaluated in Table 1. In addition, the ozonesonde measurements and simulated vertical profiles have been compared in the model evaluation of GNAQPMS. The evaluation of vertical profiles of O3 refers to Chen (2013) (shown as Figure 1).

The budget for O_3 and CO: The budgets for CO and O_3 are also displayed as a supplement in Table S2. As for CO, the total emissions are 994 Tg yr-1 in IAP-AACM. It's smaller than the other models (e.g., TM5:1159 (Huijnen et al., 2010), MOZART-4: 1210.7 (Emmons et al., 2010)). Direct emissions and oxidation contribute 43.4% and 55.4% to the total CO, respectively. The global burden is 327 Tg, smaller than the results of other

models (353~399 Tg) (Horowitz et al., 2003; Huijnen et al., 2010; Badia et al., 2017;). As for ozone, dry deposition contributes 21.3% to the total loss (4924 Tg yr-1), and photochemical reaction is responsible for the rest loss. The dry deposition (1049 Tg yr-1) is larger than the mean value of model collection of ACCENT and ACCMIP (Young et al., 2018).

Table 1 the budget of O_3 and CO compared with the other models.

Species	Process		IAP-AACM
CO	Emission ($Tg\ yr^{-1}$) Total 994	Anthrop.	546.4
		Bio. burning	336.2
		Biogenic	92.7
		Others	18.3
	Top condition inflow ($Tg\ yr^{-1}$)		28
	Chem pro ($Tg\ yr^{-1}$)		1270
	Chem lss ($Tg\ yr^{-1}$)		2292
	Dry dep ($Tg\ yr^{-1}$)		0
	Burden (Tg)		327
	Lifetime (days)		52
O_3	Top condition inflow ($Tg\ yr^{-1}$)		398
	Chemical production ($Tg\ yr^{-1}$)		4526
	Chemical loss ($Tg\ yr^{-1}$)		3875
	Dry dep. ($Tg\ yr^{-1}$)		1049
	Burden (Tg)		370
	Lifetime (days)		27.4

Changes in the manuscript: Please refer to Table S2 and Line 351-360.

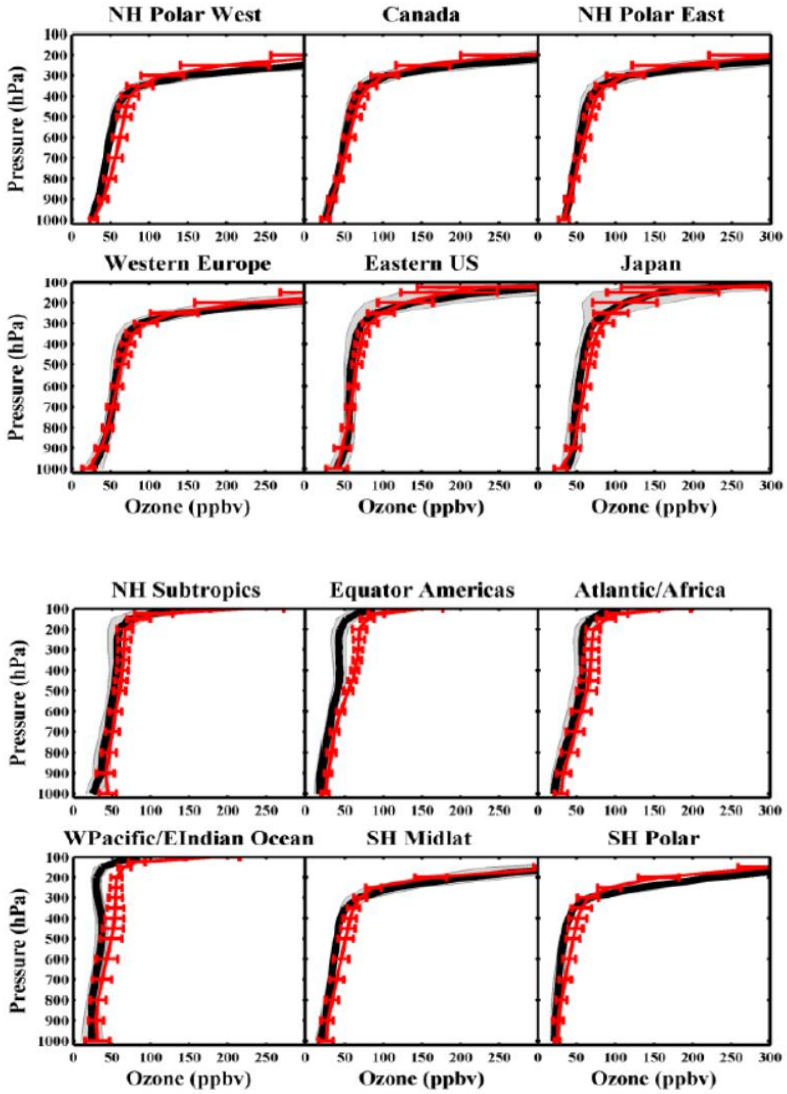

Figure 1 Comparison of vertical profiles between ozonesonde measurements and simulation in GNAQPMS, it followed the methodology of Tilmes et al. (2012) for the selection and treatment of the measurements.

The comparison with O_3 satellite observation: The vertical tropospheric column (VTC) of O_3 is compared against satellite observation derived from OMI (shown in Figure 2). In the main board, the pattern of the seasonal cycle was covered by the model. In mainland of Northern Hemisphere the higher O_3 VTC appears during June-July-August (JJA), while in Southern Hemisphere it appears during September-October-November (SON)， with a range of 40-60 DU. The model keeps a high value (40-50 DU) in tropics during DJF, possibly due to the high emission of CO in biomass burning. The underestimation of cloud cover in the Intertropical Convergence Zone may contribute, too. The O_3 VTC is underestimated over ocean in middle-high latitudes. As the stratospheric chemistry is not considered in IAP-AACM. The lack of stratospheric-tropospheric exchanges should partly be responsible for the underestimation of column burden.

Changes in the manuscript: Please refer to Fig. 8 and Line 558-568.

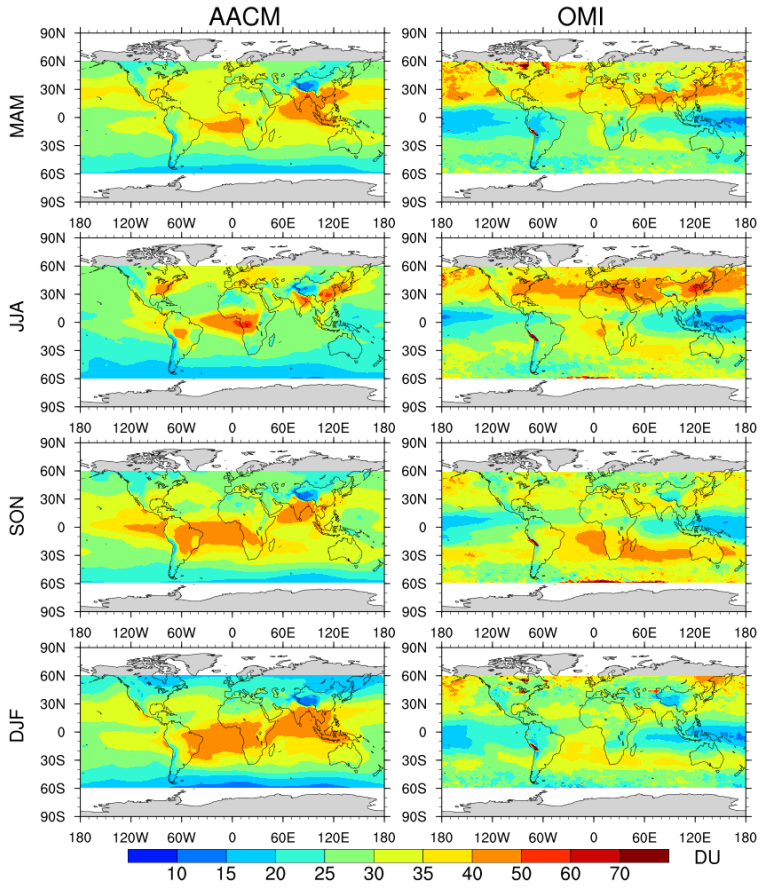

Figure 2 Seasonal mean column concentration of O_3 in IAP-AACM (left column) and OMI (right column). Seasons are defined as December-January-February (DJF), March-April-May (MAM), June-July-August (JJA), and September-October-November (SON). The unit is DU.

The comparison with NO_2 satellite observation: The VTC of NO_2 is compared against satellite observation derived from GOME-2A (shown in Figure 3). The NO_2 VTC has a range of 20-150 $\times 10^{14}$ molecule cm^{-2} in most source areas. By and large, IAP-AACM reproduced the magnitude in different regions. In addition, the model captured seasonal variations of NO_2 concentration in the vertical troposphere well. In anthropogenic source areas of Northern Hemisphere (e.g., North America, Europe, East Asia), the NO_2 VTC is higher in SON and December-January-February (DJF) while lower in JJA, caused by unfavorable diffusion conditions and weak photochemistry. The column concentration is higher during JJA in South America and South Africa, while it is higher during DJF in central Africa, due to the vegetation burning in dry season. Compared with GOME-2A, IAP-AACM showed a larger column concentration over ocean. The overestimation is also reflected in the comparison of surface concentration. This is probably caused by insufficient oxidation to nitrate and a higher injection height of emission which leads to a farther transportation distance as suggested in Badia et al. (2017). Generally, the distribution of NO_2 by the model is consistent with satellite observation.

Changes in the manuscript: Please refer to Fig. 9 and Line 569-582.

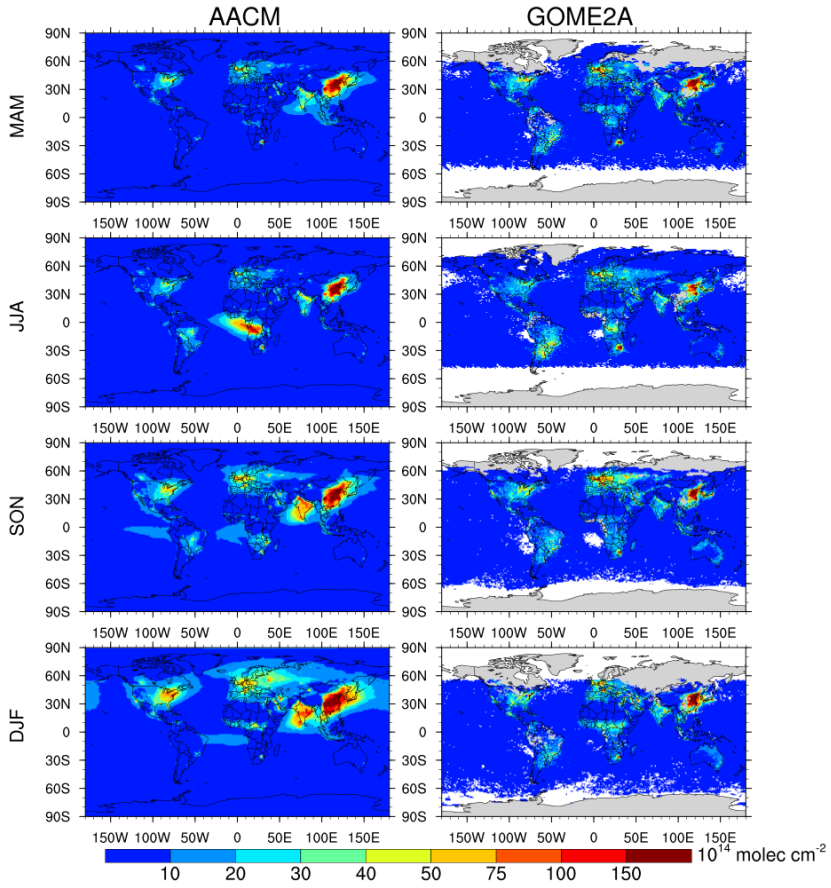

Figure 3 Seasonal mean column concentration of NO_2 in IAP-AACM (left column) and GOME-2A (right column). Seasons are defined as December-January-February (DJF), March-April-May (MAM), June-July-August (JJA), and September-October-November (SON). The unit is 10^{14} molecule cm^{-2}.

The zonal distribution of OH: Oxidation is the basic characteristic of atmospheric chemistry. As the most important oxidant in atmosphere, OH is the crucial species in CTMs. OH in troposphere is mainly produced by the reaction O3 + h ν (λ ≦320nm) + H2O → 2OH+O2. The tropospheric mean concentration of OH in IAP-AACM is 13.0×105 molec cm-3. It is a little higher than the mean OH concentration (11.1±1.6×105 molec cm-3) given by 16 ACCMIP models in Naik et al. (2013). The high concentration indicates a stronger atmospheric oxidation. This could explain the lower concentration of CO over ocean. The zonal mean OH concentrations for January, April, July and October are shown in Fig. 3. Like other chemistry models, OH concentration in the tropics keeps highest all the year round and decreases gradually from tropics to poles. This is due to the positive influence of solar radiation and water vapor concentration. The seasonal north-south shift of OH maximum area is also ascribed to the seasonal variation of these two factors. The mean inter-hemispheric (N/S) ratio of OH in the model is 1.26, in accordance with the multi-model mean ratio of 1.28±0.1 (Naik et al., 2013). Vertically, the highest concentration is in the layer of 2-4 km over the tropics. In Northern Hemisphere, the highest OH concentration appears in summer. Peak value is located at around 30 ℃N, in the atmosphere above 2km. Generally, the distribution of OH concentration is similar with other models

(Huijnen et al., 2010; Badia et al., 2017).

Changes in the manuscript: Please refer to Fig. 3 and Sect. 3.2.1.

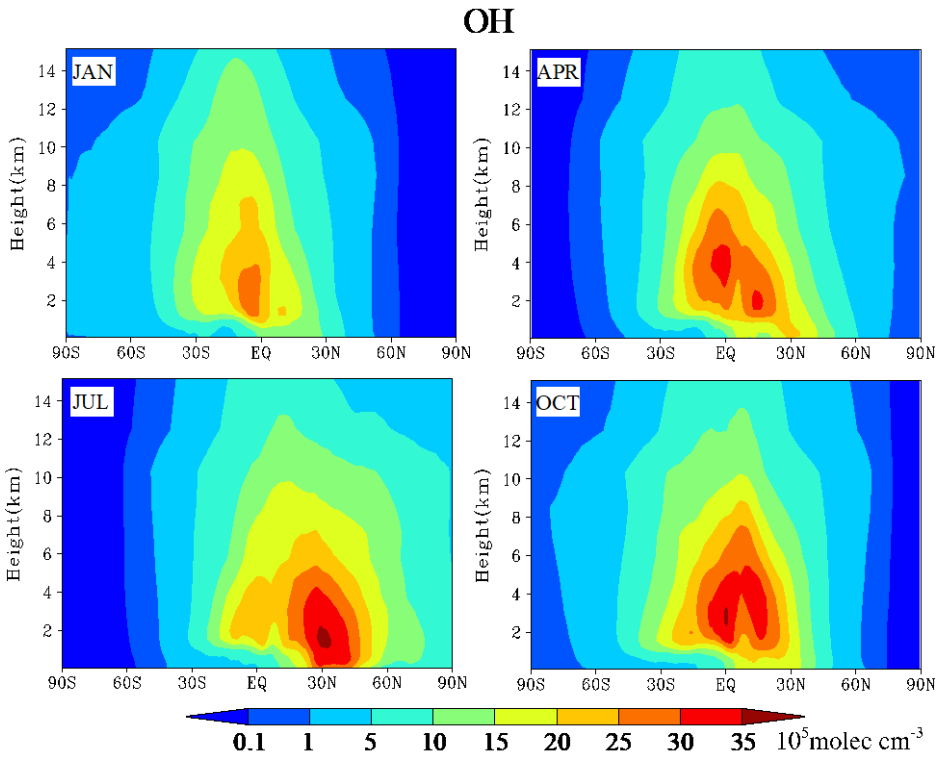

Figure 4 Zonal monthly mean concentration of OH for January, April, July and October by the IAP-AACM. The unit is 10^5 molecule cm^{-3}.

Measurement data often contain missing values and outliers and have different temporal resolutions from model simulations. Please specify how the measurement data are processed and how model results are sampled (temporally and spatially) according to measurements. In particular, satellite data contain large amounts of missing values. Near-surface NO2 measurements are contaminated by other nitrogen species, and what would be the implications for model evaluation (especially when discussing the model bias).

Reply: The measurement datasets (except CNEMC) collected in this paper are monthly or annual mean results which have been processed by the observation workgroups. The hourly CNEMC observations are processed by data quality control. The corresponding simulation data compared with aforementioned observations are sampled in the model grid cells containing observational sites. The simulation of seasonal cycle in different regions or cities are first sampled at the model grid cells containing the observational sites and then averaged within sub-regions. When compared with satellite data, the missing values of satellite data are kept and shown in the figures.

As shown in the scatter plot in Figure 12, model results for NO_2 concentrations are in good agreement with observation with NMB of -0.02. As the "NO_2" values reported by routine monitoring sites are NO_2^*, which

partially includes HNO_3 and NO_3^-. It implicates that the model may overestimate "NO_2".

Changes in the manuscript: The description of simulations sampled according to site observations is revised in Line 295-298. The discussion on model bias between NO2 and NO_2^* is revised in Line 620-622 and Fig. 11(b) in the manuscript.

The resolution dependence discussed in Sect. 3.4 has also been studied in other recent works. It would be nice to refer to or compare against previous findings.

Reply: That's a good suggestion. High-resolution helps to improve CTMs performance, but it is limited by the scale applicable to the parameterization scheme of physical and chemical processes. Recently, sensitivity to horizontal grid resolution has been discussed in many regional model works. Wang et al. (2014) showed a better simulation of particles in North China with CMAQ when increasing the resolution from 36km to 12km. A study of $PM_{2.5}$ heath impact assessment with CMAQ by Jiang et al. (2018) found that model results at 12 km generally performed better and had substantially lower computational burden, compared to 4 km resolution.

Changes in the manuscript: Previous model resolution studies are discussed in Line 722-729 in Sect. 3.4.

The spin-up time (one month) is too short for CO, ozone and other longer-lived species. This may explain part of the underestimate in CO. Please comment on the effect of spin-up time.

Reply: We agree that the spin-up time of one month is not enough for longer-lived species. It may lead to an underestimation of some trace gases such as CO. But in this study we used monthly mean concentration of CO, O_3 and NO_2 from MOZART-4 as initial conditions and top boundary conditions. It can offset the potential underestimation of CO and O_3 substantially. Furthermore, to verify the effect of shorter spin-up time here, we also run a case with spin-up time of one year. The annual mean result is similar to the case of one month spin-up time as shown in Figure 5.

The underestimation of CO potentially reflects a difference in emissions. The natural sources of CO over ocean are included in the HTAP models whereas they are not considered in IAP-AACM. Besides, it may partly owe to differences in chemical transformation between models. As shown in Figure 4, the OH concentration is a bit higher in IAP-AACM than the other models. Due to the sink reaction of CO ($CO + OH \rightarrow CO_2 + H$), the CO loss will be faster in IAP-AACM.

Changes in the manuscript: The discussion on the underestimation of CO refers to Line 396-401.

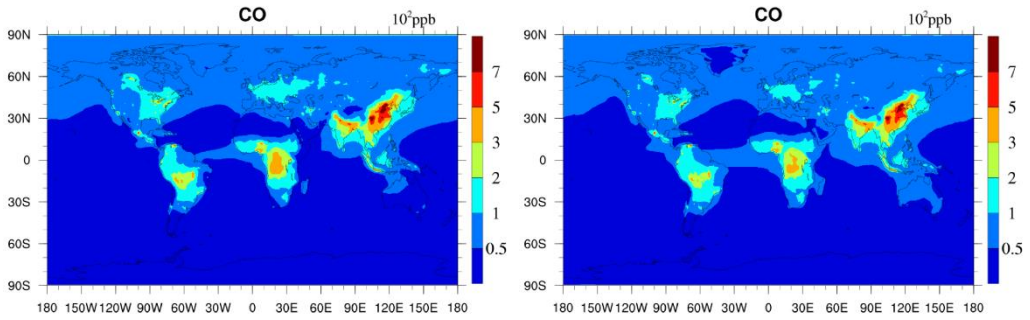

Figure 5 The annual mean surface concentration of CO. The left one is the surface distribution with one month spin-up time, the right one is with one year spin-up time.

There have been discussions in the literature on bug fixes in ISOROPIA II. Are these bugs and fixes relevant here?

Reply: No, it's not relevant here. The code bug only affects the forward (in which the concentration of both gas and aerosol of each species is fixed) stable state calculation. In IAP-AACM, we use reverse mode (in which the concentration of each species in the aerosol phase is fixed) to calculate.

Brief descriptions of WRFv3.3 would be very useful. The vertical resolution of WRF is different from that in IAP-AACM, so how is the conversion done?

Reply: The WRF version used in this study is a global version of WRFv3.3. It is an extension of mesoscale WRF that was developed for global weather research and forecasting applications. It has more general choice of map projection (to include both conformal and non-conformal map projections). The specification of planetary constants, physics parameterizations and timing conventions are also improved to allow the model to be run as a global model. Thus, it has multiscale and nesting capabilities, blurring the distinction between global and mesoscale models and enabling investigation of coupling between processes on all scales (Richardson et al., 2007).

Output of WRF is interpolated to the vertical layers defined in IAP-AACM.

Changes in the manuscript: The information of WRFv3.3 has been added in Line 231-239 of the revised manuscript. The interpretation of interpolation in the vertical is added in Line 242.

Table 1 – do you extrapolate the emissions to 2014? If not, what would be implications for your model evaluation against measurements in 2014?

Reply: Yes， we extrapolate the emission of SO_2 to 2014. As a consequence of government control policy included in the twelfth Five-Year Plan (FYP), China has achieved an obvious decrease in air pollution in the past years, especially for SO_2. The FYP controls suppress SO_2 emissions in energy and industry sectors which is the major source of SO_2. Considering the cutting effect on SO_2 (China completed the emission reduction

task of 12th FYP (2010~2015) ahead of schedule in 2014 with a reduction ratio reaching by 12.9%), we adjusted the total SO_2 emission for 2014 by a factor of 0.9 in China. For other species, the intensity of emission reduction is not so great like SO_2. The study by Zheng et al. (2018) showed that the dramatic reduction of emissions is mostly happened after 2013 for China's Clean Air Action implemented during 2013-2017. Relative change rates of China's anthropogenic emissions during 2010–2017 are estimated as follows: -62% for SO2, -17% for NOx, -27% for CO, -27% for BC and -35% for OC. And the emission mostly decreased during 2013-2017, by 59% for SO2, 21% for NOx, 23% for CO, 28% for BC and 32% for OC. Compared to 2010, emissions of trace gas in 2014 decreased not significant except SO_2 (shown in Figure 6). So we only extrapolate the emission of SO_2. It will partly be responsible for the overestimation of some species (e.g., NO_2 in Fig. 16) in our simulation.

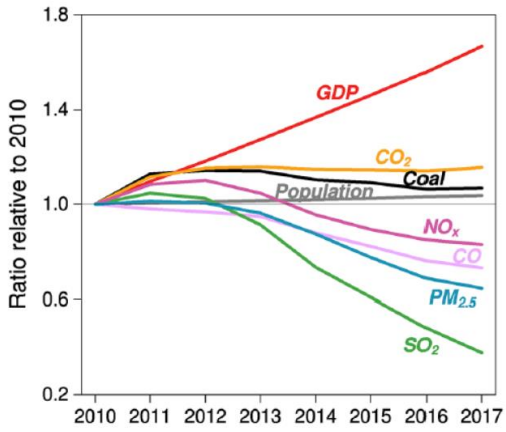

Figure 6 Emission trends and underlying social and economic factors from 2010 to 2017 by Zheng et al. (2018).

Changes in the manuscript: The interpretation and reference are added in Line 227-229.

In the comparisons over China, only a few cities are selected, although there are CEMC measurements in other cities as well. Please explain the rationale for choosing these cities.

Reply: The cities are selected in six regions (North China, Pearl River Delta, Yangtze River Delta, Northwest China, Central China, Southwest China). The six regions not only represent the major geographical regions over China, but also include regions with the most severe air pollution at present which are studied most.

Changes in the manuscript: The reason for choosing these cities are shown in Line 304-306.

Specific comments:

Abstract – please specify which part of the writing is for the evaluation of global model and which is for nested model. Also, please present the bias (in addition to R) of the model.

Reply: The global and nested description has been specified and NMB has been added in the manuscript.

Changes in the manuscript: It has been revised in the Abstract, in Line 25, Line 35-36 and Line 40.

L48-67 – the references are relatively old. Please use newer ones. Also, aerosols affect the cardiovascular diseases very significantly.

Reply: The citation of IPCC has been updated to the latest report. References for aerosols' health effect are also updated (see below).

Aerosols formatted from these precursor gases, together with aerosols from other sources, have a direct radiative forcing. By modifying cloud properties, the aerosols also have important indirect effects. As reported in the Fifth Assessment Report (AR5) of IPCC (Myhre et al., 2013), the radiative forcing of aerosols ranges from -1.9 ~ -0.1 W m^{-2}, with the direct radiative forcing ranges from -0.85 ~ 0.15 W m^{-2}. With better model performance and more robust observation network, AR5 achieved increasing confidence in the assessment compared with AR4 (Boucher et al., 2013), but the largest uncertainty to the total radiative forcing estimate is still aerosols. In addition, aerosols have adverse impacts on human health including respiratory diseases, cardiovascular risk and lung cancer, which has drawn increasing public attention (Burnett et al., 2014; Pope et al., 2011; Powell et al., 2015).

Changes in the manuscript: References for aerosols' health effect and IPCC are updated in Line 55-65.

L71 – change "prediction" to "projection"

Reply: It has been corrected in Line 72.

L87-88 – there have been model evaluation studies over China in recent years. Please refer to these studies.

Reply: Yes, there have been several model evaluation studies with observation in China. The discussion has been added in Line 725-726 in the manuscript.

L97 – remove "precise". Every model has its limitations.

Reply: It has been deleted in the revised manuscript.

L100 – change to "lateral (and upper) boundary conditions"

Reply: It has been modified in the revised manuscript in Line 102.

L147 – specify the resolution

Reply: The high resolution is 0.25 °×0.25 °, we have specified it in Line 154.

L160 – do you mean "natural dust"?

Reply: Yes，it is.

L199 – do you mean the first layer center is 50 m?

Reply: Yes, we have specified the meaning in Line 204.

Table 2 – please explain the meanings of these statistics and provide the units.

Reply: Captions and units are added to Table 2.

L279 – why not just use the WDCGG data in 2014?

Reply: The dataset of WDCGG provides a large number of trace gases observations globally. But there is no observation data for some sites in 2014. To get more data to evaluate the model over the world, we expanded the time range to ten years (2006-2015).

We have re-selected the observation data for 2014 to comparison with model results (shown in Figure 7~ Figure 9). Overall, the results have not changed much in terms of the evaluation of model's simulation capability. The simulation of NO_2 performs better with the NMB closer to zero in Asia and Europe. The underestimation of CO in Antarctica disappeared due to the change of the observed value. There are some changes in the trend of the seasonal variation of O_3 in Northern Hemisphere.

Changes in the manuscript: All the figures and tables related to these changes are updated in the manuscript (please refer to Fig. 4 and Fig.6), and the corresponding analysis is updated in the manuscript, too (please refer to Sect. 3.2.2).

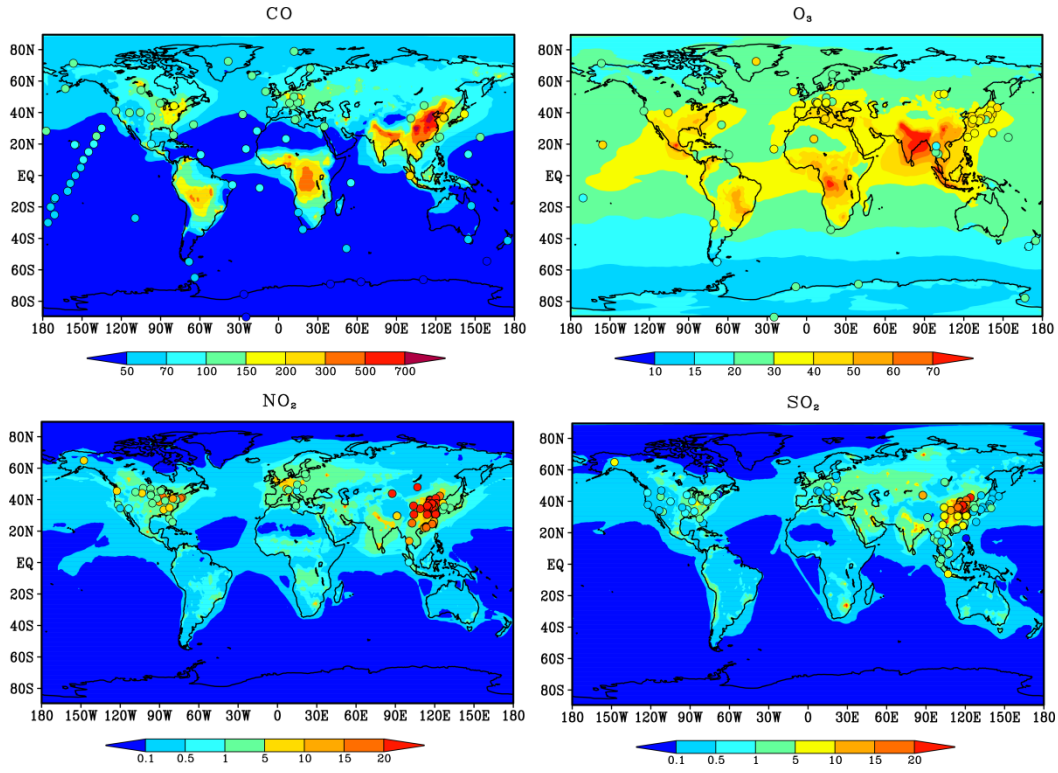

Figure 7 Annual mean concentration (ppb) of the surface layer in IAP-AACM. The circles represent site

observations. The first row is CO and O_3, the bottom row is NO_2 and SO_2.

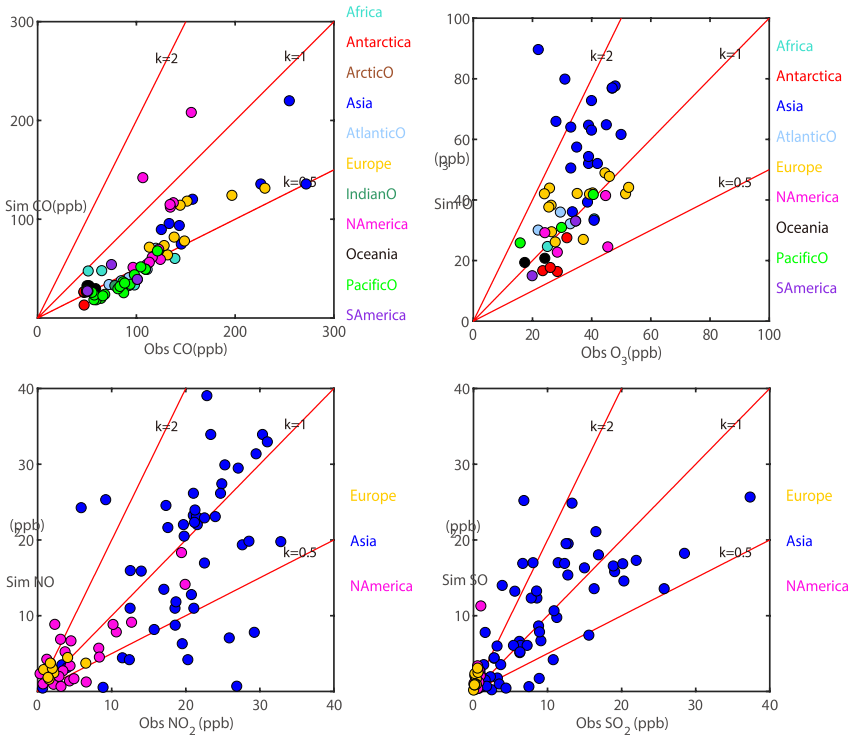

Figure 8 Scatter plots of annual mean concentrations (ppb) in Africa, Antarctica, Arctic Ocean (ArcticO), Asia, Atlantic Ocean (AtlanticO), Europe, Indian Ocean (IndianO), North America (NAmerica), South America (SAmerica), Oceania and Pacific Ocean (PacificO). The abscissa shows the observation and the ordinate shows the simulation. The color of the points represents different regions. (a) ~ (d) show CO, O_3, NO_2 and SO_2 respectively.

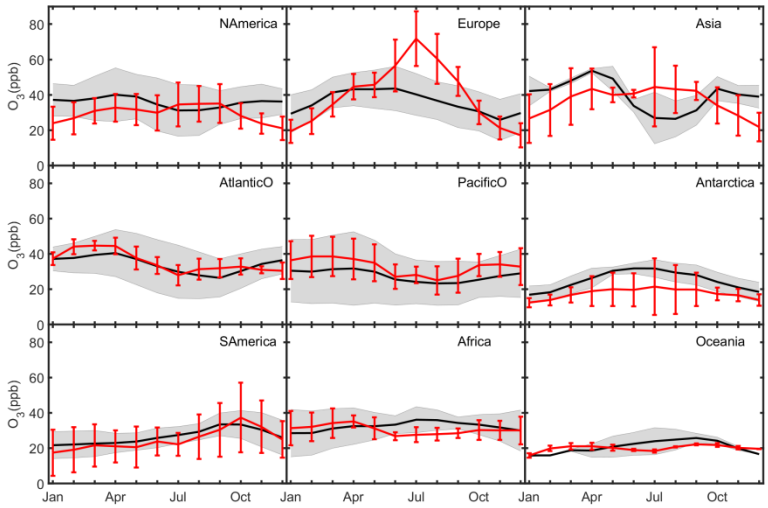

Figure 9 Mean seasonal variation of O_3 (ppb) over NAmerica, Europe, Asia, AtlanticO, PacificO, Antarctica, SAmerica, Africa and Oceania sites. Black lines and red lines represent the average of observations and

simulations respectively. Gray shaded areas and red vertical bars show 1 standard deviation over the sites for observations and for model results respectively.

CO model evaluation – could you comment on the effect of spinup time and coarse model resolution?

Reply: We agree that the spin-up time of one month is not enough for longer-lived species. It may lead to an underestimation of some trace gases such as CO and O_3. But in this study we used monthly mean concentration of CO, O_3 and NO_2 from MOZART-4 as initial conditions and top boundary conditions. It can offset potential underestimation of CO and O_3 substantially. Furthermore, to verify the effect of the shorter spin-up time here, we also run a case with spin-up time of one year. The annual mean result is almost the same with the case of one month spin-up time as shown in Figure 5.

On one hand, the results of coarse-resolution models are often lower than those of high-resolution models due to the effect of gridded average on static emission sources. On the other hand, it's difficult to reproduce the atmospheric dynamics characteristics under complex underlying surface conditions for coarse resolution models. The coarse resolution of global models can hardly represent local orographically driven flows or sharp gradients in mixing depths. It's unfavorable to simulate pollutant diffusion process.

L416 – the ozone seasonality is not very well captured in many regions. Also, this paragraph is too long.

Reply: Agree. We have reanalyzed the simulation of ozone in this part in the revised manuscript. The model showed poor performance on the seasonal cycle of surface ozone in the NH land, with overestimation in Europe and EA in summer while underestimation in winter in NH land, as shown in Figure 9 (the plot with WDCGG observations only for 2014).

The surface O_3 are also underestimated in spring over NH land. In IAP-AACM, the stratospheric chemistry is not considered. Thus the stratospheric-tropospheric exchange is weak. It leads to a large negative bias in the simulating. To date it has become apparent that the measured annual cycle of ozone shows a distinct maximum during spring. The stratosphere-to-troposphere ozone transport event occurs widely across mid-latitudes in the NH (Monks et al., 2000; Akritidis et al., 2018). Since the magnitude and frequency of the transport through tropopause is still not clear. There are large uncertainties in simulating the flux. Some researches (Munzert et al, 1985; Austin and Follows, 1991) showed that the maximum in the stratosphere to troposphere flux occurs in late winter/spring. It may partly responsible for the underestimation of O_3 in winter, too.

The surface O_3 concentrations over East Asia (sites mainly located in Japan) are overestimated in summer and early autumn. The same pattern is also found in the multi-model inter-comparison of 21 HTAP models (Fiore et al., 2009). The simulations in island countries of EA are sensitive to the timing and extent of the Asian summer monsoon (Han et al., 2008). The positive model bias in this season may stem from inadequate representation of southwesterly inflow of clean marine air.

Changes in the manuscript: The discussion on ozone evaluation is updated, please refer to Line 432-468.

L452 – please specify the quantitative difference between GFED3 and GFED4.

Reply: GFED3 and GFED4 are both monthly burned area emission data gridded to 0.5 °×0.5 °and 0.25 °×0.25 °, respectively. Due to the impact of a reduction of combustion area and decreasing in fuel consumption, there is about a reduction of 20%~30% for CO emissions in GFED4 compared with GFED3 in the burned areas (Werf et al., 2017).

Changes in the manuscript: The specific difference has been added to the manuscript, please refer to Line 412-417.

L485-499 – please comment on the effect of difference in time (2006 for measurements and 2014 for model simulation).

Reply: As the simulation used emissions of 2010 but the measurements are for 2006, there is a mismatch on emission scenario. Besides, the meteorological conditions also play a role.

As the analysis of the CAWNET observation over China (Zhang et al., 2015), there is no significant changes happened in the proportion of chemical component of PM_{10} from 2006 to 2013. For the annual average trends of carbonaceous shown in Figure 10, both Southwest China and North China experienced a process of declining first and then rising due to the unfavorable weather conditions. Pearl River Delta showed a significant falling (about half). Yangtze River Delta had a slight decreasing. Generally, it is reasonable to infer that the distribution of BC and OC in most areas have changed a little from 2006 to 2014, except for the Pearl River Delta region.

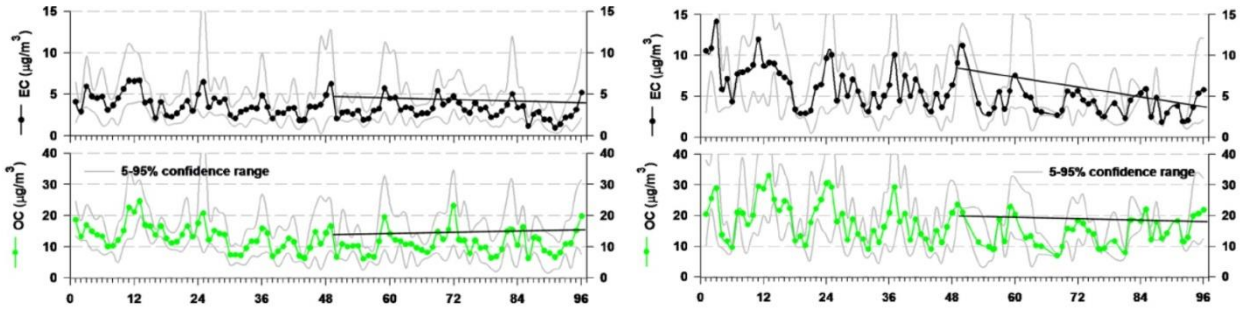

YRD PRD

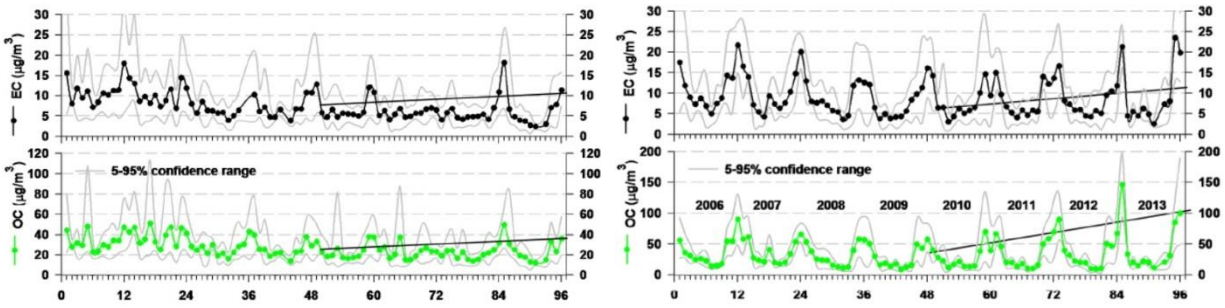

SWC NC

Figure 10 Monthly mean concentrations of OC and EC from 2006 to 2013 by Zhang et al., 2015. YRD, PRD, SWC and NC represents Yangtze River Delta, Pearl River Delta, Southwest China and North China, respectively.

L495 – BC depends on emissions and deposition processes.

Reply: Yes, it has been corrected, please refer to Line 533.

L500 – please clarify which components are included in PM2.5

Reply: To be uniform in the context, the figures of $PM_{2.5}$ showed in the revised manuscript are all calculated with components of primary $PM_{2.5}$, BC, POA, SOA and SNA.

Changes in the manuscript: The clarification is added to the manuscript in Line 626.

L506 – please specify the version of MODIS AOD and how data are selected/sampled.

Reply: The product version is MYD04_L2-MODIS/Aqua Aerosol 5-Min L2 Swath 10km. It is available at the website: http://dx.doi.org/10.5067/MODIS/MYD04_L2.006.

Changes in the manuscript: The product version and website is supplemented in the revised manuscript. Please refer to Line 286.

L512 – LAC or BC?

Reply: It should be BC, it has been revised in Line 589.

L522-531 – please consider to present the seasonality results in a line figure.

Reply: That's a good suggestion. A more detailed comparison of the global gridded average AOD on the seasonality variation is displayed in Figure 11. As the seasonality cycle is different in different regions, we not only showed the global average value, but also showed the gridded average value of Africa, South America and East Asia, which are major aerosol emission areas. Generally, the model captured seasonal variation in different regions. The discrepancy in East Asia potentially stemmed from the bias of dust simulation in spring.

Changes in the manuscript: The figure is supplemented as Fig. S4, and the analysis is shown in Line 307-308 in the revised manuscript.

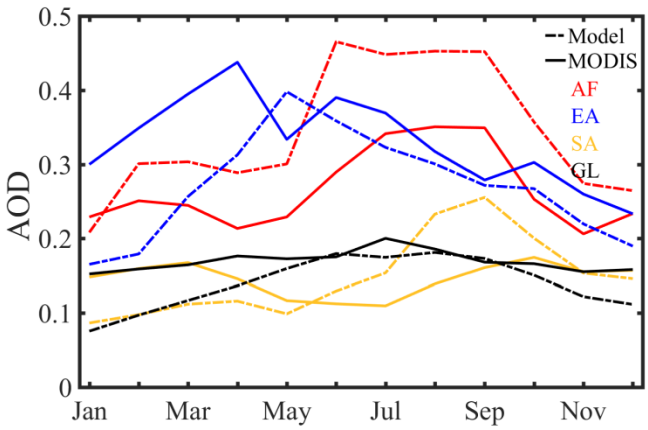

Figure 11 Gridded mean value of monthly averaged AOD for 2014, AF, EA, SA and GL represents Africa, East Asia, South America and global. Dash line and solid line represents model results and observation derived from MODIS, respectively.

L526 – In the model, DJF is not the season with the highest AOD over East China.

Reply: Yes, it's an incorrect expression here and we have deleted it. In fact, the highest AOD may not be in DJF, it often appears in MAM. Since East Asia is frequently affected by dust in spring, this phenomenon is common in other model evaluation studies (e.g., GISS-TOMAS (Lee et al., 2010)). The seasonal variation of relative humidity also impacts the simulating of AOD.

L548-558 – please be more quantitative.

Reply: To be more quantitative, we provided scatter plots of simulations in the nested domain in Figure 12. As shown in Figure 12, model results for NO_2, SO_2 and $PM_{2.5}$ are mostly within the factor of two with NMB within ±0.3. PM_{10} concentrations are underestimated at all sites with NMB of -0.51 due to the simulation without dust.

Changes in the manuscript: The figure is added in the revised manuscript, as Fig. 11(b). Descriptions refer to Line 621-625.

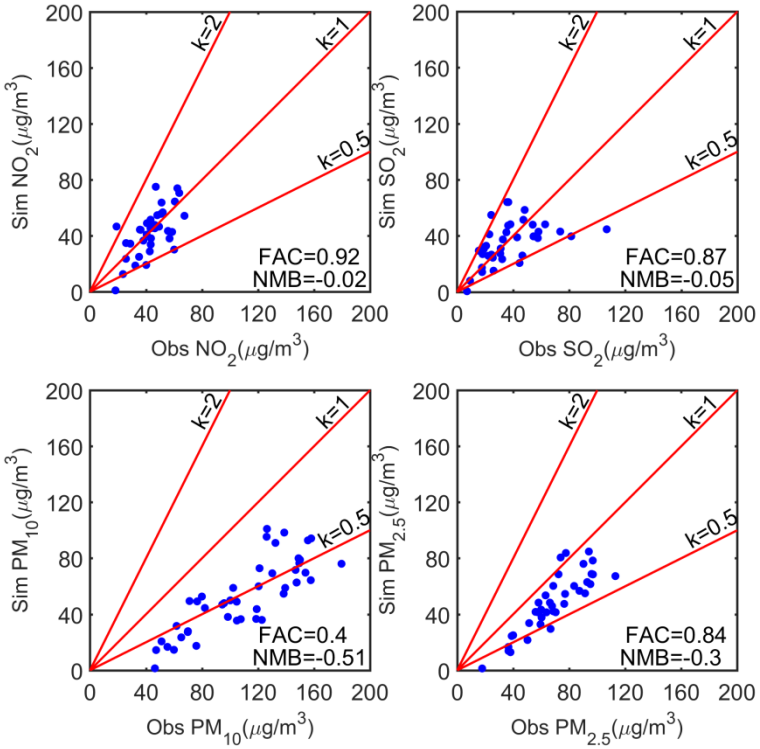

Figure 12 Scatter plots of annual mean concentrations (μg m^{-3}) in nested domain. (a)~(f) is SO_2, NO_2, PM_{10} and $PM_{2.5}$ respectively. The abscissa shows the observation and the ordinate shows the simulation.

L567-568 – please provide model versions.

Reply: the model versions are CMAQv4.7.1, WRF-Chemv3.9 respectively.

Changes in the manuscript: This has been added in the revised manuscript. Please refer to Line 628-629.

L572 – do you mean "other regional models"?

Reply: It means the regional model. Here we compared the simulation of the nested domain in IAP-AACM with regional models of MICS-Asia.

L575-576 – what are the differences in emissions?

Reply: The differences of emissions between IAP-AACM and MICS-Asia models are natural sources. For anthropogenic source, IAP-AACM uses MIX inventory (incorporated into HTAP for Asia) as same as MICS-Asia models. For biogenic source, IAP-AACM uses MEGAN-MACC but models of MICS-Asia uses an earlier version of MEGANv2.04. For biomass burning source, IAP-AACM uses GFEDv4 but MICS-Asia models uses GFEDv3.

Fig. 14 – please specify the components in PM2.5

Reply: To be uniform in the context, the figures of $PM_{2.5}$ showed in the revised manuscript are all calculated

with components of primary $PM_{2.5}$, BC, POA, SOA and SNA.

Changes in the manuscript: It is added in the caption of Fig. 15.

Table 6 – please specify which one is global model and which one is regional model. Also, please provide the mean values over these cities.

Reply: Do you mean Table 7 in the ACPD document, the statistics for 12 cities in global and nested domains? If so, all the results in this table are calculated with outputs from the global model IAP-AACM. The difference between D1 and D2 is the horizontal resolution. D1 represents domain 1 (1 °×1 °), D2 represents domain 2 (0.33 °×0.33 °).

Changes in the manuscript: The mean values over these cities are added in Table 6.

Anonymous Referee #2

Major comments:

The main purpose of this paper is to clearly show the ability and/or inability of their model to simulate the observed spatial and temporal variation in the concentration of the chemical species in the atmosphere. Based on those findings the authors and also the readers of the paper can understand what kind applications are suitable for this model and what aspect of the model should be further improved in order to apply it to a particular issue. From this point of view, the self-evaluation about the ability of the model by authors were often insufficient and unclear. The good points and also the shortcomings of the model should be described more specifically in the text. I pointed out some of those points as specific comments in the following, but I strongly recommend the authors to reexamine the descriptions particularly in the model evaluation parts.

Reply: We greatly appreciate the reviewer for insight comments on the manuscript. To respond to the reviewer's major concerns, we made thoroughly revisions and corrections according to all the insight comments of the reviewers. Besides, more crucial information and analysis will be added in the revised manuscript, as follows:

(1) A new evaluation with the WDCGG datasets only for 2014 is updated, and the evaluation is more quantitative.

(2) We provide more information to discuss the model's performance on the underestimation of CO over ocean, including a comparison of the profile concentration of OH with other models.

(3) More discussions and descriptions are added in the evaluation of ozone. The bias of inter-models and model-observation are discussed. In particular, the poor performance on the seasonal cycle in NH land is interpreted. We further showed the seasonal cycle of ozone compared against sites separated by the terrain.

(4) The model's ability in aerosol simulating is discussed in detail. Especially, the SOA formation mechanism and the multiphase processes in the model are described.

(5) Overall, more analysis on the model's performance are shown, and some improvements are put forward in the model's further work.

Specific comments:

- L24: What are the aerosol effects here?

Reply: The aerosol effects refer to climate effect (direct, semi-direct and indirect effect) and health effect

(mainly of respiratory diseases, cardiovascular risk and lung cancer).

Changes in the manuscript: It has been added in Line 25 in the revised manuscript.

- L38: Only R-value can not ensure the accuracy of the simulation. How about MB or NMB?

Reply: For most of the cities, NMB for the nested simulations are within ±0.5, and MB for the nested simulations are within ±25.

Changes in the manuscript: The description has been added in the Abstract. Please refer to Line 40.

-L58: Why didn't you cite the latest AR5 report here?

Reply: Thanks for your suggestion, the citation are updated to the latest report.

Changes in the manuscript: The update refer to Line 55-62.

- L79: Typo? e.g.

Reply: 'For example' is used to introduce the work by Badia et al. (2017), Mann et al. (2010) and Tsigaridis et al. (2014) instead of 'e.g.' in the manuscript.

- L86: EA, this should be defined at its first appearance in the text.

Reply: Thanks, the definition has been added at its first appearance (Line 91) in the revised manuscript.

- L108-109: What do you mean here? Could you use more words to explain "localization of the process parameterization"?

Reply: In the dust module, the deflation mechanism and dust loading parameterization are based on a detailed analysis of the meteorological conditions, landform, and climatology from daily weather records at about 300 local stations in North China. For the heterogeneous chemistry scheme, the parameterization of uptake coefficients improved the simulating of sulfate and nitrate in severe haze period in China.

Changes in the manuscript: It has been added in the manuscript. Please refer to Line 110-115.

- L135-139: Are there citable references for CoLM , and IAP-OBGCM?

Reply: the references for CoLM (Dai et al., 2015), and IAP-OBGCM (Li et al., 2012) has been supplemented in the revised manuscript.

Changes in the manuscript: Please refer to Line 143 and Line 146.

-L158: What is the main difference between these two models (GNAQPMS and IAP-AACM)?

Reply: Generally, IAP-AACM is similar to GNAQPMS. IAP-AACM has the same model framework with GNAQPMS but has some improvements. It extended the gas phase chemistry from CBMZ to an alternative

simplified scheme specifically for CAS-ESM. The model was renamed when it joined the CAS-ESM.

- L204: What does "synchronous time step" mean ?

Reply: It is the time step of model's integration calculation. In order to keep the stability of calculation in the model, the integration time step will be cut into shorter sub-integration time step in different modules (e.g., advection and gas chemistry processes).

- L206: What is the reason for choosing the year 2014 as the focal year?

Reply: The year 2014 is closest year to 2010 having global emission inventory. In addition, observation data sets were only available in 2014 since Chinese National Environmental Monitoring Network (CNEMC) started to publish data in 2013.

- L224-225: Emission data used in the study are not up-to-date, the base year of each database is a bit old. Therefore, adjusting the emission data to input them to the model is suitable for the purpose of this study. However, you only mentioned about the adjustment of SO2 emission in China in the text. Did you adjust other species emission?

Reply: No, we only adjust the emission of SO_2 for its dramatic variation in the past years in China. During 2010~2014, the change of SO_2 emissions are significant in China, due to a strict controlling policy by the government. The study by Zheng et al. (2018) shows that relative change rates of China's anthropogenic emissions during 2010–2017 are estimated as follows: -62% for SO2, -17% for NOx, -27% for CO, -27% for BC and -35% for OC. But the emissions decreased by 59% for SO2, 21% for NOx, 23% for CO, 28% for BC and 32% for OC during 2013-2017. The dramatic reduction of emissions is mostly happened after 2013 (shown in Figure 6) for China's Clean Air Action implemented during 2013-2017. Compared to 2010, emissions of trace gas in 2014 decreased slightly except SO_2. So we only adjust the emission of SO_2.

Changes in the manuscript: More words to explain are added in Line 227-229 in the revised manuscript.

- Figure2: Why did you compare with NCEP R1, not with NCEP-FNL? What is the purpose of it?

Reply: Because the meteorological field of WRF is nudged to FNL datasets. We used NCEP R1 to compare with the simulation considering data independence.

- L244: This statement is not correct. The difference in RH2 between WRF and Reanalysis is much larger in general as shown in Fig2 over land area.

Reply: The statement is correct. The figure is wrong and it has been replaced.

Changes in the manuscript: Please refer to Fig. 2.

- Table2 and L246-248: If you want to mention only the correlation coefficient of annual mean values, you

should remove Table 2. If you want to retain Table2, you should explain the table more precisely here. Table 2 is hard to read and insufficient caption.

Reply: Thank you for your good suggestion. The simulation of the meteorological factors are close to the site records in different season, with mean bias (MB) of -0.3 ~ 0 ℃, -0.8 ~ -0.5 m/s and -4~ -2.3% for T_2, W_{10} and RH_2 respectively. The model underestimates T_2 in all the seasons. The summer showed a negative bias with Root Mean Square Error (RMSE) of 2 ℃. As for W_{10}, it's also underestimated the most in summer, with MB of -0.8m/s and RMSE of 1.9 m/s. As for RH2, the underestimation is more obvious in summer (MB= -3.2%) and autumn (MB= -3.2%), mainly stem from the insufficient precipitation. Overall, the agreement in T_2 and RH_2 with observations is better than that of W_{10}, with annual correlation coefficients (R) of 0.98, 0.84 and 0.53, respectively. Generally, the meteorology calculated by WRF can rationally reproduce the characteristics of observations.

Changes in the manuscript: Captions and units are added in Table 2. The description about Table 2 refers to Line 257-267.

- L270: Why did you take average of 2006-2015 only for WDCGG?

Reply: The WDCGG datasets provides a large number of trace gases observations globally. The datasets can help to evaluate model performance of CO and ozone in different regions, but there are no observations for some sites in 2014. To get more data to evaluate the model over the world, we expanded the time range to ten years (2006-2015) and take the average of 2006-2015 as the statement of the air in the initial evaluation.

We have re-selected the observation data for 2014 to comparison with model results. Overall, the results have not changed much in terms of the evaluation of model's simulation capability. The simulation of NO_2 performed better with the NMB closer to zero in Asia and Europe. The underestimation of CO in Antarctica disappeared due to the change of the observed value. There are some changes in the trend of the seasonal variation of O_3 in Northern Hemisphere.

Changes in the manuscript: All the figures and tables related to these changes are updated in the manuscript (please refer to Fig. 4 and Fig.6), and the corresponding analysis is updated in the manuscript, too (please refer to Sect. 3.2.2).

- Table3: It is better to include the information of region of each observation datasets.

Reply: That's a good suggestion, we have added the region of each observation datasets in Table3.

- L298: The value (23.3) differs from that in Table4.

Reply: Thanks, it's a typo. We have corrected it to 22.8 in the sentence in Line 324.

- Table5: Table 5 is not completely filled with the necessary information for OM (other sources and total sink

are missing).

Reply: Other sources and total sink are added to Table 5.

- Figure4: Fig4c and 4d should be switched to be in accordance with the order of panels in Fig3.

Reply: The subplot in Fig. 4(b) has been switched to the same order as Fig. 4(a) in the revised manuscript.

- L363: Typo?: Northern Hemisphere

Reply: Yes, we have revised it. Please refer to Line 407.

L368-369: Why did IAP-AACM show the lowest concentration of CO over ocean among the models considered here?

Reply: It potentially reflects a difference in emissions. The natural sources of CO over ocean are included in the HTAP models whereas they are not considered in IAP-AACM. Besides, it may reflect differences in chemical transformation between models. The tropospheric (200hpa to the surface) mean OH concentration of IAP-AACM is 13.0×10^5 molec cm^{-3}. It is a little higher than the mean OH concentration study ($11.1\pm1.6\times10^5$ molec cm^{-3}) from 16 ACCMIP models for 2000 by Naik et al. (2013). It potentially leads to strong atmospheric oxidation. As shown in Figure 4, there is a slightly higher peak concentration of 30-35 molec cm^{-3} in IAP-AACM, compared with the other models (under 30 molec cm^{-3}) (Huijnen et al., 2010; Badia et al., 2017). Due to the sink reaction of CO ($CO + OH \rightarrow CO_2 + H$), the CO loss is larger in IAP-AACM.

Changes in the manuscript: More discussion on the underestimation of CO refers to Line 396-401.

- L378-380: The seasonal variation of surface O3 should be different in different environment even in the same region. So, I recommend the authors to compare separately for different environment (e.g. maritime area vs mountainous area). Otherwise, I can not regard the Fig6 as an evidence that the model can well simulate the seasonal variation of surface O3.

Reply: That's a helpful suggestion. The seasonal cycle of ozone shows different characteristics in different topographic conditions due to different control factors. We separate the observational sites as maritime area, inland and mountain due to the altitudes (shown in Figure 13). For inland, the model tends to overestimate O_3 concentrations in summer time. The simulation of cloud may contribute to the positive bias. Furthermore, uncertainties in volatile organic compounds (VOCs)-NOx-O_3 chemistry may contribute. The natural source of isoprene from vegetation is important in the O_3 formation due to its high proportion of VOCs emission in summer (as estimated to be 40.9 Tg/yr in China by Fu et al., 2012).

Changes in the manuscript: Please refer to 456-464.

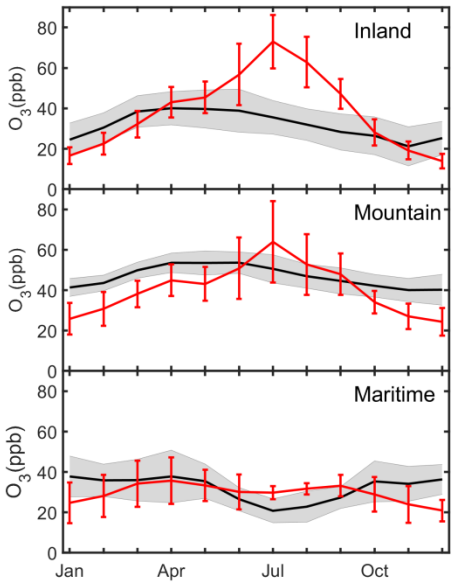

Figure 13 Mean seasonal variation of O_3 (ppb) over inland, mountain and maritime area in Northern Hemisphere compared with site records. Black lines and red lines represent average observations and simulations respectively. Gray shaded areas and red vertical bars show 1 standard deviation over the sites for observations and for model results respectively.

- L385: Underestimation in Antarctica is not small. Such an underestimation could be seen in the other CTMs. Can you use more words about this issue here?

Reply: In IAP-AACM, ozone concentration is about 5~15 ppb lower than site observations in Antarctica. It may be caused by the lack of halogen chemistry in the model. Remarkable ozone depletion events which is driven by halogen chemistry (mostly notably as bromine) is observed in the polar boundary layer (Simpson et al., 2007). The model study by Falk & Sinnhuber (2018) indicated that there are missing sources of bromine release from ice and snow in EMAC v2.52. The over prediction of dry deposition velocity to sea ice also plays a role here. The dry deposition velocity to ice is under 0.02 cm s^{-1} across 15 HTAP models (Hardecre et al., 2015). In IAP-AACM, it's higher (0.035~0.048 cm s^{-1}) than those models, as shown in Figure 14.

Changes in the manuscript: The discussion on the underestimation of ozone in Antarctica refers to Line 465-471

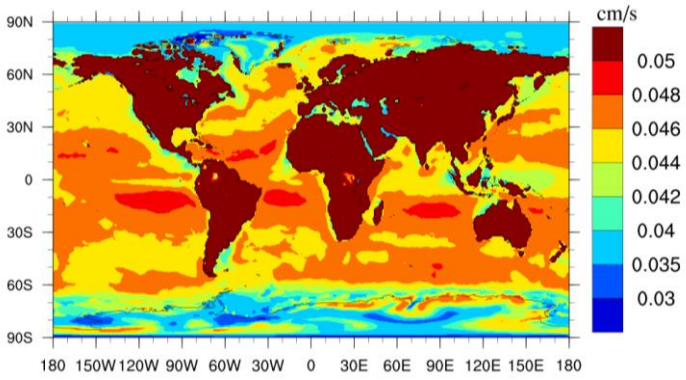

Figure 14 Annual mean dry deposition velocity of ozone in IAP-AACM. The unit is cm s^{-1}.

- L385-387: In the NH land area, it seems that the model completely failed to represent the seasonal cycle of surface O3, but the author regarded it as just a positive bias during July-September. More words for this issue are necessary. For example, what do you think the apparent underestimation in cold season in NAmerica and Europe?

Reply: Yes, the model showed poor performance on the seasonal cycle of surface ozone in the NH land, with overestimation in Europe and EA in summer while underestimation in NH land in winter, as shown in Figure 9 (the comparison drawn with WDCGG observation only for 2014).

The surface O_3 are underestimated in cold seasons over NH land. In IAP-AACM, the stratospheric chemistry is not considered. Thus the stratospheric-tropospheric exchange is weak. It leads to a large negative bias in simulation. To date it has become apparent that the measured annual cycle of ozone shows a distinct maximum during spring. The stratosphere-to-troposphere ozone transport event occurs widely across mid-latitudes in the NH (Monks et al., 2000; Akritidis et al., 2018). Since the magnitude and frequency of the transport through tropopause is still not clear. There are large uncertainties in simulating the flux. Some researches (Munzert et al, 1985; Austin and Follows, 1991) showed that the maximum in the stratosphere to troposphere flux occurs in late winter/spring. It may partly explain the underestimation of O_3 in winter.

The surface O_3 concentrations over East Asia (sites mainly located in Japan) are overestimated in summer and early autumn. The same pattern is also found in the multi-model inter-comparison of 21 HTAP models (Fiore et al., 2009). The simulations in island countries of EA are sensitive to the timing and extent of the Asian summer monsoon (Han et al., 2008). The positive model bias in this season may stem from inadequate representation of southwesterly inflow of clean marine air. Furthermore, the underestimation of cloud cover in summer may also responsible for the overestimation of O_3 due to stronger photochemistry. Additionally, it's difficult for global model with coarse resolution to resolve local orographically driven flows or sharp gradients in mixing depths under complex underlying surface conditions in lands.

Changes in the manuscript: The discussion on the seasonal cycle of ozone in NH land refers to Line 435-456.

- L388-390: In Badia et al (2017), they suspected the excessive emission height of NOx which will cause low NOx at surface and consequently might lead to weak NO titration. Do the same things happen in your model?

Reply: Yes, there is the same situation in our model. In Badia et al. (2017), all the land-based anthropogenic emissions are emitted in the first 500m of the model. In IAP-AACM, the energy emissions and industry emissions are emitted in the first five layers considering the stack height.

- L390-391: The AACM apparently showed larger concentration of surface O3 in the tropical regions (central Africa, South America, and Southeast Asia) than the other models. However, the concentration of O3 precursor species (CO and NOx) in these regions are not so different among the models. Can you give discussion about the issue here?

Reply: Yes, the concentrations of CO and NOx in the tropical regions are not so different among the models. There are several uncertainties in the model performance. Even the same module schemes applied in different models may display different result (Tsigaridis et al. 2014; Hardecre et al., 2015). Furthermore, the meteorological conditions also play an important role in simulation. The chemical reactions and dynamical processes (transportation and diffusion) of the matters are sensitive to meteorological field (e.g., wind, precipitation, cloud cover, temperature). In addition, the biomass burning emissions used in IAP-AACM is different from the other models. For multi-model activities of HTAP, groups use GFED3 data as the biomass burning emissions (Galmarini et al., 2017). In IAP-AACM, we use GFED4. A comparison of different versions of GFED emissions (Werf et al., 2017) shows the impact of a minor reduction in burned area and decreasing fuel consumption.

- L391-394: These two sentences are not consistent to each other. In general, the region of high O3 concentration can be different in different season. If you look at the "annual mean" concentration, the highest O3 usually occur in the source region in summer, but that in the downwind region in winter. However, if you see the different index such as MD8H O3, you can see completely different seasonal cycle. I strongly recommend the author to carefully revise these sentences.

Reply: We totally agree with your comment. We have revised those sentences. Please refer to Line 425-430.

- L402-403: An overall evaluation of O3 dry deposition in global CTMs can be seen in Hardecre et al. (2015). I recommend to check it out. Hardacre et al. (2015) An evaluation of ozone dry deposition in global scale chemistry climate model, Atmos. Chem. Phys., 15, 6419–6436, doi:10.5194/acp-15-6419-2015.

Reply: Thanks for your suggestion. According to Hardecre et al. (2015), the dry deposition velocity to sea varies little (around 0.05 cm s^{-1}) in different CTMs models using the deposition scheme by Wesely (1989). Besides, the study of Ganzeveld et al. (2009) shows that surface ozone differed by up to 60% if the deposition velocity of ozone varies from 0.01 to 0.05 cm s^{-1}. In IAP-AACM, the deposition velocity over the oceans varies from 0.042 to 0.05 cm s^{-1}, as shown in Figure 14. The variation in absolute terms between IAP-AACM

and the other models is smaller than 0.008 cm s^{-1}. Hence the difference of surface ozone caused by dry deposition should be less than 12%.

Changes in the manuscript: We revised sentences in the manuscript. Please refer to Line 428-434.

- L416-418: The concentration of NOx over oceanic areas are larger in AACM than in other models, which might stem from larger emission or longer life time of NOx in AACM than the other models. I recommend to discuss this issue further here.

Reply: We totally agree with reviewer's suggestion. Compared with the other models shown in Fig. 5, the surface NO_2 over ocean is larger in IAP-AACM. This may reflect larger emission or less sinks of NO_2 in IAP-AACM. The higher injection height of emission sources leads to further transportation distance and low NO_x at surface of source areas. Consequently, it leads to higher concentration of surface ozone in NH source areas due to weak NOx titration.

Changes in the manuscript: This is added in Line 585-590 in the revised manuscript.

- L436-438: This is misleading statement. The model results are not generally with in a factor of two, but they apparently tend to overestimate the observation in all the three regions. The NMB value for sulfate in Europe, 0.11, is incorrect which is 1.1 in Table 6.

Reply: The '0.11' is a typo, we have corrected it and renewed a new description about the simulation of sulfate as follows. As shown in Fig. 8, Sulfate is overestimated more or less. Specifically, in Asia, the simulations at most sites here are within a factor of two of observations, with NMB of 0.36. However, In NAmerica and Europe, it's overestimated with NMB of 1.94 and 1.1 respectively.

Changes in the manuscript: Please refer to Line 505-508.

- L438-439: How can you conclude like this (2ugm-3 higher)? What is the ground of this statement?

Reply: We calculated the sites average value in the model and compared it against the observation but we didn't mention it, we have added this description in the revised paper.

Changes in the manuscript: Please refer to Line 508-510.

- L442-443: What aspect of the observation do you think your model can reproduce? You should be more specific.

Reply: As shown in Fig. 8 in the revised manuscript, the concentration of nitrate is higher in eastern America and lower in western America. IAP-AACM reproduces the distribution of nitrate in western America well but overestimates it in eastern America. The model doesn't fully capture the spatial variation over Europe, with an overestimation at most of the sites. As for Asia, there is an underestimation in Southeast Asia and Japan.

Changes in the manuscript: We have provided a detailed description of the distribution in the revised

manuscript. Please refer to Line 514-518.

- L446-449: About the simulation of ammonium, I can see obvious underestimation in NAmerica and overestimation in Asia and Europe.

Reply: The performance of ammonium varies in different regions since there are more uncertainties in the emission of NH3 (precursor of ammonium) from croplands (Xu et al., 2019). There is slight negative bias in America and positive bias in Asia, with NMB less than ±1 (-0.46 and 0.85 respectively). In Europe, there is significant positive bias with NMB of 1.49.

Changes in the manuscript: This has been added to the revised manuscript. Please refer to Line 520-525.

- L455-457: The concentration of OC were obviously underestimated by the model.

Reply: Yes, the meteorological conditions and emission inventories in the model are inconsistent with the observation year (2006) of carbonaceous in China. This may be partially responsible for the bias of OC. According to recent study, there is a slightly increasing (less than 0.1Tg) of both BC and OC emissions from 2006 to 2010 in China (Lu et al., 2011; Fu et al., 2012). As shown in Fig. 7, the simulation of BC at most sites are close to observations while the simulation of OC is significantly underestimated. The study by Fu et al. (2012) showed a significant underestimation of OC emissions over China. Furthermore, Zhao et al. (2016) found that the pathway of intermediate volatile organic compounds (IVOC) to SOA is very important for the formation of SOA. Their model experiments suggest that IVOCs constitute over 40% of OM concentrations in Eastern China. Yang et al. (2018) also showed the significant increase of SOA concentration in an observation-based box model which included the IVOCs reactions. IVOC reactions are not included in our SOA module. The SOA module in IAP-AACM is Two-Product scheme. Model studies with Two-Product scheme estimated an underestimation of OM by 40-78% in China (Lin et al., 2016; Han et al., 2016). Thus the closely simulating of BC but greatly underestimating of OC requires an improvement in SOA formation mechanism in IAP-AACM.

Changes in the manuscript: The discussion refers to Line 536-553.

- L491-492: The highest AOD in DJF in east China is not clearly seen both in satellite and model AOD.

Reply: Yes, it's an incorrect expression here and we have deleted it. In fact, the highest AOD may not be in DJF, it often appears in MAM. Since East Asia is frequently affected by dust in spring, this phenomenon is common in other model evaluation studies (e.g., GISS-TOMAS (Lee et al., 2010)). The seasonal variation of relative humidity also impacts the simulating of AOD.

- Figure10: It's better to show scatter plots too, at least as a supplement figure.

Reply: The figure is added in the revised manuscript, as Fig. 11(b). Descriptions refer to Line 621-625.

- Figure11: The area and the map projection of the figures for all models should be united.

Reply: The model results have been adapted to the same area and projection (shown in Figure 15).

Changes in the manuscript: The new figure is updated to Fig. 12 in the manuscript.

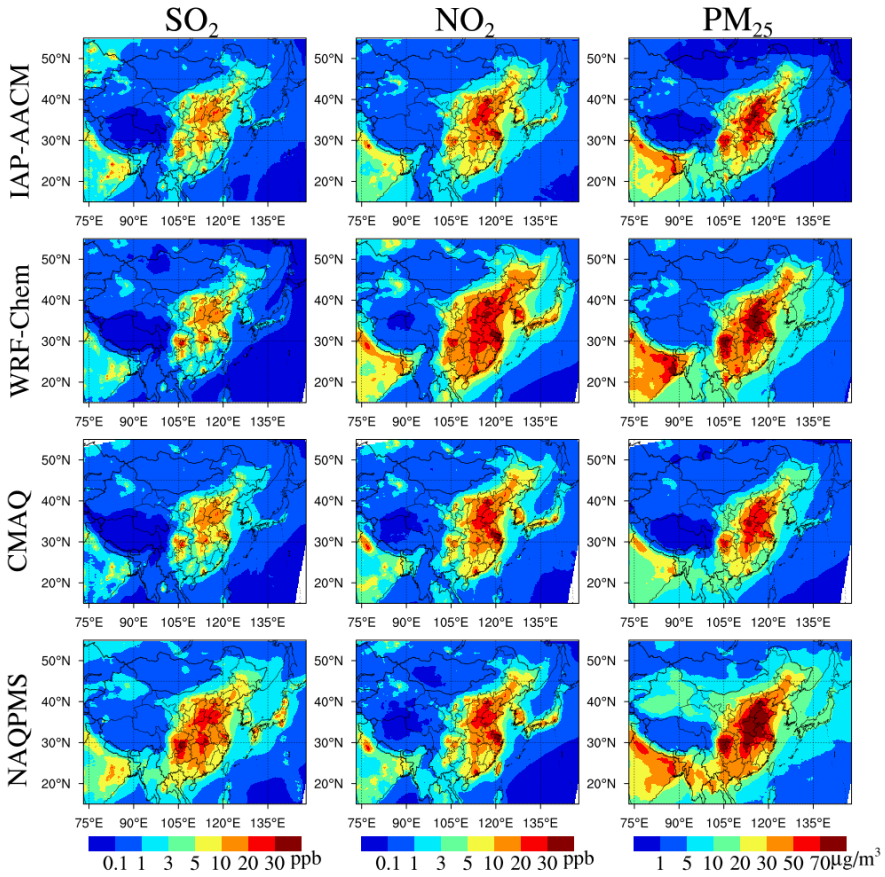

Figure 15 Annual surface distributions from nested IAP-AACM compared with regional models from MICS-Asia. Each row from top to bottom represents IAP-AACM, WRF-Chem, CMAQ and NAQPMS respectively. The left column is SO_2 (ppb), the middle column is NO_2 (ppb) and the right column is $PM_{2.5}$ (μg m^{-3}).

- L517-519: I'm sorry I can not understand what you want to mean here.

Reply: Since the boundary conditions are provided by the parent grids in IAP-AACM, it's updated real-time. The spatial distribution of pollutant near boundary areas varies consecutively if we check the hourly simulation. But as for the annual averaged results, the discrepancy is masked.

L545-547: What do you want to mean here? Your model overestimated the NO2 in summer in NC and YRD regions. If you don't use the NO2* observation, the model's overestimation should become worse.

Reply: As shown in Figure 12, the annual mean simulations of NO_2 are in good agreement with observations. Due to the NO_2* observation, it implicates that the model may overestimate "NO_2". As shown in Fig. 14 in the

manuscript, the NO_2 is overestimated in some cities in summer. It is associated with deposition removal process and multiphase chemistry in IAP-AACM. The overestimation of NO_2 and underestimation of nitrate in daytime of summer and autumn relates to over decomposition of nitric acid at high temperature condition in the thermodynamic equilibrium module. Moreover, heterogeneous chemical reactions in the model should partly be responsible for the overestimation in summer. The heterogeneous chemical module coupled in IAP-AACM has been applied in North China in winter (Li et al, 2018). The mechanism significantly improved sulfate simulation under highly polluted conditions (contributing 50%-80% of total concentration of sulfate) and reduced the overestimation of nitrate. However, the simulations excluded heterogeneous chemical processes showed better performance of NO_2 (shown in Fig. S5). It indicates that a more reasonable mechanism should be considered in model development.

Changes in the manuscript: The discussion on the overestimation of NO_2 is revised in Line 663-674. The seasonal cycle of NO_2 ($\mu g\ m^{-3}$) simulated without heterogeneous chemical process is supplemented as Fig. S5.

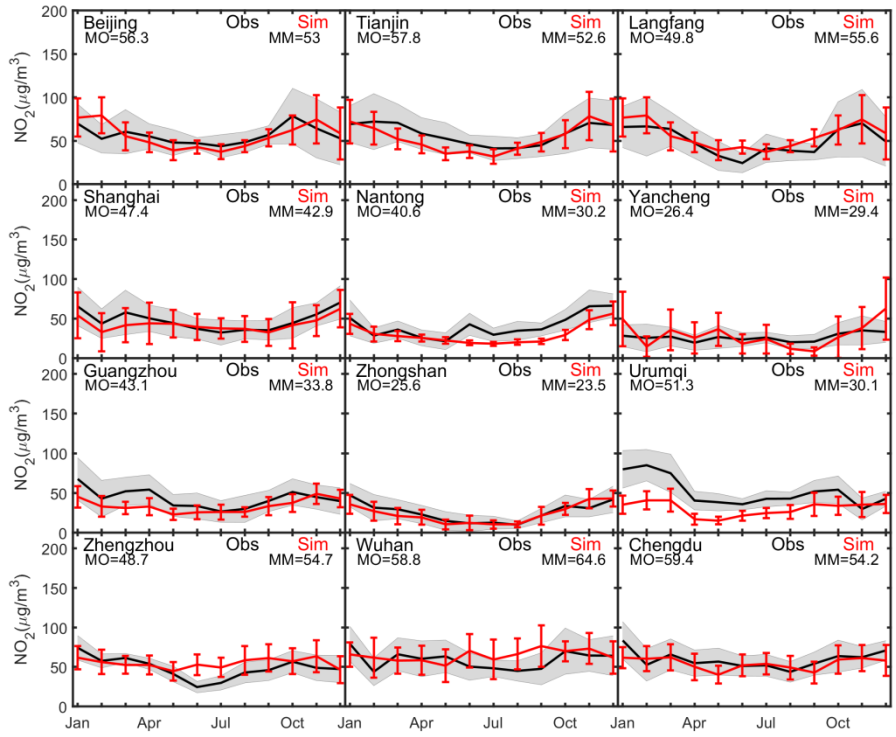

Figure 16 Seasonal cycle of NO_2 ($\mu g\ m^{-3}$) simulated without heterogeneous chemical process over China. The black line and red line represent monthly mean concentration of city-averaged observation and simulation respectively. Gray shaded areas and red vertical bars show 1 standard deviation over the sites for observations and for model results, respectively. MO and MM stand for annual mean concentration of observation and simulation respectively.

- L547-550: I can not understand what aspect of seasonal difference in NO2 column observation were reproduced by your model. You should describe more specifically on it.

Reply: As shown in Fig. S3, the model captures seasonal variations of NO_2 column concentrations in the vertical troposphere well. In China, the NO_2 VTC is higher during September-October-November and December-January-February while lower in June-July-August, due to unfavorable diffusion conditions and weaker photochemical reactions.

Changes in the manuscript: The updated description refers to Line 676-679.

- L595: Typo? respects ! aspects

Reply: Yes, we have revised it.

- Conclusions should be revised according to the modifications made to respond the reviewers comments.

Reply: Yes, Conclusions and Abstract has been updated in the manuscript.

Changes in the manuscript: Please refer to Abstract and Conclusions.

References

Akritidis, D., Katragkou, E., Zanis, P.， et al. A deep stratosphere-to-troposphere ozone transport event over Europe simulated in CAMS global and regional forecast systems: analysis and evaluation. Atmospheric Chemistry and Physics, 18, 15515–15534, doi: 10.5194/acp-18-15515-2018, 2018.

Badia, A., Jorba, O., Voulgarakis, A., Dabdub, D., Pérez García-Pando, C., & Hilboll, A., et al. : Description and evaluation of the multiscale online nonhydrostatic atmosphere chemistry model (NMMB-MONARCH) version 1.0: gas-phase chemistry at global scale, Geoscientific Model Development, 10, 1-47, doi:10.5194/gmd-10-609-2017, 2017.

Boucher, O., D. Randall, P. Artaxo, C. Bretherton, G. Feingold, P. Forster, V.-M. Kerminen, Y. Kondo, H. Liao, U. Lohmann, P. Rasch, S.K. Satheesh, S. Sherwood, B. Stevens and X.Y. Zhang, 2013: Clouds and Aerosols. In: Climate Change 2013: The Physical Science Basis. Contribution of Working Group I to the Fifth Assessment Report of the Intergovernmental Panel on Climate Change [Stocker, T.F., D. Qin, G.-K. Plattner, M. Tignor, S.K. Allen, J. Boschung, A. Nauels, Y. Xia, V. Bex and P.M. Midgley (eds.)]. Cambridge University Press, Cambridge, United Kingdom and New York, NY, USA.

Burnett, R. T., Arden Pope, C., Ezzati, M., Olives, C., Lim, S. S., Mehta, S., Shin, H. H., Singh, G., Hubbell, B., Brauer, M., Ross, Anderson, H., Smith, K. R., Balmes, J. R., Bruce, N. G., Kan, H., Laden, F., Prüss-Ustün, A., Turner, M. C., Gapstur, S. M., Diver, W. R., and Cohen, A: An integrated risk function for estimating the global burden of disease attributable to ambient fine particulate matter exposure, Environ. Health Persp., 122, 397, https://doi.org/10.1289/ehp.1307049, 2014.

Dai, Y. J., Zeng, X. B., Dickinson, R. E. , Baker, I. ,Bonan, G. B. & Bosilovich, M. G.: The common land model. Bulletin of the American Meteorological Society, 84(8), 1013-1023, 2015. doi:10.1175/BAMS-84-8-1013, 2015.

Emmons, L. K. , Walters, S. , Hess, P. G. , J.-F., L. , Pfister, G. G. , & Fillmore, D. , et al. Description and

evaluation of the Model for Ozone and Related Chemical Tracers, version 4 (MOZART-4). Geosci. Model Dev., 3, 43–67, 2010

Falk, S., & Sinnhuber, B. M. Polar boundary layer bromine explosion and ozone depletion events in the chemistry-climate model EMAC v2.52: implementation and evaluation of airsnow algorithm. Geoscientific Model Development, 11(3), 1-15, https://doi.org/10.5194/gmd-11-1115-2018, 2018.

Fiore，A. M., Dentener，F. J., Wild, O., et al. Multimodel estimates of intercontinental source-receptor relationships for ozone pollution. JOURNAL OF GEOPHYSICAL RESEARCH, 114, D04301, doi:10.1029/2008JD010816, 2009, 2009.

Fu， T.-M., Cao, J. J., Zhang, X. Y., Lee, S. C., & Henze, D. K.: Carbonaceous aerosols in china: top-down constraints on primary sources and estimation of secondary contribution. Atmospheric Chemistry and Physics, 12(5), 2725-2746, doi:10.5194/acp-12-2725-2012, 2012.

Galmarini, S., Koffi, B., Solazzo, E., Keating, T., Hogrefe, C., & Schulz, M., et al. Technical note: coordination and harmonization of the multi-scale, multi-model activities HTAP2, AQMEII3, and MICS-Asia3: simulations, emission inventories, boundary conditions, and model output formats. Atmospheric Chemistry and Physics Discuss, 17(2), 1543-1555, 2017.

Ganzeveld, L., Helmig, D., Fairall, C. W. , Hare, J. , & Pozzer, A. . Atmosphere-ocean ozone exchange: a global modeling study of biogeochemical, atmospheric, and waterside turbulence dependencies. Global Biogeochemical Cycles, 23(4), doi:10.1029/2008GB003301,2009.

Han, Z., et al. MICS-Asia II: Model intercomparison and evaluation of ozone and relevant species, Atmos. Environ., 42, 3491 – 3509, doi:10.1016/j.atmosenv.2007.07.031, 2008.

Han, Z., Xie, Z., Wang, G., Zhang, R., & Tao, J. Modeling organic aerosols over east china using a volatility basis-set approach with aging mechanism in a regional air quality model. Atmospheric Environment,124, 186-198, 2016.

Hardacre, C., Wild, O., & Emberson, L.. An evaluation of ozone dry deposition in global scale chemistry climate models. Atmospheric Chemistry and Physics, 15(11), 6419-6436, doi:10.5194/acp-15-6419-2015, 2015.

Horowitz, L. W., Walters, S., Mauzerall, D. L., Emmons, L. K., Rasch, P. J., Granier, C., Tie, X., Lamarque, J.-F., Schultz, M. G., Tyndall, G. S., Orlando, J. J., and Brasseur, G. P.: A global simulation of tropospheric ozone and related tracers: Description and evaluation of MOZART, version 2, J. Geophys. Res.-Atmos., 108, 4784, doi:10.1029/2002JD002853, 2003.

Huijnen, V., Williams, J., van Weele, M., van Noije, T., Krol, M., Dentener, F., and et al. The global chemistry transport model TM5: description and evaluation of the tropospheric chemistry version 3.0, Geosci. Model Dev., 3, 445–473, doi:10.5194/gmd-3-445-2010, 2010.

Jiang, X. , & Yoo, E. H. The importance of spatial resolutions of community multiscale air quality (CMAQ) models on health impact assessment. Science of The Total Environment, 627, 1528-1543, doi: 10.1016/j.scitotenv.2018.01.228, 2018.

Lee, Y. H., & Adams, P. J. : Evaluation of aerosol distributions in the GISS-TOMAS global aerosol microphysics model with remote sensing observations. Atmospheric Chemistry & Physics, 10(5), 2129-2144,

2010.

Li, J., Chen, X., Wang, Z., Du, H., Yang, W., & Sun, Y., et al. : Radiative and heterogeneous chemical effects of aerosols on ozone and inorganic aerosols over East Asia, Science of the Total Environment, 622, 1327-1342, https://doi.org/10.1016/j.scitotenv.2017.12.041, 2018.

Li, Y., & Xu, Y..: Uptake and storage of anthropogenic CO_2 in the pacific ocean estimated using two modeling approaches. Advances in Atmospheric Sciences, 29(4), 795-809, 2012. doi: 10.1007/s00376-012-1170-4, 2012.

Lin, J., An, J., Yu, Q., Yong, C., Ying, L., & Tang, Y., et al. Local and distant source contributions to secondary organic aerosol in the Beijing urban area in summer. Atmospheric Environment, 124, 176-185, 2016.

Lu, Z, Zhang, Q, & Streets, D. G.: Sulfur dioxide and primary carbonaceous aerosol emissions in China and India, 1996–2010. Atmospheric Chemistry and Physics, 11(18), 9839-9864, 2011.

Monks, P. S. A review of the observations and origins of the spring ozone maximum. Atmospheric Environment, 34(21), 3545-3561, 2000.

Myhre, G., D. Shindell, F.-M. Bréon, W. Collins, J. Fuglestvedt, J. Huang, D. Koch, J.-F. Lamarque, D. Lee, B. Mendoza, T. Nakajima, A. Robock, G. Stephens, T. Takemura and H. Zhang, 2013: Anthropogenic and Natural Radiative Forcing. In: Climate Change 2013: The Physical Science Basis. Contribution of Working Group I to the Fifth Assessment Report of the Intergovernmental Panel on Climate Change [Stocker, T.F., D. Qin, G.-K. Plattner, M. Tignor, S.K. Allen, J. Boschung, A. Nauels, Y. Xia, V. Bex and P.M. Midgley (eds.)]. Cambridge University Press, Cambridge, United Kingdom and New York, NY, USA.

Naik, V., Voulgarakis, A., Fiore, A. M., Horowitz, L. W., Lamarque, J.-F., Lin, M., Prather, M. J., Young, P. J., Bergmann, D., Cameron-Smith, P. J., Cionni, I., Collins, W. J., Dalsøren, S. B., Doherty, R., Eyring, V., Faluvegi, G., Folberth, G. A., Josse, B., Lee, Y. H., MacKenzie, I. A., Nagashima, T., van Noije, T. P. C., Plummer, D. A., Righi, M., Rumbold, S. T., Skeie, R., Shindell, D. T., Stevenson, D. S., Strode, S., Sudo, K., Szopa, S., and Zeng, G.: Preindustrial to present-day changes in tropospheric hydroxyl radical and methane lifetime from the Atmospheric Chemistry and Climate Model Intercomparison Project (ACCMIP), Atmos. Chem. Phys., 13, 5277–5298, doi:10.5194/acp-13-5277-2013, 2013.

Pope III, C. A., Burnett, R. T., Turner, M. C., Cohen, A., Krewski, D., Jerrett, M. et al.: Lung cancer and cardiovascular disease mortality associated with ambient air pollution and cigarette smoke: shape of the exposure–response relationships, Environ. Health Persp., 119, 1616, https://doi.org/10.1289/ehp.1103639, 2011.

Powell, H., Krall, J. R., Wang, Y., Bell, M. L., and Peng, R. D.: Ambient coarse particulate matter and hospital admissions in the Medicare Cohort Air Pollution Study, 1999–2010, Environ. Health Persp., 123, 1152, https://doi.org/10.1289/ehp.1408720, 2015.

Richardson, M. I., Toigo, A. D. and Newman, C. E: Planet WRF: A General Purpose, Local to Global Numerical Model for Planetary Atmosphere and Climate Dynamics, Journal of Geophysical Research, 112, E09001, doi:10.1029/2006JE002825, 2007.

Simpson, W. R., von Glasow, R., Riedel, K., Anderson, P., Ariya, P., Bottenheim, J., Burrows, J., Carpenter, L. J., Frieß, U., Goodsite, M. E., Heard, D., Hutterli, M., Jacobi, H.-W., Kaleschke, L., Neff, B., Plane, J., Platt, U., Richter, A., Roscoe, H., Sander, R., Shepson, P., Sodeau, J., Steffen, A., Wagner, T., and Wolff, E.:

Halogens and their role in polar boundary-layer ozone depletion, Atmos. Chem. Phys., 7, 4375–4418, doi:10.5194/acp-7- 4375-2007, 2007.

Tilmes, S., Lamarque, J.-F., Emmons, L. K., Conley, A., Schultz, M. G., Saunois, M., Thouret, V., Thompson, A. M., Oltmans, S. J., Johnson, B., and Tarasick, D.: Technical Note: Ozonesonde climatology between 1995 and 2011: description,evaluation and applications, Atmos. Chem. Phys., 12, 7475–7497, doi:10.5194/acp-12-7475-2012, 2012.

Tsigaridis, K., Daskalakis, N., Kanakidou, M., Adams, P. J., & Zhang, X.. The aerocom evaluation and intercomparison of organic aerosol in global models. Atmos. Chem. Phys., 14(19), 6027-6161, doi:10.5194/acp-14-10845-2014, 2014.

Xu, R. T., Tian, H. Q., Pan, S. F., Prior, S. A., Feng, Y. C., & Batchelor, W. D., et al.: Global ammonia emissions from synthetic nitrogen fertilizer applications in agricultural systems: Empirical and process-based estimates and uncertainty. Global Change Biology, 25, 314-325, doi: 10.1111/gcb.14499, 2019.

Wang, L. T., Wei, Z., Yang, J., Zhang, Y., Zhang, F. F., & Su, J., et al. The 2013 severe haze over southern Hebei, China: model evaluation, source apportionment, and policy implications. Atmospheric Chemistry and Physics, 14(11), 28395-28451, doi:10.5194/acp-14-3151-2014, 2014.

Werf, G. R. V. D., Randerson, J. T. , Giglio, L. , Leeuwen, T. T. V. , Chen, Y. , & Rogers, B. M. , et al. Global fire emissions estimates during 1997–2016. Earth System Science Data, 9(2), 697-720. https://doi.org/10.5194/essd-9-697-2017, 2017.

Yang, W. Y., Li, J., Wang, M., Sun Y. L., Wang, Z. F.. A Case Study of Investigating Secondary Organic Aerosol Formation Pathways in Beijing using an Observation-based SOA Box Model, Aerosol and Air Quality Research, 18: 1606–1616, doi: 10.4209/aaqr.2017.10.0415, 2018.

Young, P. J., Naik, V., Fiore, A. M., et al. 2018 Tropospheric Ozone Assessment Report: Assessment of global-scale model performance for global and regional ozone distributions, variability, and trends. Elem Sci Anth, 6: 10. DOI: https://doi.org/10.1525/elementa.265,2018.

Zhang, X. Y. , Wang, J. Z. , Wang, Y. Q. , Liu, H. L. , Sun, J. Y. , & Zhang, Y. M. . Changes in chemical components of aerosol particles in different haze regions in china from 2006 to 2013 and contribution of meteorological factors. Atmospheric Chemistry and Physics,15,22(2015-11-22), 15(22), 12935-12952, doi:10.5194/acp-15-12935-2015, 2015.

Zhao, B., Wang, S., Donahue, N. M., Jathar, S. H., & Robinson, A. L. .. Quantifying the effect of organic aerosol aging and intermediate-volatility emissions on regional-scale aerosol pollution in china. Scientific Reports, 6, 2016.

Zheng, B., Tong, D., Li, M., Liu, F., Hong, C. P., Geng, G. N., et al. : Trends in China’s anthropogenic emissions since 2010 as the consequence of clean air actions, Atmospheric Chemistry & Physics, 18(19), 14095-14111. https://doi.org/10.5194/acp-18-14095-2018, 2018.

IAP-AACM v1.0： Global to regional evaluation of the atmospheric chemistry model in CAS-ESM

Ying Wei[1,2], Xueshun Chen[1,4], Huansheng Chen[1], Jie Li[1], Zifa Wang[1,2,4], Wenyi Yang[1], Baozhu Ge[1], Huiyun Du[1,2], Jianqi Hao[1,*], Wei Wang[3], Jianjun Li[3], Yele Sun[1], Huili Huang[1]

[1] The State Key Laboratory of Atmospheric Boundary Layer Physics and Atmospheric Chemistry, Institute of Atmospheric Physics, Chinese Academy of Sciences, Beijing 100029, China

[2] University of Chinese Academy of Sciences, Beijing 100049, China

[3] China National Environmental Monitoring Center, Beijing 100012, China

[4] Center for Excellence in Regional Atmospheric Environment, Institute of Urban Environment, Chinese Academy of Sciences, Xiamen 361021, China

[*] Now at: School of Civil and Environmental Engineering, Georgia Institute of Technology, Atlanta, GA, 30332, USA

Correspondence to: Zifa Wang (zifawang@mail.iap.ac.cn)

Abstract:

In this study, a full description and comprehensive evaluation of a global-regional nested model, the Aerosol and Atmospheric Chemistry Model of the Institute of Atmospheric Physics (IAP-AACM), is presented for the first time. Not only the global budgets and distribution, but also a comparison of nested simulation over China against multi-datasets are investigated, benefiting from the access of air quality monitoring data in China since 2013 and the Model Inter-Comparison Study for Asia

project. The model results and analysis can greatly help reduce uncertainties and understand model diversity in assessing global and regional aerosol effects on climate and human health, especially over East Asia and areas affected by East Asia. For global simulation, the 1-year simulation for 2014 shows that the IAP-AACM is within the range of other models. Overall, it reasonably reproduces spatial distribution and seasonal variation of trace gases and aerosols in both surface concentrations and column burdens (mostly within the factor of two). The model well captures spatial variation for carbon monoxide with a bit underestimation over ocean, which implicates uncertainties on ocean source. The simulations well matches the seasonal cycle of ozone except for lands in the northern hemisphere, partly due to the lack of stratospheric-tropospheric exchange. For aerosols, the simulation of fine-mode particulate matter ($PM_{2.5}$) matches observation well. The simulation on primary aerosols (Normalized Mean Bias (NMB) are within $\pm$0.64) is better than secondary aerosols (NMB are greater than 1.0 in some regions). For nested regional simulation, IAP-AACM shows the superiority of higher resolution simulation using the nested domain over East Asia. The model reproduces variation of sulfur dioxide (SO_2), nitrogen dioxide (NO_2) and $PM_{2.5}$ accurately in typical cities, with correlation coefficients (R) above 0.5 and NMB within $\pm$0.5. Compared to the global simulation, the nested simulation exhibits an improved ability to capture the high temporal and spatial variability over China. In particular, R for SO_2 and NO_2 and $PM_{2.5}$ are raised by ~0.15, ~0.2 and ~0.25 respectively in the nested grid. Based on the evaluation and analysis, model improvements needed are suggested.

Key words: IAP-AACM, model evaluation, multi-model inter-comparison, $PM_{2.5}$, China

1. Introduction

Atmospheric composition can affect climate and environment through direct and indirect effects (Intergovernmental Panel on Climate Change (IPCC), 2001). The composition of the troposphere has changed a lot due to anthropogenic activities over the past decades (Akimoto, 2003; Tsigaridis et al., 2006). Changes in the concentration of trace gases such as sulfur dioxide (SO_2) and nitrogen oxides (NO_x = NO + NO_2) have a substantial impact on acid deposition (Mathur et al., 2003), atmospheric oxidation (Calvert, 1984), and gas-particle transformation processes (Saxena et al., 1987). Aerosols formatted from these precursor gases, together with aerosols from other sources, have a direct radiative forcing. By modifying cloud properties, the aerosols also have important indirect effects. As reported in the Fifth Assessment Report (AR5) of IPCC (Myhre et al., 2013), the radiative forcing of aerosols ranges from -1.9 ~ -0.1 W m^{-2}, with the direct radiative forcing ranges from -0.85 ~ 0.15 W m^{-2}. With better model performance and more robust observation network, AR5 achieved increasing confidence in the assessment compared with AR4 (Boucher et al., 2013), but radiative forcing associated with aerosols still has large uncertainties. In addition, aerosols have adverse impacts on human health including respiratory diseases, cardiovascular risk and lung cancer, which has drawn increasing public attention (Burnett et al., 2014; Pope et al., 2011; Powell et al., 2015). It is necessary to represent the key physical and chemical parameters controlling trace

gases and aerosols in order to quantify these adverse effects and project the influence of aerosols in the future.

Chemical Transport Models (CTMs) are mathematical tools for studying the evolution of chemical constituents in the atmosphere. CTMs have irreplaceable advantages in terms of source and sink assessment of trace gases, historical process reproduction, and future scenario projection. Together with observations and laboratory simulations, CTMs have become the main methods for atmospheric environmental research (Wang et al., 2008). But there are numerous uncertain factors affecting model results (e.g. meteorology, emissions and model framework and physiochemical schemes). Therefore, model evaluation is essential for model development and scientific analysis. To date, many assessments with a single model using various observation datasets and multi-model inter-comparisons (with or without observations) have provided us with a comprehensive understanding of model performance and uncertainty. For example, Badia et al. (2017) evaluated the gas-phase chemistry of the Multi-scale Online Nonhydrostatic Atmosphere Chemistry model (NMMB-MONARCH), Mann et al. (2010) evaluated both mass concentration and number concentration of the Global Model of Aerosol Processes (GLOMAP), and Tsigaridis et al. (2014) gave a detail evaluation of organic aerosol in the Aerosol Comparisons between Observations and Models Project (AeroCom). However, evaluations against site observations mainly focused on America and Europe and it's inadequate for EA due to a limited set of data (Søvde et al., 2012; Lee et al., 2015; Kaiser et al. 2018). Spatial distribution of aerosols affects estimation of radiative

forcing (Shindell et al., 2013; Giorgi et al., 2003). Thus using more observations to assess the model results helps to reduce uncertainties of climate effect prediction over East Asia (EA).

Along with economic development and urbanization, most megacities in China have been plagued by haze in recent years. There are many reports on observation and simulation studies addressing particulate matter. The model studies mainly focus on the relationship between haze and weather conditions (Zhang et al., 2015; Tie et al., 2015, 2017), pollutants source apportionment (Wang et al., 2014; Wang et al., 2014), and chemical mechanism of particulate formation (Cheng et al., 2016). Regional models are more often used in local air pollution researches due to its advantage in capturing the variation of inputs (e.g. meteorology, underlying surface and emissions) and therefrom the temporal and spatial variation of pollutants. However, the regional models can't study the long range transport between AE and its downwind/upwind regions due to the limits of lateral (and upper) boundary conditions.

Based on the Global Nested Grid Air Quality Prediction Model System (GNAQPMS) (Chen et al., 2015), we developed the Aerosol and Atmospheric Chemistry Model of the Institute of Atmospheric Physics (IAP-AACM) and coupled it into the Earth System Model of the Chinese Academy of Sciences (CAS-ESM) as the atmosphere chemistry component of the model, using the framework of coupler 7 (CPL7) (Tang et al., 2015; Zhu et al., 2018). IAP-AACM incorporated the localization of several modules, such as dust emission and heterogeneous chemistry. For the dust module, the deflation mechanism and dust loading parameterization are based on a

detailed analysis of the meteorological conditions, landform, and climatology from daily weather records at about 300 local stations in North China (NC) (Wang et al., 2000). For the heterogeneous chemistry scheme, the parameterization of uptake coefficients improved the simulation of sulfate and nitrate in China during the severe haze period (Li et al., 2018). With the ability of multi-scale nesting, it has advantage in application in EA. The development of IAP-AACM allows us to quantify climate effects on a global scale and elucidate air pollution problems on a regional scale over China. Here a large number of datasets are used to evaluate the model, including a dataset of city sites covering China. Continuous year-round observations at city sites can help study of air pollution and model evaluation in China. As we are currently building a global forecasting platform, the model evaluation across a wide range of cities will also provide knowledge for global model forecasting and assessment.

In this study, the off-line IAP-AACM is applied to a 1-year simulation for 2014 and the model results of trace gases and aerosol mass concentration are evaluated against other model datasets and a wide range of observational datasets, including site observations and satellite data. Firstly we present the global evaluation in section 3.1~3.2. The global budgets of sulfur (dimethylsulfide (DMS), SO_2 and sulfate) and carbonaceous (organic matter (OM) and black carbon (BC)) aerosol are compared with other aerosol models in section 3.1. The global distribution and evaluation of trace gases and aerosol are shown in section 3.2. In section 3.3~3.4, we focus on the model simulation of $PM_{2.5}$ and its components in Chinese cities. The nested simulation is compared with an abundant dataset of city sites which cover most areas

in China, and the impact of different resolutions on model performance is also explored. An inter-comparison with the Model Inter-Comparison Study for Asia (MICS-Asia) models is presented in section 3.3, to give a general comparison across EA.

2. Model description and setup

2.1 Model description

2.1.1 CAS-ESM

CAS-ESM is the Earth System Model developed by the Chinese Academy of Sciences. It is a coupled model incorporating the Atmospheric General Circulation Model of IAP (IAP-AGCM) (Su et al., 2014), the Climate System Ocean Model (LICOM) (Liu et al., 2012), the Common Land Model (CoLM) (Dai et al., 2015), the sea ice model (CICE), the Dynamic Global Vegetation Model of IAP (IAP-DGVM) (Zhu et al., 2018), the IAP-AACM, and the land and ocean biogeochemical models of IAP (IAP-OBGCM) (Li et al., 2012). The IAP-AACM provides mass concentration of trace gases and aerosols for CAS-ESM and responds to the feedback of aerosols on meteorological fields. Currently, global climate and ecological environment change is not only one of the core issues of international climate and environment diplomacy, but also an important factor governing the sustainable development of China. Earth system model is a basic tool to understand and solve these problems. The resolution of the CAS-ESM is 1°×1°currently and later will be updated to 0.25°×0.25°. The CAS-ESM will be used for the climate numerical experiment with high resolution

(0.25 °×0.25 °) for 100 years (1950 ~ 2050) and provide simulation results for the CMIP6 and IPCC AR6.

2.1.2 IAP-AACM

The IAP-AACM is developed on the basis of the Nested Grid Air Quality Prediction Model System (NAQPMS) (Wang et al. 2006b) and the Global Nested Grid Air Quality Prediction Model System (GNAQPMS) (Chen et al., 2015). NAQPMS/GNAQPMS is widely used in the simulation of dust (Li et al., 2012), ozone (O_3) (Wang et al., 2006a; Li et al., 2007), deposition (Ge et al., 2014), air pollution policy control (Wu et al., 2011; Li et al., 2016; Wei et al., 2017) and the global transportation of mercury (Chen et al., 2015).

Like GNAQPMS, the IAP-AACM is a multi-scale nested model that describes atmospheric chemistry and aerosol process on both global and regional scales. In the IAP-AACM, sea salt and dust emissions are calculated online. The dust scheme originates from the wind erosion model developed by Wang et al. (2000) and improved by Luo et al. (2006). The simulation of sea salt is based on the scheme of Athanasopoulou et al. (2008). Dry deposition processes are based on the resistance model approach of Zhang et al. (2003). The gas-phase chemistry scheme is Carbon Bond Mechanism Z (CBM-Z) (Zaveri et al., 1999). The cloud convection, aqueous chemistry, in-cloud and below-cloud scavenging use the second generation of Regional Acid Deposition Model (RADM2) (Stockwell et al., 1997). For aerosols, the thermodynamic equilibrium module ISORROPIA (Nenes et al., 1998, 1999) is used to calculate gas-particle partitioning of inorganic aerosols and aerosol water content.

Furthermore, an aerosol microphysics dynamic module (APM) (Yu et al., 2009) was added to expand the simulation from mass concentration to size distribution (Chen et al., 2015, 2017). The secondary organic aerosol (SOA) module is based on the mechanism developed by Strader (1999), considering two anthropogenic emission precursors (toluene and other aromatic hydrocarbons) and four bio-emission precursors (isoprene, monoterpene, etc.) (Li et al., 2011).

In addition, the IAP-AACM includes an updated DMS emission module from Lana et al. (2011). The DMS concentration in seawater is calculated using 47,313 observations of the Global Surface Waters DMS database (http://saga.pmel.noaa.gov/dms/) and an additional 63 observations in the South Pacific (Lee et al., 2010). The IAP-AACM also provides simplified gas-phase chemistry mechanism specially designed for CAS-ESM to provide the major aerosol components (sulfate, OM, BC, dust and sea salt). Retaining aerosols with significant climatic radiative effects while cutting computational load, nitrate and its chemical reactions are excluded. This approach is common in global aerosol models such as the Integrated Massively Parallel Atmospheric Chemical Transport (IMPACT) model (Liu et al., 2005) and GLOMAP (Mann et al., 2010). The simplified scheme contains sulfur species (SO_2, DMS, and sulfur acid gas (H_2SO_4)), ammonia (NH_3) and hydrogen peroxide. Offline monthly fields of the oxidants hydroxyl radical (OH), nitrate ion radical (NO_3), O_3 and super oxidation of hydrogen (HO_2), generated from a simulation of the standard version of IAP-AACM, are read in and interpolated. Chemical processes in the simplified version are the same as those in the standard

version except for the gas-phase scheme mentioned above. In this paper we focus on evaluating simulation results of the standard version model driven by a global version of Weather Research and Forecasting (WRF).

2.2 IAP-AACM setup

In this study, the simulation region covers the globe at 1 °×1 ° resolution and has a nested domain over EA at 0.33 °×0.33 °. Vertically, the model uses 20 layers, from the bottom layer center of 50m to the model top of 20km, and about 10 layers are located below 3 km. The model domain is shown in Fig. 1. The synchronous time step of integration is 1800 s. The meteorology input frequency is 6 hour in the global domain but 3 hour in the nested domain. The simulation period is from December 1st, 2013 to December 31th, 2014, and the first month is spin up time. Lateral boundary conditions for the nested region are real-time calculated by the parent grid. The initial conditions and top boundary conditions of O_3, NO_x and CO are prescribed from the Model for Ozone and Related Chemical Tracers version4 (MOZART-4) (Emmons et al., 2010).

2.3 Emissions

By integrating data from publicly-released emission inventories, we compiled a global high-resolution (0.1 ° × 0.1 °) emission dataset with source categories (29 species and 14 sectors) and interpolate it to the model resolution. The benchmark year is 2010. Detailed information on the emissions is shown in Table 1. We note that volcanic emissions are not yet considered here.

As a consequence of government control policy included in the Five-Year Plan (FYP), China has achieved an obvious decrease in air pollution in the past ten years,

especially for SO_2. According to an announcement by the Ministry of Environmental Protection of China (http://www.zhb.gov.cn/gkml/hbb/qt/201507/t20150722_307020.htm), the country completed the emission reduction task of 12th FYP (2010~2015) ahead of schedule in 2014 with a reduction ratio reaching by 12.9%. As the FYP controls suppressed SO_2 emissions mainly in the energy and industry sectors, we adjusted the total SO_2 emission for 2014 by a factor of 0.9 in China. The annual mean SO_2 emission is shown in Fig. 1. According to the latest emission inventory study for China (Zheng et al., 2018), the other species of emissions didn't decrease so much from 2010 to 2014. Thus we didn't modify the other emissions.

2.4 Meteorology and evaluation

Meteorological fields were provided offline by the global WRF. The global WRF is an extension of mesoscale WRF that was developed for global weather research and forecasting applications. It has more general choice of map projection (to include both conformal and non-conformal map projections). The specification of planetary constants, physics parameterizations and timing conventions are also improved to allow the model to be run as a global model. Thus, it has multiscale and nesting capabilities, blurring the distinction between global and mesoscale models and enabling investigation of coupling between processes on all scales (Richardson et al., 2007). In the study we used WRF version 3.3 (WRFv3.3). The temporal and horizontal spatial resolution of WRFv3.3 was consistent with IAP-AACM. The atmosphere was divided into 27 vertical layers up to 10 hundred Pascal (hPa). Output

of WRF is interpolated to the vertical layers defined in IAP-AACM. WRF was driven by the National Centers for Environmental Prediction (NCEP) Final Analysis (FNL) data and the calculation is nudged to the FNL data.

A comparison of annual mean meteorological fields (temperature, wind and relative humidity) between WRF and reanalysis data (NCEP Reanalysis 1) are presented in Fig. 2. A comparison of annual mean precipitation between the model and reanalysis data from the Global Precipitation Climatology Project is also shown in Fig. S1. Globally, as shown in Fig. 2, the difference in temperature at 2 m (T_2) and wind at 10 m (W_{10}) between the model and observation is within 2 ℃ and 2 m s^{-1} respectively, except in high-latitude areas. The relative humidity at 2 m (RH_2) is generally underestimated on land and overestimated over the ocean, the difference in most areas is within ±10%. The difference in precipitation is within 2 mm day^{-1} except equatorial regions. The frequently strong convection in tropical areas is difficult to reproduce in the model. 443 surface sites in the nested domain are also analyzed with the National Climate Data Center (NCDC) data and the statistical parameters are shown in Table 2. The simulation of the meteorological factors are close to the site records in different season, with mean bias (MB) of -0.3 ~ 0 ℃, -0.8 ~ -0.5 m/s and -4~ -2.3% for T_2, W_{10} and RH_2 respectively. The model underestimates T_2 in all the seasons, especially in summer with Root Mean Square Error (RMSE) of 2 ℃. As for W_{10}, it's also underestimated with MB of -0.8m/s. As for RH2, the underestimation is more obvious in summer (MB= -3.2%) and autumn (MB= -3.2%) than in spring (MB= -2.3%) and winter (MB= -2.8%), mainly stem from the

insufficient prediction of precipitation. The agreement in T_2 and RH_2 with observations is better than that of W_{10}, with annual correlation coefficients (R) of 0.98, 0.84 and 0.53, respectively. Generally, the meteorology calculated by WRF can rationally reproduce the characteristics of observations.

2.5 Observation data

Trace gas observation data for CO, O_3, SO_2, and NO_2 in this paper are collected from the World Data Center for Greenhouse Gas (WDCGG) (http://ds.data.jma.go.jp/gmd/wdcgg/cgi-bin/wdcgg/catalogue.cgi), the Acid Deposition Monitoring Network in East Asia (EANET) (http://www.eanet.asia/product/index.html#datarep), and the Chinese National Environmental Monitoring Center (CNEMC) (http://www.cnemc.cn). Annual observation data of particle and aerosol species are from the European Monitoring and Evaluation Program (EMEP) (http://www.emep.int/), EANET, the United States Environmental Protection Agency (EPA) (http://aqsdr1.epa.gov/aqsweb/aqstmp/airdata/download_files.html#Daily) and the Interagency Monitoring of Protected Visual Environments (IMPROVE) network (http://vista.cira.colostate.edu/improve/). As there is no data published for BC and organic carbon (OC) in Asia in 2014, we collected earlier records from the China Atmosphere Watch Network (CAWNET) reported by Zhang et al. (2008). Hourly air quality data in China are downloaded from CNEMC. The other aerosol observations in China are collected from monitoring sites of Nanjing and Wuhan, and scientific observation at Xinzhou and Beijing (Chen et al., 2015). Aerosol Optical Depth (AOD)

product of MYD04_L2 (http://dx.doi.org/10.5067/MODIS/MYD04_L2.006) from the Moderate Resolution Imaging Spectroradiometer (MODIS) is used to evaluate the simulated AOD. Total column product from the Global Ozone Monitoring Experiment 2 aboard METOP-A (GOME-2A) (https://www.ospo.noaa.gov/Products/atmosphere/gome/gome-A.html) and the Ozone Monitoring Instrument (OMI) (https://earthdata.nasa.gov/earth-observation-data/near-real-time/download-nrt-data/omi-nrt) are also used to evaluate the vertical tropospheric column (VTC) of NO_2 and O_3, respectively. All these datasets are for 2014, except that the CAWNET is for 2006. The corresponding simulations at observation sites are sampled at model grid cells containing those sites. The simulation of seasonal cycle in different regions or cities are first sampled at the model grid cells containing the observational sites and then averaged within sub-regions. The observation datasets are summarized in Table 3 and detailed information for observation sites is given in Table S1. Note that the observed species in Table 3 are not always available at the corresponding sites.

To investigate the model performance over China, we selected 89 stations in 12 cities representing typical areas (NC, Yangtze River Delta (YRD), Pearl River Delta (PRD), Northwest China (NWC), Central China (CC), Southwest China (SWC)) in China (shown in Fig. 1). The six regions represent the major geographical regions over China and they are also the regions on which severe air pollution researches focus. The daily mean city-averaged concentration of pollutants are displayed in figures and used to calculate statistics. In addition, we collected the mass

concentrations of BC, OM, sulfate, nitrate and ammonium in Beijing, Xinzhou, Nanjing and Wuhan (shown in Fig. 1) to evaluate the model performance in simulating aerosol components.

3 Model results and evaluation

3.1 Budgets

On account of the significant radiative effect of sulfate and carbonaceous aerosols, their budgets play an important role in the climate change (Penner et al., 1998). Here we elucidate the budgets of sulfate with its precursor gases (DMS and SO_2) and carbonaceous aerosols.

The global budgets for DMS, SO_2 and sulfate in IAP-AACM are summarized in Table 4. For comparison, Table 4 also lists results from other global aerosol models including IMPACT (Liu et al., 2005), Goddard Institute for Space Studies General Circulation Model with TwO-Moment Aerosol Sectional (GISS-TOMAS) (Lee et al., 2010), Atmospheric Chemistry and Climate Model Intercomparison Project (ACCMIP) models (Lee et al., 2013) and the AeroCom models (Textor et al., 2006). The DMS emission (23.3 TgS yr^{-1}) of IAP-AACM is within the range of other models (10.7~22.8 TgS yr^{-1}). The dry deposition of DMS is zero in IAP-AACM. Therefor the sink is only oxidation. This treatment is common in other models such as ModelE2-TOMAS and ModelE2-OMA (Lee et al., 2015). As a result, we have a higher burden of DMS of 0.19 TgS, just outside the range (0.05~0.15 TgS), and a longer lifetime of 3 days. For SO_2, the emissions are a bit lower than the reference range (54.3 TgS yr^{-1} vs. 63.4~94.9 TgS yr^{-1}). This is ascribed to the lack of volcanic

emissions. The volcanic emissions of SO_2 is about 12.5 TgS yr^{-1} used in most models, based on the work of Andres and Kasgnoc (1998) and Dentener et al. (2006). The oxidation of DMS to SO_2 is 22.8 TgS yr^{-1}, within the range of other models' results. The aqueous-phase process is responsible for 61% of the oxidation to sulfate and gas-phase processes are responsible for the remaining 39%. Although it's a bit lower conversion efficiency for aqueous-phase chemistry compared with other models (about 70% ~ 80%), both aqueous phase and gas phase oxidation are well within the range of other models. Due to the lower removal in aqueous-phase oxidation (29.8 Tg S) and wet deposition (as zero), the lifetime of SO_2 in the model is a little longer than other models (3 days vs. 0.6~2.6 days). In IAP-AACM, the emission of H_2SO_4 is assumed as 2.5% of the total sulfur emission. With a strong wet scavenging effect, 94% of sulfate is removed by wet deposition and the rest by dry deposition.

Table 5 lists the budgets for BC and OM in IAP-AACM. They are in the range of results from other models including Liu et al. (2005), Lee et al. (2013), Lee et al. (2015), Textor et al. (2006), and those listed in Liu et al. (2005). The emissions of BC/OM are at the low end compared with other models (BC: 7.42 TgS yr^{-1} vs. 7.4~19.0 TgS yr^{-1}; OM: 56.7 TgS yr^{-1} vs 34~144 TgS yr^{-1}). The ratio of dry deposition to wet deposition for BC and OM is 15.8% and 13.6%, respectively. Both the burden and lifetime of carbonaceous aerosol are within the other models' results. The burden of BC and OM is 0.13 Tg and 1.16 Tg respectively and the lifetime is 6.4 days and 7.4 days respectively.

The budgets for CO and O_3 are displayed in Table S2. As for CO, the total

emissions are 994 Tg yr^{-1} in IAP-AACM. It's smaller than those in the other models (e.g., 1159 Tg yr^{-1} in Huijnen et al. (2010), 1210.7 Tg yr^{-1} in Emmons et al. (2010)). Direct emissions and oxidation contribute 43.4% and 55.4% to the total CO, respectively. The global annual burden is 327 Tg, smaller than the other models of 353~399 Tg (Horowitz et al., 2003; Huijnen et al., 2010; Badia et al., 2017;). As for ozone, dry deposition contributes 21.3% to the total loss (4924 Tg yr^{-1}), and photochemical reaction is responsible for the rest loss. The dry deposition (1049 Tg yr^{-1}) is larger than values of model collection of ACCENT and ACCMIP (Young et al., 2018).

3.2 Global distribution and evaluation

3.2.1 Hydroxyl radical (OH)

Oxidation is the basic characteristic of atmospheric chemistry. As the most important oxidant in atmosphere, OH is the crucial species in CTMs. OH in troposphere is mainly produced by the reaction $O_3 + h\nu$ ($\lambda \leqq 320$nm) + H2O → 2OH+O2. The tropospheric mean concentration of OH in IAP-AACM is 13.0×10^5 molec cm^{-3}. It is a little higher than the mean OH concentration ($11.1 \pm 1.6 \times 10^5$ molec cm^{-3}) given by 16 ACCMIP models in Naik et al. (2013). The high concentration indicates a stronger atmospheric oxidation. This could explain the lower concentration of CO over ocean. The zonal mean OH concentrations for January, April, July and October are shown in Fig. 3. Like other chemistry models, OH concentration in the tropics keeps highest all the year round and decreases gradually from tropics to poles. This is due to the positive influence of solar radiation and water vapor concentration.

The seasonal north-south shift of OH maximum area is also ascribed to the seasonal variation of these two factors. The mean inter-hemispheric (N/S) ratio of OH in the model is 1.26, in accordance with the multi-model mean ratio of 1.28±0.1 (Naik et al., 2013). Vertically, the highest concentration is in the layer of 2-4 km over the tropics. In Northern Hemisphere, the highest OH concentration appears in summer. Peak value is located at around 30°N, in the atmosphere above 2km. Generally, the distribution of OH concentration is similar with other models (Huijnen et al., 2010; Badia et al., 2017).

3.2.2 Trace gases

Global annual-averaged surface-layer trace gas distributions from IAP-AACM are evaluated against site observations in Fig. 4(a). Scatter plots of observations and simulations divided into 11 regions are exhibited in Fig. 4(b). Fig. 5 shows the comparison of annual surface concentrations of CO, O_3 and NO_2 between IAP-AACM and HTAP CTMs including CAM-Chem (Lamarque et al., 2012), OsloCTM3 (Søvde et al., 2012), and CHASER(Sudo et al., 2002).

Overall, the global surface CO simulation of IAP-AACM is lower than observations, especially in natural source regions. The difference over ocean reaches ~100 ppb, with NMB ranging from -0.59 to -0.45 shown in Table S3. In anthropogenic source regions, the model is close to site records in North America (NAmerica), EA, and Europe with NMB of -0.23, -0.34, -0.39 respectively. The scatter plot clearly shows a negative bias between the model and observations. The lower model results should be related to underestimated emissions and overestimated

OH. As discussed in Sect. 3.2.1, the OH concentration in troposphere is slightly higher than the other models. As shown in Fig. 3, in IAP-AACM, the peak concentration of OH (30-35 molec cm^{-3}) is higher than the other models (under 30 molec cm^{-3}). Due to the sink reaction of CO (CO + OH → CO_2 + H), the CO loss is larger in IAP-AACM. Moreover, the anthropogenic emission of CO is 546.4 Tg yr^{-1} in IAP-AACM (shown in Table S2). It's lower than other emission inventory (e.g. MOZART-4 with 642 Tg yr^{-1} (Emmons et al., 2010), ACCMIP with 610.5 Tg yr^{-1} (Badia et al., 2017)). Janssens-Maenhout et al. (2015) pointed out that CO emission from HTAPv2 has an uncertainty of 15~100% and 35~150% in data from well maintained countries and poorly maintained countries respectively. Furthermore, Shindell et al. (2006) evaluated 26 global models and showed that all the model results are lower than observations in the Northern Hemisphere (NH) except in the tropics. It's related to a lower CO emission source. The spatial distribution of CO concentrations in IAP-AACM is similar to that in other models from HTAP in 2010. High values are found in industrial areas such as NAmerica, Europe and EA, and biomass burning areas (BBAs) such as South Africa (SAfrica) and South America (SAmerica). Overall, IAP-AACM shows lower concentration in BBAs. The difference probably relates to the different fire emissions used in IAP-AACM and HTAP models (GFED4 vs. GFED3) (Janssens-Maenhout et al., 2015). Due to the impact of a reduction of combustion area and decreasing in fuel consumption, there is a reduction of about 20%~30% in BBAs for CO emissions in GFED4, compared with GFED3 (Werf et al., 2017).

The surface distribution of O_3 simulated by IAP-AACM is in a good agreement with observations. The O_3 simulations at most sites are within a factor of two of observations and all the regions have NMB within ±0.2 (Table S3) except for Antarctica and Asia. There are three sites in Southeast Asia exhibit concentrations more than twice the observed values. As the sites are located at coast, simulations in the coarse grids can't capture the steep variation. Besides, South Asia is a high-emission area for biogenic VOCs. Uncertainties in the biogenic emission inventory also cause large errors in O_3 simulation due to photochemical processes. As shown in Fig. 5, IAP-AACM exhibits generally similar surface distribution of O_3 to the other models. But the model shows lower concentrations in high-latitude areas (especially over ocean) than the other models. That should be partly related to the dry deposition over sea ice. The dry deposition velocity to ice is under 0.02 cm s^{-1} across 15 HTAP models (Hardecre et al., 2015). In IAP-AACM, it's higher (0.035~0.048 cm s^{-1}) than those models, as shown in Fig. S2. Additionally, the dry deposition velocity over ocean is 0.042~0.05 cm s^{-1} in IAP-AACM. compared with the HTAP models (around 0.05 cm s^{-1}), there should be a difference less than 12% according to the research in Ganzeveld et al. (2009).

As shown in Fig. 6, the model shows a good skill in capturing the seasonal variation of surface O_3 in the Southern Hemisphere (SH) and the NH oceans. Over ocean, O_3 concentration is higher in spring and lower in summer. In contrast, it's higher in autumn or summer in the SH land. The model shows poor performance on seasonal cycle of surface ozone in the NH, with underestimation in NH land in cold

seasons and overestimation in Europe and EA in summer. In IAP-AACM, the stratospheric-tropospheric exchange is not considered. It leads to a large negative bias in the simulation. The stratosphere-to-troposphere ozone transport event occurs widely across mid-latitudes in the NH (Monks et al., 2000; Akritidis et al., 2018). Researches (Munzert et al, 1985; Austin and Follows, 1991) showed that the maximum of stratosphere to troposphere flux occurs in late winter/spring. The surface O_3 concentrations over EA (sites mainly located in Japan) are overestimated in summer and early autumn. The same pattern is also found in the multi-model inter-comparison of 21 HTAP models (Fiore et al., 2009). The simulations in island countries of EA are sensitive to the timing and extent of the Asian summer monsoon (Han et al., 2008). The positive model bias in this season may stem from inadequate representation of southwesterly inflow of clean marine air. Furthermore, the underestimation of cloud cover in summer may also responsible for the overestimation of O_3 due to stronger photochemistry. Additionally, it's difficult for global model with coarse resolution to resolve local orographically driven flows or sharp gradients in mixing depths under complex underlying surface conditions in lands. As the seasonal variation of surface O_3 should be different in different environment, a seasonal cycle comparison with these NH sites which are separated as land, mountain and marine are also shown in Fig. S3. To varying degrees, the underestimation in cold seasons and overestimation in summer are found in different environments. For inland, the model tends to overestimate O_3 concentrations in summer time. Uncertainties in volatile organic compounds (VOCs)-NOx-O_3

chemistry may contribute. The natural source of isoprene from vegetation is important in the O_3 formation due to its high proportion of VOCs emission in summer (as estimated to be 40.9 Tg/yr in China by Fu et al., 2012). In IAP-AACM, ozone concentration is about 5~15 ppb lower than site observations in Antarctica. It may be caused by the lack of halogen chemistry in the model. Remarkable ozone depletion events which is driven by halogen chemistry (mostly notably as bromine) is observed in the polar boundary layer (Simpson et al., 2007). The model study by Falk & Sinnhuber (2018) indicated that there are missing sources of bromine release from ice and snow in EMAC v2.52. The over prediction of dry deposition velocity to sea ice also plays a role here, as aforementioned discussion.

NO_2 mainly distributes in the anthropogenic source areas, which is well captured by IAP-AACM, see Fig. 4(a). In the NH, the maxima are located in urban areas due to fossil fuel combustion in traffic and industry. The surface concentration of NO_2 is much higher in eastern China (>20 ppb) than that in eastern NAmerica and Europe (3-10 ppb). In the SH, the maxima are located in SAmerica and SAfrica due to biomass burning, where NO_2 ranges of 1-10 ppb. The simulations are in good agreement with observations in NAmerica, Europe, and most parts of EA. As shown in Fig. 4(b), simulations are within a factor of two of observations at most sites, with NMB of -0.14, 0.16 and -0.14 for Asia, Europe and NAmerica, respectively. As we use the same anthropogenic emission inventory, the distribution of NO_2 in NH between IAP-AACM and other models is similar (shown in Fig. 6). The concentration in in SAmerica and SAfrica is slightly lower (~3 ppb) than the other models, due to

aforementioned different version of GFED data used in IAP-AACM and HTAP models. Compared with the other models, the surface NO_2 over ocean is larger in IAP-AACM. In IAP-AACM, the emissions of energy and industry are emitted in the first five layers considering the stack height. The higher injection height of emissions leads to further transportation distance and lower NO_x at surface of source areas (Badia et al., 2017). Consequently, it also leads to higher concentration of surface ozone in NH source areas due to weak NO_x titration.

Similar to NO_2, SO_2 shows high value in the NH land, mainly due to human activities associated with fossil fuel combustion. Maximum concentrations are mainly found in NAmerica, Europe, India and EA, ranging of 5-20ppb. It's even over 20 ppb in Eastern China. SO_2 over ocean is mainly due to DMS oxidation from marine organisms, ranging of 0.1-1ppb. The model shows a distribution of 0.1-20 ppb in EA and 0.1-5 ppb in western NAmerica, which is consistent with observations. The simulation of SO_2 in eastern NAmerica and Europe is about 1-10 ppb, which are overestimated with NMB=3.51 and NMB=3.79 respectively, as shown in Table S3.

3.2.3 Aerosol composition

Fig. 7 shows the annual surface concentrations of aerosols in IAP-AACM in comparison with site observations. The formation of sulfate, nitrate and ammonium (SNA) are due to gas-to-particle conversion in the atmosphere. The distribution of SNA are consistent with the precursor gases (SO_2, NO_x, NH_3), mainly in the NH land. As shown in Fig. 7(a), the surface distribution of SNA in IAP-AACM is close to the site records generally. As shown in Fig. 7(b), sulfate is overestimated more or less.

Specifically, in Asia, the simulations at most sites here are within a factor of two of observations, with NMB of 0.36. However, In NAmerica and Europe, it's overestimated with NMB of 1.94 and 1.1 respectively. The sites average simulation is 1.67 μg m^{-3} and 1.56 μg m^{-3} higher than observations in NAmerica and Europe respectively. The overestimation is consistent with the high level of SO_2 described previously. There are more uncertainties in the simulation of nitrate. Since the volatility of HNO_3 makes nitrate formation more sensitive to environmental factors such as temperature and relative humidity in the atmosphere. The complex photochemical reactions of NO_x also contribute to the uncertainties. The concentration of nitrate is higher in eastern America and lower in western America. IAP-AACM reproduces the distribution of nitrate in western America well but overestimates it in eastern America. The model doesn't fully capture the spatial variation over Europe, with an overestimation at most of the sites. For EA, there is an underestimation of ~5 μg m^{-3} in Southeast Asia and Japan. Overall, the NMB are within ±0.8 (as 0.5, 0.74 and -0.61 for NAmerica, Europe and EA respectively). The performance of ammonium varies in different regions since there are more uncertainties in the emission of NH_3 (precursor of ammonium) from croplands (Xu et al., 2019). There is slight negative bias in America and positive bias in Asia, with NMB less than ±1 (-0.46 and 0.85 respectively). In Europe, there is significant positive bias with NMB of 1.49.

Due to the large contribution of biomass burning and fossil fuel combustion with old technology, carbonaceous aerosols are higher in developing countries than in

developed regions such as NAmerica and Europe. The concentration of BC and OC ranges 2-10 μg m^{-3} and 5-10 μg m^{-3} respectively in China and India, while it ranges ~1 μg m^{-3} and 3-10 μg m^{-3} respectively in SAfrica and SAmerica. By and large, the model results are consistent with observations in the three regions shown in Fig. 7, with the NMB within ±0.65 and ±0.7 for BC and OC respectively. The accuracy of the simulation mainly depends on emissions and deposition processes, since BC is quite inert to chemical reactions.

The simulation of BC in China is accurate with 70% of the stations within a factor of two of observation while OC is underestimated by about 5-10 μg m^{-3}. The meteorological conditions and emission inventories in the model are inconsistent with the observation year (2006) of carbonaceous in China. This may be partially responsible for the bias of OC. According to recent study, there is a slightly increasing (less than 0.1Tg) of both BC and OC emissions from 2006 to 2010 in China (Lu et al., 2011; Fu et al., 2012). As shown in Fig. 7, the simulation of BC at most sites are close to observations while the simulation of OC is significantly underestimated. The study by Fu et al. (2012) showed a significant underestimation of OC emissions over China. Furthermore, Zhao et al. (2016) found that the pathway of intermediate volatile organic compounds (IVOC) to SOA is very important for the formation of SOA. Their model experiments suggest that IVOCs constitute over 40% of OM concentrations in Eastern China. Yang et al. (2018) also showed the significant increase of SOA concentration in an observation-based box model which included the IVOCs reactions. IVOC reactions are not included in our SOA module. The SOA

module in IAP-AACM is Two-Product scheme. Model studies with Two-Product scheme estimated an underestimation of OM by 40-78% in China (Lin et al., 2016; Han et al., 2016). Thus the closely simulating of BC but greatly underestimating of OC requires an improvement in SOA formation mechanism in IAP-AACM.

Generally, the model shows good skill in simulating $PM_{2.5}$. Model results at most sites are close to observations as shown in Fig. 7(b), especially in Europe and Asia with NMB of -0.35 and -0.36 respectively. The underestimation in western China should be related to uncertainties in emissions and unrepresentative simulation with coarse grids.

3.2.4 Comparison with satellite data

The VTC of O_3 is compared against satellite observation derived from OMI (shown in Fig. 8). In the main board, the pattern of the seasonal cycle was covered by the model. In mainland of Northern Hemisphere, the higher O_3 VTC appears during June-July-August (JJA), while in SH, it appears during September-October-November (SON) with a range of 40-60 DU. The model keeps a high value (40-50 DU) in tropics during December-January-February (DJF), possibly due to the high concentration of CO emit from biomass burning. The underestimation of cloud cover in the Intertropical Convergence Zone may contribute, too. The O_3 VTC is significantly underestimated over ocean in middle-high latitudes. As the stratospheric chemistry is not considered in IAP-AACM， the lack of stratospheric-tropospheric exchanges should partly be responsible for the underestimation of column burden.

The VTC of NO_2 is also compared against satellite observation derived from

GOME-2A (shown in Fig. 9). The NO_2 VTC has a range of 20-150 $\times 10^{14}$ molecule cm^{-2} in most source areas. By and large, IAP-AACM reproduced the magnitude in different regions. In addition, the model captured seasonal variations of NO_2 concentration in the vertical troposphere well. In anthropogenic source areas of NH (e.g., NAmerica, Europe, EA), the NO_2 VTC is higher in SON and DJF while lower in JJA. The column concentration is higher during JJA in SAmerica and SAfrica, while it is higher during DJF in central Africa, due to the vegetation burning in dry season. Compared with GOME-2A, IAP-AACM showed a larger column concentration over ocean. The overestimation is also reflected in the comparison of surface concentration. This is probably caused by insufficient oxidation to nitrate and a higher injection height of emission which leads to a farther transportation distance as suggested in Badia et al. (2017). Generally, the distribution of tropospheric NO_2 by the model is consistent with satellite observation.

In order to evaluate the column burden of aerosol in IAP-AACM, we compared the AOD from IAP-AACM with MODIS satellite data as shown in Fig. 10. The calculation of light-extinction coefficient, b_{ext550} (1/Mm, at 550nm), follows equation (1) given by Li et al. (2011):

$$b_{ext550} = 3.0\times f_{SNA}(RH)\{[(NH_4)SO_4]+[(NH_4)NO_3]\}+4.0\times[OC] \\ +10.0\times[BC]+1.0\times[FD]+0.6\times[CD]+1.7\times f_{SS}(RH)\times[SS] \quad (1)$$

where $f_{SNA}(RH)$ and $f_{SS}(RH)$ represent the hygroscopic growth factor for SNA and sea salt respectively, and the variables in brackets are the mass concentration of aerosol species (OC: organic carbon; BC: black carbon; FD: fine dust; CD: coarse dust; SS: sea salt).

In Fig. 10, the model reproduces the spatial features of AOD exhibited by satellites globally. For example, the high value around 60 ℃S, ranging from 0.1 to 0.3, is due to high concentrations of sea salt. The maximum in SAmerica and SAfrica is due to the large amount of carbonaceous aerosol produced by biomass burning. The desert maximum over 0.5 is caused by mineral dust in NAfrica, Arabian Peninsula and western China. High AOD in NAmerica, Europe, India, and EA is caused by anthropogenic aerosols. Furthermore, there is a good agreement of the seasonal variations with satellite observations. For example, the AOD in the desert areas of NH reaches a maximum in March-April-May (MAM) since there are frequent dust storms in the period. SAmerica and SAfrica exhibits the highest AOD during JJA as there is more biomass burning in this season. However, there are several biases between model and observation. The model shows a weaker AOD in Southeast Asia than observation where the value is mainly controlled by biomass burning. The AOD from IAP-AACM is lower than observation to about ~0.4 in eastern China, mainly due to the negative bias in anthropogenic aerosols simulation. Furthermore, the underestimation of RH2 in eastern China (shown in Fig. 2) is also responsible for the lower simulation of AOD. The comparison of monthly gridded average AOD (shown in Fig. S4) shows a discrepancy in EA, due to the bias of dust simulation in spring.

3.3 Nested simulation evaluation

3.3.1 Distribution of pollutants in EA

Fig. 11(a) shows the annual distribution of the four pollutants SO_2, NO_2, PM_{10} and $PM_{2.5}$, against 45 city stations from the nested simulation. In general, the

simulation shows better agreement with sites in Eastern China than Western China. The distribution of $PM_{2.5}$ and its precursors show high levels in Eastern China and low in Western China, which is related to large emissions in the east. The simulation is in good agreement with observations at most sites. Concentrations of precursor gases and particles in Tibet are greatly underestimated. Because the model's coarse resolution can't represent the emission for the city. As shown in Fig. 11(b), model results for NO_2, SO_2 and $PM_{2.5}$ are mostly within the factor of two, with NMB within $\pm$0.3. The "NO_2" values reported by routine monitoring sites are NO_2^*, which partially includes HNO_3 and NO_3^-. It implicates that the model may overestimate "NO_2". PM_{10} concentrations are underestimated at all sites with NMB of -0.51. The model results of PM_{10} and $PM_{2.5}$ include primary $PM_{2.5}$, BC, POA, SOA and SNA. As natural dust contributes a lot to particles in Northwest China, it's underestimated in this area.

Model inter-comparison can give some insights into model uncertainties. Here a comparison between IAP-AACM and several regional models of MICS-Asia is presented in Fig. 12. The MICS-Asia models shown here are WRF-Chem(v3.9) (Tuccella et al., 2012), CMAQ(v4.7.1) (Mebust et al., 2003) and NAQPMS (Wang et al., 2006b). The simulations are for 2010 with the same meteorological fields, emissions and horizontal resolution (45 km). Overall, the IAP-AACM shows similar annual distribution as MICS-Asia models in EA, as the emission inventories used in IAP-AACM are largely the same as MICS-Asia models. The simulation of SO_2 in IAP-AACM is similar to WRF-Chem and CMAQ. The simulation of NO_2 in

IAP-AACM is lower in source area (e.g., eastern China, Japan) but higher over downwind areas, compared with CMAQ. It's possibly related to the higher injection height in IAP-AACM. Although using the same dynamic framework, SO_2 and NO_2 in IAP-AACM are lower than NAQPMS. It should be related to the different dry deposition scheme as Zhang et al. (2003) and Wesely (1989) used in IAP-AACM and NAQPMS respectively. Furthermore, the $PM_{2.5}$ from NQAPMS is higher than IAP-AACM in Northwest of China because it includes dust aerosol in NQAPMS. Overall, the simulation in the nested domain of global model is comparable to regional model.

3.3.2 Trace gas evaluation in cities

To get deeper insight into the performance of IAP-AACM in cities, the nested simulation was compared with daily averaged observations in 12 cities across China. We first focus on NO_2 and SO_2 since they are precursors of SNA aerosols. The monthly variation of SO_2 and NO_2 against observations is shown in Fig. 13 and Fig. 14. Three-quarters of cities show an annual concentration of SO_2 of around 25 μg m^{-3}, only a half of NO_2 in summer and autumn, owing to the strict SO_2 emission reduction policy implemented since 2005. For SO_2, the model shows good agreement with observations except in Wuhan. This probably implies an overestimation of emissions in this city. Furthermore, IAP-AACM reproduces the seasonal variation well, showing good comparison to observations with R over 0.5 in most cities as shown in Table 6. In particular, the cities in NC have a high R of 0.76-0.89.

As illustrated in Fig. 14, the model shows a good performance for NO_2 in cities of

PRD and SWC, matching observations well with RMSE less than 20 μg m^{-3}. The model captures the daily variations well with R of 0.49-0.7 in NC, YRD and PRD. However, the model overestimated NO_2 in NC, YRD and CC in summer. The overestimation of NO_2 in summer is associated with deposition removal process and multiphase chemistry in IAP-AACM. The overestimation of NO_2 and underestimation of nitrate in daytime of summer and autumn relates to over decomposition of nitric acid (HNO_3) at high temperature condition in the thermodynamic equilibrium module. Moreover, heterogeneous chemical reactions in the model should partly be responsible for the overestimation in summer. The heterogeneous chemical module coupled in IAP-AACM has been applied in North China in winter (Li et al, 2018). The mechanism significantly improved sulfate simulation under highly polluted conditions (contributing 50%-80% of total concentration of sulfate) and reduced the overestimation of nitrate. However, the simulations excluded heterogeneous chemical processes showed better performance of NO_2 (shown in Fig. S5). It indicates that a more reasonable mechanism should be considered in model development. Here we also give a comparison of NO_2 VTC over the nested domain between the model and GOME-2A in Fig. S6. Generally, the model captures seasonal variations of NO_2 VTC well. In China, the NO_2 VTC is higher during SON and DJF while lower in JJA, due to unfavorable diffusion conditions and weaker photochemical reactions in autumn and winter.

3.3.3 Aerosol composition evaluation in cities

As shown in Fig. 15, the model performs very well in the simulation of $PM_{2.5}$.

The model reproduces $PM_{2.5}$ variation over the 12 cities well, particularly in NC, YRD and SWC, with an R of 0.70-0.79, 0.71-0.80 and 0.77 respectively. The model results are close to or slightly lower than site observations with city averaged NMB of -0.12. The concentration in NC in winter days is below the observations. Underestimation of $PM_{2.5}$ in severe haze periods is common in CTMs, mainly as a result of the deficiency in the simulation of SNA and Secondary Organic Aerosol (SOA) (Zheng et al., 2015; Donahue et al., 2006). Additionally, the simulation of meteorology (e.g., RH, wind speed, planetary boundary layer height) is more uncertain in severe haze periods. There is a clear underestimation in PRD and Urumqi where mean values are less than half of the observations, with NMB around -0.5. For PRD, it should be related to the underestimation of precursor emission and decomposition of HNO_3. For Urumqi, it should be more related to the unrepresentative simulation with coarse grids. Compared with the scale of urban area and local emissions in Urumqi, the model grids area is too large. Thus the averaged value of grids is significant lower than the local site records. Furthermore, dust is an important component of $PM_{2.5}$ in Urumqi, and this is not included in the result.

To assess the performance of IAP-AACM in representing aerosol components, we compared the model results with 4 stations in NC, YRD and CC in Fig. 16. Generally, the model represents the variation of BC well with R ranging from 0.5 to 0.8 and the values are close to observations. As primary specie, its simulation depends on emission inventory and meteorological conditions. Unlike BC, OM is underestimated at these stations, with a negative bias of 8-12 μg m^{-3}. For SNA

aerosols, sulfate is close to observations in the northern cities (Beijing and Xinzhou), but is underestimated in southern and central cities (Nanjing and Wuhan) by about 10 μg m^{-3}. As the concentration of SO_2 in Wuhan is overestimated, this suggests the underestimation of transportation or the insufficient oxidation of sulfate. The insufficient conversion has been discussed widely in recent years (Cheng et al., 2016; He et al., 2014). Moreover, SO_2 emitted by coal power plants plays a vital role in the formation of sulfate. The coarse grid resolution is insufficient to reproduce the rapid conversion of H_2SO_4 to particles in the plume. The gas-phase oxidation (SO_2 + OH → H_2SO_4(g)) is very sensitive to meteorological variables (particularly radiation and temperature) and gas (OH and NOx) concentration around the stacks (Stevens et al., 2012). The results for ammonium show similar characteristics. The simulation of nitrate is highly underestimated with a difference of 6-16 μg m^{-3}. The underestimation is due to a high frequency of 'zero' value in daytime in summer and autumn. As discussed in 3.3.2, this is caused by over decomposition of HNO_3 in high temperature in the thermodynamic equilibrium module. Schaap et al. (2011) found the same phenomenon in the LOTOSEUROS model using ISORROPIA and recommended improvements in the equilibrium module, including coarse mode nitrate.

3.4 Global versus regional results

High-resolution helps improve CTMs performance, but it is limited by the applicability of parameterization schemes of physical and chemical processes. Recently, sensitivity to horizontal grid resolution has been discussed in some model studies. Wang et al. (2014) showed a better simulation of particles in North China

with CMAQ when increasing the resolution from 36km to 12km. A study of $PM_{2.5}$ heath impact assessment with CMAQ by Jiang et al. (2018) found that model results at 12 km generally performed better and had substantially lower computational burden, compared to 4 km resolution. Here, we compared the global simulation (1 °×1 °) with the nested simulation (0.33 °×0.33 °) over China. Table 6 gives the statistics of $PM_{2.5}$, SO_2 and NO_2 simulated at different resolutions. The nested domain can effectively improve the simulating of city pollutants, especially $PM_{2.5}$, because high-resolution grid can provide better resolved emissions and meteorological fields in urban and rural areas. As shown in Table 6, the correlation coefficients of the three species in the nested simulations are significantly higher than in the global simulations. The RMSE of the nested results in most cities are reduced. For $PM_{2.5}$, the R for Guangzhou and Zhongshan increase by 0.2 and 0.25 respectively, and the R for Urumqi increases by 0.19. Moreover, the RMSE decreases over 9 cities. The improvements in SO_2 simulation is clear, with R increased over 8 cities and RMSE decreased over 9 cities. In particular, the simulation in NC, YRD and SCW improves significantly, with better representation of monthly variation and closer comparison to observations. For NO_2, the R is significantly increased in 9 cities and RMSE is decreased in 7 cities. The best performance is in Beijing with R increased from 0.48 to 0.68.

4. Conclusions

A global-nested aerosol and atmospheric chemistry model coupled into CAS-ESM is introduced in this study. The aim is to provide more precise information on climate effects and air pollution on both global and regional scales.

For the global simulation, the surface distribution of trace gases in the model agrees reasonably well with site observations, mostly within a factor of two. IAP-AACM underestimates CO over ocean mainly due to a higher oxidation loss and the underestimation of emissions over ocean. The model reproduces the annual distribution of O_3 well, with NMB ranging from -0.34 to 0.1 except Asia. Furthermore, the model represents seasonal variation of O_3 over most regions. The model shows an antifact of the ascending-in-spring and descending-in-summer pattern in the NH land. On one hand, the simulation bias is always associated with inaccurate meteorological conditions due to their impacts on photochemistry and intercontinental transportation. On the other hand, it's difficult for global models (with coarse resolution) to resolve the sharp gradient of underlying on the land. The simulation of NO_2 is consistent with site records with NMB within ±0.16. For SO_2, it shows a good agreement with observations except for an overestimation in eastern America and Europe. With a weak scavenging rate by deposition and oxidation, SO_2 in the model has a longer lifetime compared with other models and the burden (0.63 Tg S yr^{-1}) is at the high end of the range 0.2-0.69 Tg S yr^{-1}. The budgets of both carbonaceous aerosols and sulfate are similar to other models. At surface, IAP-AACM shows much closer results to observations for BC but more variable performance for secondary aerosols. In EA, simulations match records on sulfate (NMB=0.36). In NAmerica, simulations match records on nitrate and ammonium (NMB within ±0.5). It overestimates sulfate and ammonium (NMB=1.1 and 1.49 respectively) in Europe and overestimates sulfate (NMB=1.94) in America. The underestimation of OC is mainly due to the inadequate

formation of SOA and the underestimated emission for OC. Above the surface, IAP-AACM generally captures the seasonal and spatial features of O_3 and NO_2 VTC and AOD shown in the satellite products.

For the nested simulation, IAP-AACM shows a very similar annual distribution over EA and a more reasonable distribution on the boundary, compared with regional models from the MICS-Asia project. IAP-AACM shows a good agreement with observations from Chinese cities for spatio-temporal variation. The model compares well with observations for SO_2, with three-quarters cities' R ranging 0.6~0.89 and more than half of the cities' NMB within ±0.5. For NO_2, although more than half of the cities have a correlation above 0.5, there is an overestimation in NC, YRD and CC in summer. The model shows an over decomposition of HNO_3 in warm seasons due to the thermodynamic equilibrium module and heterogeneous mechanism. The underestimation of nitrate also relates to this problem. In most cities, IAP-AACM shows very good simulation skill for $PM_{2.5}$, with R near or above 0.7. For aerosol compositions, the simulation of BC shows better correlation coefficients (above 0.5) in all cities. The simulation of OC is lower than observations. The model results of sulfate and ammonium in NC are close to observations, but it underestimates the concentration in South China. The comparison between global (1 °×1 °) and nested (0.33 °×0.33 °) results indicates that the model reproduces the spatial variation of pollutants in the cities better at fine resolution, as large gradient of emissions between urban and nonurban areas and atmospheric circulations can be better captured by higher resolution grids.

In general, the model shows a favorable performance for trace gases and carbonaceous aerosols. Nevertheless, the simulation of secondary aerosols shows some weaknesses. To reduce uncertainties in the simulation of SNA, more work is needed to improve not only aerosol chemistry but also emission inventories. Moreover, the SOA module should be upgraded to incorporate a comprehensive scheme (e.g. Volatility Bias Set by Donahue et al. (2006)) and verified with observations.

Acknowledgments:

Thanks to Jiangsu Environmental Monitoring Center and Wuhan Environmental Monitoring Center for their support with aerosol composition data of Nanjing and Wuhan respectively. We sincerely thank Prof. Hajime Akimoto at National Institute for Environmental Studies for his suggestion in improving this manuscript. We are particularly grateful to Prof. Oliver Wild at Lancaster University for his support with the HTAP model data and help in improving the language of this manuscript. This research is supported by the National Major Research High Performance Computing Program of China the National Major Research High Performance Computing Program of China (Grant NO. 2016YFB0200800), the Chinese Ministry of Science and Technology (Grant NO. 2017YFC0212402) and the Natural Science Foundation of China (Grant NO. 41571130034; 91544227; 91744203; 41705108; 41620104008).

References

Akimoto, H.: Global air quality and pollution. Science, 302(5651), 1716, 2003.

Akritidis, D., Katragkou, E., Zanis, P.， et al. : A deep stratosphere-to-troposphere ozone transport event over Europe simulated in CAMS global and regional forecast systems: analysis and evaluation. Atmospheric Chemistry and Physics, 18, 15515–15534, doi: 10.5194/acp-18-15515-2018, 2018.

Andres, R. J., & Kasgnoc, A. D. :A time-averaged inventory of subaerial volcanic sulfur emissions, Journal of Geophysical Research Atmospheres, 103(D19), 25251-25261, doi: 10.1029/98JD02091 , 1998.

Athanasopoulou, E., Tombrou, M., Pandis, S. N., & Russell, A. G. : The role of sea-salt emissions and heterogeneous chemistry in the air quality of polluted coastal areas, Atmospheric Chemistry & Physics, 8(19), 5755-5769, doi: 10.5194/acp-8-5755-2008, 2008.

Austin, J.F., Follows, M.J. : The ozone record at Payerne: an assessment of the cross-tropopause flux. Atmospheric Envirnoment 25A, 1873-1880, doi: 10.1016/0960-1686(91)90270-H, 1991.

Badia, A., Jorba, O., Voulgarakis, A., Dabdub, D., Pérez Garcı́a-Pando, C., & Hilboll, A., et al. : Description and evaluation of the multiscale online nonhydrostatic atmosphere chemistry model (NMMB-MONARCH) version 1.0: gas-phase chemistry at global scale, Geoscientific Model Development, 10, 1-47, doi:10.5194/gmd-10-609-2017, 2017.

Boucher, O., D. Randall, P. Artaxo, C. Bretherton, G. Feingold, P. Forster, V.-M. Kerminen, Y. Kondo, H. Liao, U. Lohmann, P. Rasch, S.K. Satheesh, S. Sherwood, B. Stevens and X.Y. Zhang, 2013: Clouds and Aerosols. In: Climate Change 2013: The Physical Science Basis. Contribution of Working Group I to the Fifth Assessment Report of the Intergovernmental Panel on Climate Change [Stocker, T.F., D. Qin, G.-K. Plattner, M. Tignor, S.K. Allen, J. Boschung, A. Nauels, Y. Xia, V. Bex and P.M. Midgley (eds.)]. Cambridge University Press, Cambridge, United Kingdom and New York, NY, USA.

Burnett, R. T., Arden Pope, C., Ezzati, M., Olives, C., Lim, S. S., Mehta, S., Shin, H. H., Singh, G., Hubbell, B., Brauer, M., Ross, Anderson, H., Smith, K. R., Balmes, J. R., Bruce, N. G., Kan, H., Laden, F., Prüss-Ustün, A., Turner, M. C., Gapstur, S. M., Diver, W. R., and Cohen, A: An integrated risk function for estimating the global burden of disease attributable to ambient fine particulate matter exposure, Environ. Health Persp., 122, 397, https://doi.org/10.1289/ehp.1307049, 2014.

Calvert, J. G. : SO_2, NO and NO_2 oxidation mechanisms: atmospheric considerations, 1984.

Chen, C., Sun, Y. L., Xu, W. Q., Du, W., Zhou, L. B., & Han, T. T., et al. : Characteristics and sources of submicron aerosols above the urban canopy (260 m) in Beijing, china, during the 2014 APEC summit, Atmospheric Chemistry and Physics, 15, 12879–12895, doi: 10.5194/acp-15-12879-2015, 2015.

Chen, H. S., Wang, Z. F., Li, J., Tang, X., Ge, B. Z., & Wu, X. L., et al. : GNAQPMS-HG v1.0, a global nested atmospheric mercury transport model: model description, evaluation and application

to trans-boundary transport of Chinese anthropogenic emissions, Geoscientific Model Development, 8(5), 6949-6996, doi:10.5194/gmd-8-2857-2015, 2015.

Chen X. S., Wang, Z. F., Li, J. et al. : Simulation of particle number size distribution in Beijing in winter using NAQPMS+APM model. (in Chinese), 20 (6): 611−619, doi:10.3878/j.issn.1006-9585.2015.15095, 2015.

Chen, X. S., Wang, Z. F., Yu, F. Q., Pan, X. L., Li, J., & Ge, B. Z., et al. : Estimation of atmospheric aging time of black carbon particles in the polluted atmosphere over central-eastern china using microphysical process analysis in regional chemical transport model. Atmospheric Environment, 163(5): 44-56, doi: 10.1016/j.atmosenv.2017.05.016, 2017.

Cheng, Y., Zheng, G., Wei, C., Mu, Q., Zheng, B., & Wang, Z., et al. : Reactive nitrogen chemistry in aerosol water as a source of sulfate during haze events in china. Science Advances, 2(12), doi: 10.1126/sciadv.1601530, 2016.

Dai, Y. J., Zeng, X. B., Dickinson, R. E. , Baker, I. ,Bonan, G. B. & Bosilovich, M. G.: The common land model. Bulletin of the American Meteorological Society, 84(8), 1013-1023, 2015. doi:10.1175/BAMS-84-8-1013, 2015.

Dentener, F., Kinne, S., Bond, T., Boucher, O., Cofala, J., & Generoso, S., et al. : Emissions of primary aerosol and precursor gases in the years 2000 and 1750 prescribed data-sets for AeroCom. Atmospheric Chemistry & Physics, 6(12), 4321-4344, , doi:10.5194/acp-6-4321-2006, 2006.

Donahue N. M., Robinson A. L., Stanier C. O., et al. : Coupled partitioning, dilution, and chemical aging of semivolatile organics. Environmental Science & Technology, 40(8):2635-2643, doi: 10.1021/es052297c, 2006.

Emmons, L. K. , Walters, S. , Hess, P. G. , J.-F., L. , Pfister, G. G. , & Fillmore, D. , et al. : Description and evaluation of the Model for Ozone and Related Chemical Tracers, version 4 (MOZART-4). Geosci. Model Dev., 3, 43–67, doi: 10.5194/gmd-3-43-2010, 2010

Falk, S., & Sinnhuber, B. M. Polar boundary layer bromine explosion and ozone depletion events in the chemistry-climate model EMAC v2.52: implementation and evaluation of airsnow algorithm. Geoscientific Model Development, 11(3), 1-15, https://doi.org/10.5194/gmd-11-1115-2018, 2018.

Fiore，A. M., Dentener，F. J., Wild, O., et al. : Multimodel estimates of intercontinental source-receptor relationships for ozone pollution. JOURNAL OF GEOPHYSICAL RESEARCH, 114, D04301, doi:10.1029/2008JD010816, 2009, 2009.

Fu， T.-M., Cao, J. J., Zhang, X. Y., Lee, S. C., & Henze, D. K.: Carbonaceous aerosols in china: top-down constraints on primary sources and estimation of secondary contribution. Atmospheric Chemistry and Physics, 12(5), 2725-2746, doi:10.5194/acp-12-2725-2012, 2012.

Ganzeveld, L., Helmig, D., Fairall, C. W. , Hare, J. , & Pozzer, A. : Atmosphere-ocean ozone exchange: a global modeling study of biogeochemical, atmospheric, and waterside turbulence dependencies. Global Biogeochemical Cycles, 23(4), doi:10.1029/2008GB003301,2009.

Ge, B. Z., Wang, Z. F., Xu, X. B., Wu, J. B., Yu, X. L., and Li, J. Wet deposition of acidifying substances in different regions of China and the rest of East Asia: Modeling with updated NAQPMS. Environment Pollution, 187, 10-21, doi: 10.1016/j.envpol.2013.12.014, 2014.

Giorgi, F., Bi, X., & Qian, Y. : Indirect vs. direct effects of anthropogenic sulfate on the climate of East Asia as simulated with a regional coupled climate-chemistry/aerosol model. Climatic Change, 58(3), 345-376, 2003.

Granier, C., Lamarque, J. F., Mieville, A., Muller, J. F., and Olivier, J.: POET. : a database of surface emissions of ozone precursors, tech. report, available at: http://www.aero.jussieu.fr/projet/ACCENT/POET.php , 2005.

Han, Z., et al. MICS-Asia II: Model intercomparison and evaluation of ozone and relevant species, Atmos. Environ., 42, 3491 – 3509, doi:10.1016/j.atmosenv.2007.07.031, 2008.

Han, Z., Xie, Z., Wang, G., Zhang, R., & Tao, J. : Modeling organic aerosols over east china using a volatility basis-set approach with aging mechanism in a regional air quality model. Atmospheric Environment,124, 186-198, doi: 10.1016/j.atmosenv.2015.05.045, 2016.

Hardacre, C. , Wild, O. , & Emberson, L., et al. : An evaluation of ozone dry deposition in global scale chemistry climate models. Atmospheric Chemistry and Physics, 15, 6419–6436, doi:10.5194/acp-15-6419-2015, 2015.

He, H., Wang, Y., Ma, Q., Ma, J., Chu, B., & Ji, D., et al. : Corrigendum: mineral dust and nox promote the conversion of so2 to sulfate in heavy pollution days. Sci Rep, 4(1), 4172, doi: 10.1038/srep06092, 2014.

Horowitz, L. W., Walters, S., Mauzerall, D. L., Emmons, L. K., Rasch, P. J., Granier, C., Tie, X., Lamarque, J.-F., Schultz, M. G., Tyndall, G. S., Orlando, J. J., and Brasseur, G. P.: A global simulation of tropospheric ozone and related tracers: Description and evaluation of MOZART, version 2, J. Geophys. Res.-Atmos., 108, 4784, doi:10.1029/2002JD002853, 2003.

Houghton, J. E. T., Ding, Y. H., Griggs, J., Noguer, M., Pj, V. D. L., & Dai, X., et al. : IPCC 2001. Climate Change 2001: the scientific basis. Climate Change 2001: The Scientific Basis, 2001:227-239, 2001.

Huijnen, V., Williams, J., van Weele, M., van Noije, T., Krol, M., Dentener, F., and et al. : The global chemistry transport model TM5: description and evaluation of the tropospheric chemistry version 3.0, Geosci. Model Dev., 3, 445–473, doi:10.5194/gmd-3-445-2010, 2010.

Janssens-Maenhout, G., Crippa, M., Guizzardi, D., Dentener, F., Muntean, M., & Pouliot, G., et al. : HTAP_v2.2: a mosaic of regional and global emission grid maps for 2008 and 2010 to study hemispheric transport of air pollution. Atmospheric Chemistry & Physics, 15(8), 12867-12909, doi: 10.5194/acp-15-11411-2015, 2015.

Jiang, X. , & Yoo, E. H. : The importance of spatial resolutions of community multiscale air quality (CMAQ) models on health impact assessment. Science of The Total Environment, 627, 1528-1543, doi: 10.1016/j.scitotenv.2018.01.228, 2018.

Kaiser, J. C., Hendricks, J., Righi, M., Jöckel, P.,Tost, H.,Kandler, K., et al. : Global aerosol

modeling with MADE3 (v3.0) in EMAC (based on v2.53): model description and evaluation. Geoscientific Model Development Discussion. https://doi.org/10.5194/gmd-2018-185, 2018

Lamarque, J. F., Emmons, L. K., Hess, P. G., Kinnison, D. E., Tilmes, S., & Vitt, F., et al. : Cam-chem: description and evaluation of interactive atmospheric chemistry in the Community Earth System Model. Geoscientific Model Development, 5(2), 369-411, doi:10.5194/gmd-5-369-2012, 2012.

Lana, A., Bell, T. G., Simó, R., Vallina, S. M., Ballabrera-Poy, J., & Kettle, A. J., et al. : An updated climatology of surface dimethlysulfide concentrations and emission fluxes in the global ocean. Global Biogeochemical Cycles, 25(1), 3-25, doi: 10.1029/2010GB003850, 2011.

Lee, Y. H., & Adams, P. J. : Evaluation of aerosol distributions in the GISS-TOMAS global aerosol microphysics model with remote sensing observations. Atmospheric Chemistry & Physics, 10(5), 2129-2144, doi: 10.5194/acp-10-2129-2010, 2010.

Lee, Y. H., Lamarque, J. F., Flanner, M. G., Jiao, C., Shindell, D. T., & Berntsen, T., et al. : Evaluation of preindustrial to present-day black carbon and its albedo forcing from Atmospheric Chemistry and Climate Model Intercomparison Project (ACCMIP). Atmospheric Chemistry & Physics, 13(5), 2607-2634, doi: 10.5194/acp-13-6553-2013, 2013.

Lee, Y. H., Adams, P. J., & Shindell, D. T. : Evaluation of the global aerosol microphysical ModelE2-TOMAS model against satellite and ground-based observations. Geoscientific Model Development, 8(3), 631-667, doi:10.5194/gmd-8-631-2015, 2015.

Li, J., Z. Wang, et al. : Modeling study of ozone seasonal cycle in lower troposphere over east Asia. Journal of Geophysical Research-Atmospheres, 112(D22), doi: 10.1029/2006jd008209, 2007.

Li, J., Wang, Z., Wang, X., Yamaji, K., Takigawa, M., & Kanaya, Y., et al. : Impacts of aerosols on summertime tropospheric photolysis frequencies and photochemistry over central eastern china. Atmospheric Environment, 45(10), 1817-1829, doi: 10.1016/j.atmosenv.2011.01.016 , 2011.

Li, J., Z. Wang, et al. Mixing of Asian mineral dust with anthropogenic pollutants over East Asia: a model case study of a super-duststorm in March 2010. Atmospheric Chemistry and Physics, 12(16): 7591-7606, doi: 10.5194/acpd-12-2743-2012, 2012.

Li, J., Yang, W., Wang, Z., Chen, H., Hu, B., et al. Modeling study of surface ozone source-receptor relationships in East Asia. Atmospheric Research, 167, 77-88, doi: 10.1016/j.atmosres.2015.07.010, 2016.

Li, J., Chen, X., Wang, Z., Du, H., Yang, W., & Sun, Y., et al. : Radiative and heterogeneous chemical effects of aerosols on ozone and inorganic aerosols over East Asia, Science of the Total Environment, 622, 1327-1342, https://doi.org/10.1016/j.scitotenv.2017.12.041, 2018.

Li, Y., & Xu, Y..: Uptake and storage of anthropogenic CO_2 in the pacific ocean estimated using two modeling approaches. Advances in Atmospheric Sciences, 29(4), 795-809, 2012. doi: 10.1007/s00376-012-1170-4, 2012.

Lin, J., An, J., Yu, Q., Yong, C., Ying, L., & Tang, Y., et al. Local and distant source contributions to secondary organic aerosol in the Beijing urban area in summer. Atmospheric

Environment, 124, 176-185, doi: 10.1016/j.atmosenv.2015.08.098, 2016.

Liu, H., Lin, P., Yu, Y. Q., & Zhang, X. : The baseline evaluation of LASG/IAP climate system ocean model (LICOM) version 2. Journal of Meteorological Research, 26(3), 318-329, 2012.

Liu, X., Penner, J. E., & Herzog, M. : Global modeling of aerosol dynamics: model description, evaluation, and interactions between sulfate and nonsulfate aerosols, Journal of Geophysical Research Atmospheres, 110(D18), doi: 10.1029/2004JD005674, 2005

Lu, Z, Zhang, Q, & Streets, D. G.: Sulfur dioxide and primary carbonaceous aerosol emissions in China and India, 1996–2010. Atmospheric Chemistry and Physics, 11(18), 9839-9864, doi: 10.5194/acp-11-9839-2011, 2011.

Luo, G., & WANG Z. F. A Global Environmental Atmospheric Transport Model (GEATM): Model Description and Validation, Atmospheric Science, 30(3), 504-518, doi: 10.1016/S1003-6326(06)60040-X, 2006.

Mann, G. W., Carslaw, K. S., Spracklen, D. V., Ridley, D. A., Manktelow, P. T., & Chipperfield, M. P., et al. : Description and evaluation of GLOMAP-mode: a modal global aerosol microphysics model for the UKCA composition-climate model, Geoscientific Model Development, 3(2), 519-551, doi: 10.5194/gmd-3-519-2010, 2010.

Mathur, R., & Dennis, R. L. : Seasonal and annual modeling of reduced nitrogen compounds over the eastern United States: Emissions, ambient levels, and deposition amounts, Journal of Geophysical Research Atmospheres, 108(D15), 22-1 – 22-15, 2003.

Mebust, M. R., Eder, B. K., Binkowski, F. S., & Roselle, S. J. : Models-3 Community Multiscale Air Quality (CMAQ) model aerosol component 2. model evaluation. Journal of Geophysical Research Atmospheres, 108(D6), doi: 10.1029/2001JD001410, 2003.

Monks, P. S. A review of the observations and origins of the spring ozone maximum. Atmospheric Environment, 34(21), 3545-3561, doi: 10.1016/s1352-2310(00)00129-1, 2000.

Munzert, K. , Reiter, R. , Kanter, H. J. , & K. Pötzl. : Effect of Stratospheric Intrusions on the Tropospheric Ozone. In Proceedings of the Quad. Ozone Symposium, Halkidiki, Reidel, Dordecht, pp. 735-739, doi: 10.1007/978-94-009-5313-0_144, 1985.

Myhre, G., D. Shindell, F.-M. Bréon, W. Collins, J. Fuglestvedt, J. Huang, D. Koch, J.-F. Lamarque, D. Lee, B. Mendoza, T. Nakajima, A. Robock, G. Stephens, T. Takemura and H. Zhang, 2013: Anthropogenic and Natural Radiative Forcing. In: Climate Change 2013: The Physical Science Basis. Contribution of Working Group I to the Fifth Assessment Report of the Intergovernmental Panel on Climate Change [Stocker, T.F., D. Qin, G.-K. Plattner, M. Tignor, S.K. Allen, J. Boschung, A. Nauels, Y. Xia, V. Bex and P.M. Midgley (eds.)]. Cambridge University Press, Cambridge, United Kingdom and New York, NY, USA.

Naik, V., Voulgarakis, A., Fiore, A. M., Horowitz, L. W., Lamarque, J.-F., Lin, M., Prather, M. J., Young, P. J., Bergmann, D., Cameron-Smith, P. J., Cionni, I., Collins, W. J., Dalsøren, S. B., Doherty, R., Eyring, V., Faluvegi, G., Folberth, G. A., Josse, B., Lee, Y. H., MacKenzie, I. A., Nagashima, T., van Noije, T. P. C., Plummer, D. A., Righi, M., Rumbold, S. T., Skeie, R., Shindell, D. T., Stevenson, D. S., Strode, S., Sudo, K., Szopa, S., and Zeng, G.: Preindustrial

to present-day changes in tropospheric hydroxyl radical and methane lifetime from the Atmospheric Chemistry and Climate Model Intercomparison Project (ACCMIP), Atmos. Chem. Phys., 13, 5277–5298, doi:10.5194/acp-13-5277-2013, 2013.

Nenes, A., S. Pandis, et al. : ISORROPIA: A New Thermodynamic Equilibrium Model for Multiphase Multicomponent Inorganic Aerosols, Aquatic Geochemistry, 4(1): 123-152, doi: 10.1023/a:1009604003981, 1998.

Nenes, A., S. N. Pandis, et al. : Continued development and testing of a new thermodynamic aerosol module for urban and regional air quality models, Atmospheric Environment, 33(10): 1553-1560, doi: 10.1016/s1352-2310(98)00352-5, 1999.

Penner, J. E., Chuang, C. C. and Grant, K. : Climate forcing by carbonaceous and sulfate aerosols, Climate Dynamics, 14(12), 839-851, doi: 10.1007/s003820050259, 1998.

Penner, J. E., Andreae, M., Annegarn, H., et al. : climate change 2001: the scientific basis, contribution of working group I to the third assessment report of the IPCC, 2001.

Pope III, C. A., Burnett, R. T., Turner, M. C., Cohen, A., Krewski, D., Jerrett, M. et al.: Lung cancer and cardiovascular disease mortality associated with ambient air pollution and cigarette smoke: shape of the exposure–response relationships, Environ. Health Persp., 119, 1616, https://doi.org/10.1289/ehp.1103639, 2011.

Powell, H., Krall, J. R., Wang, Y., Bell, M. L., and Peng, R. D.: Ambient coarse particulate matter and hospital admissions in the Medicare Cohort Air Pollution Study, 1999–2010, Environ. Health Persp., 123, 1152, https://doi.org/10.1289/ehp.1408720, 2015.

Price, C., J. Penner, & M. Prather. : NOx, from lightning: 1. global distribution based on lightning physics. Journal of Geophysical Research: Atmospheres, 102(D5), 5929-5941, 1997.

Randerson, J. T., G. R. vander Werf, L. Giglio, G. J. Collatz, and P. S. Kasibhatla. : Global Fire Emissions Database, Version 4, (GFEDv4). ORNL DAAC, Oak Ridge, Tennessee, USA. https://doi.org/10.3334/ORNLDAAC/1293, 2015.

Richardson, M. I., Toigo, A. D. and Newman, C. E: Planet WRF: A General Purpose, Local to Global Numerical Model for Planetary Atmosphere and Climate Dynamics, Journal of Geophysical Research, 112, E09001, doi:10.1029/2006JE002825, 2007.

Saxena, P., and Seigneur, C.: On the oxidation of SO_2 to sulfate in atmospheric aerosols. Atmospheric Environment, 21(4), 807-812, 1987.

Schaap, M., Otjes, R. P., and Weijers, E. P. : Illustrating the benefit of using hourly monitoring data on secondary inorganic aerosol and its precursors for model evaluation. Atmospheric Chemistry & Physics, 11(21), 11041-11053, doi: 10.5194/acpd-10-12341-2010, 2011.

Shindell, D. T., G. Faluvegi, et al. : Multimodel simulations of carbon monoxide: Comparison with observations and projected near-future changes, Journal of Geophysical Research-Atmospheres111 (D19), doi: 10.1029/2006JD007100, 2006.

Shindell, D. T., Lamarque, J. F., Schulz, M., Flanner, M., Jiao, C., & Chin, M., et al. Radiative forcing in the ACCMIP historical and future climate simulations, Atmospheric Chemistry &

Physics, 13(3), 2939-2974, doi:10.5194/acp-13-2939-2013, 2013.

Simpson, W. R., von Glasow, R., Riedel, K., Anderson, P., Ariya, P., Bottenheim, J., Burrows, J., Carpenter, L. J., Frieß, U., Goodsite, M. E., Heard, D., Hutterli, M., Jacobi, H.-W., Kaleschke, L., Neff, B., Plane, J., Platt, U., Richter, A., Roscoe, H., Sander, R., Shepson, P., Sodeau, J., Steffen, A., Wagner, T., and Wolff, E.: Halogens and their role in polar boundary-layer ozone depletion, Atmos. Chem. Phys., 7, 4375–4418, doi:10.5194/acp-7-4375-2007, 2007.

Sindelarova, K., Granier, C., Bouarar, I., Guenther, A., Tilmes, S., Stavrakou, T., Müller, J.-F., Kuhn, U., Stefani, P., and Knorr, W. : Global dataset of biogenic VOC emissions calculated by the MEGAN model over the last 30 years, Atmospheric Chemistry & Physics, 14(17), 10725-10788, doi:10.5194/acpd-14-10725-2014, 2014.

Søvde, O. A., Prather, M. J., Isaksen, I. S. A., & Berntsen, T. K. : The chemical transport model OSLO CTM3. Geoscientific Model Development, 5(6), 1441-1469, doi: doi:10.5194/gmd-5-1441-2012, 2012.

Stevens, R. G., Pierce, J. R., Brock, C. A., Reed, M. K., Crawford, J. H., & Holloway, J. S., et al. : Nucleation and growth of sulfate aerosol in coal-fired power plant plumes: sensitivity to background aerosol and meteorology. Atmospheric Chemistry & Physics, 12(1), 189-206, doi: 10.5194/acp-12-189-2012, 2012.

Stockwell, W. R., Kirchner, F., Kuhn, M., & Seefeld, S. : A new mechanism for regional atmospheric chemistry modeling, Journal of Geophysical Research Atmospheres, 102(D22), 25847-25879, doi: 10.1029/97JD00849, 1997.

Strader, R., F. Lurmann, et al. : Evaluation of secondary organic aerosol formation in winter, Atmospheric Environment, 33(29): 4849-4863, doi: 10.1016/s1352-2310(99)00310-6 , 1999.

Sudo, K., Takahashi, M., Kurokawa, J. I., & Akimoto, H. : Chaser: A global chemical model of the troposphere 1. Model description. Journal of Geophysical Research Atmospheres, 107(D17), ACH-1-ACH 7-20, 10.1029/2001jd001113, 2002.

Su, T., Xue, F., & Zhang, H. : Simulating the intraseasonal variation of the East Asian summer monsoon by IAP AGCM 4.0, Advances in Atmospheric Sciences, 31(3), 570-580, 2014.

Tang Y., Dong, W., Li, L., Xue, W., Wang, B.. : CPL7 and its application prospect in the Earth system models of China, Advances in Earth Science, 30(5):620-625, 2015. (in Chinese)

Textor, C., Schulz, M., Guibert, S., Kinne, S., Balkanski, Y., & Bauer, S., et al. : Analysis and quantification of the diversities of aerosol life cycles within AEROCOM, Atmospheric Chemistry & Physics, 6, 1777-1813, doi: 10.5194/acpd-5-8331-2005, 2006.

Tie, X., Zhang, Q., He, H., Cao, J., Han, S., & Gao, Y., et al. : A budget analysis of the formation of haze in Beijing. Atmospheric Environment, 100, 25-36, 2015.

Tie X, Huang R J, Cao J, et al. Severe Pollution in China Amplified by Atmospheric Moisture, Scientific Reports, 7(1):15760, 2017.

Tsigaridis, K., Krol, M., Dentener, F. J., & Balkanski, Y. : Change in global aerosol composition since preindustrial times, Atmospheric Chemistry & Physics, 6(12), 5143-5162, 2006.

Tsigaridis, K., Daskalakis, N., Kanakidou, M., Adams, P. J., Artaxo, P., & Bahadur, R., et al. : The AEROCOM evaluation and intercomparison of organic aerosol in global models, Atmospheric Chemistry & Physics, 14(5), 6027-6161, 2014.

Tuccella, P., Curci, G., Visconti, G., Bessagnet, B., Menut, L., & Park, R. J. : Modeling of gas and aerosol with wrf/chem over europe: evaluation and sensitivity study, Journal of Geophysical Research Atmospheres, 117(D3), doi: 10.1029/2011JD016302, 2012.

Wang, L. T., Wei, Z., Yang, J., Zhang, Y., Zhang, F. F., & Su, J., et al. : The 2013 severe haze over the southern Hebei, China: Model evaluation, source apportionment, and policy implications, Atmospheric Chemistry & Physics, 14(6), 3151-3173, doi: 10.5194/acp-14-3151-2014, 2014.

Wang, Y. X., Mcelroy, M. B., Jacob, D. J., & Yantosca, R. M. : A nested grid formulation for chemical transport over Asia: Applications to CO, Journal of Geophysical Research, 109(D22), 2285-2311, 2008.

Wang, Y., Li, L., Chen, C., Huang, C., Huang, H., & Feng, J., et al. : Source apportionment of fine particulate matter during autumn haze episodes in Shanghai, China, Journal of Geophysical Research Atmospheres, 119(4), 1903–1914, DOI: 10.1002/2013JD019630, 2014.

Wang, Z. F., Ueda, H., & Huang, M. : A deflation module for use in modeling long-range transport of yellow sand over East Asia, Journal of Geophysical Research Atmospheres, 105(D22), 26947-26959, doi: 10.1029/2000JD900370, 2000.

Wang, Z., Li, J., Wang, X., Pochanart, P., & Akimoto, H. Modeling of regional high ozone episode observed at two mountain sites (MT. Tai and Huang) in East China. Journal of Atmospheric Chemistry, 55(3), 253-272, doi: 10.1007/s10874-006-9038-6, 2006a.

Wang, Z. F., Xie, F. Y., Wang X. Q., An J. L., Zhu, J. : Development and Application of Nested Air Quality Prediction Modeling System, Chinese Journal of Atmospheric Sciences, 30(5),778-790, 2006b. (in Chinese)

Wang, Z. F., Xie, F., Sakurai, T., Ueda, H., Han, Z., & Carmichael, G. R., et al. : Mics-Asia II: model inter-comparison and evaluation of acid deposition, Atmospheric Environment, 42(15), 3528-3542, 2008.

Wei, Y., Li, J., Wang, Z. F., Chen, H. S., Wu, Q. Z., et al. Trends of surface $PM_{2.5}$ over Beijing–Tianjin–Hebei in 2013–2015 and their causes: emission controls VS. meteorological conditions, Atmospheric and Oceanic Science Letters, 10(4), 276-283, doi: 10.1080/16742834.2017.1315631, 2017.

Werf, G. R. V. D., Randerson, J. T. , Giglio, L. , Leeuwen, T. T. V. , Chen, Y. , & Rogers, B. M. , et al. : Global fire emissions estimates during 1997–2016. Earth System Science Data, 9(2), 697-720. https://doi.org/10.5194/essd-9-697-2017, 2017.

Wesely, M. L. : Parameterization of surface resistances to gaseous dry deposition in regional-scale numerical models, Atmospheric Environment, 23(6), 1293-1304, doi:

10.1016/0004-6981(89)90153-4, 1989.

Wu, Q. Z., Z. F. Wang, et al. A numerical study of contributions to air pollution in Beijing during CAREBeijing-2006, Atmospheric Chemistry and Physics, 11(12), 5997-6011, 2011.

Xu, R. T., Tian, H. Q., Pan, S. F., Prior, S. A., Feng, Y. C., & Batchelor, W. D., et al.: Global ammonia emissions from synthetic nitrogen fertilizer applications in agricultural systems: Empirical and process-based estimates and uncertainty. Global Change Biology, 25, 314-325, doi: 10.1111/gcb.14499, 2019.

Yan, X. Y., Ohara, T., & Akimoto, H. : Statistical modeling of global soil NOx emissions. Global Biogeochemical Cycles, 19(3), 2005.

Yang, W. Y., Li, J., Wang, M., Sun Y. L., Wang, Z. F. : A Case Study of Investigating Secondary Organic Aerosol Formation Pathways in Beijing using an Observation-based SOA Box Model, Aerosol and Air Quality Research, 18: 1606–1616, doi: 10.4209/aaqr.2017.10.0415, 2018.

Young, P. J., Naik, V., Fiore, A. M., et al. 2018 Tropospheric Ozone Assessment Report: Assessment of global-scale model performance for global and regional ozone distributions, variability, and trends. Elem Sci Anth, 6: 10. DOI: https://doi.org/10.1525/elementa.265,2018.

Yu, F. and Luo, G.: Simulation of particle size distribution with a global aerosol model: contribution of nucleation to aerosol and CCN number concentrations, Atmos. Chem. Phys., 9, 7691– 7710, doi:10.5194/acp-9-7691-2009, 2009.

Zaveri, R. and L. Peters: A new lumped structure photochemical mechanism for large-scale application, Journal of Geophysical Research-Atmospheres, 104(D23), doi: 10.1029/1999JD900876, 1999.

Zhang, L. M., Brook, J. R., & Vet, R. : A revised parameterization for gaseous dry deposition in air-quality models, Atmos.chem.phys, 3(2), 2067-2082, doi: 10.5194/acp-3-2067-2003, 2003.

Zhang, Q., Quan, J., Tie, X., Li, X., Liu, Q., & Gao, Y., et al. : Effects of meteorology and secondary particle formation on visibility during heavy haze events in Beijing, China, Science of the Total Environment, 502, 578-584, 2015.

Zhang, X. Y., Wang, Y. Q., Zhang, X. C., Guo, W., & Gong, S. L. : Carbonaceous aerosol composition over various regions of china during 2006, Journal of Geophysical Research, 113(D14), doi: 10.1029/2007JD009525, 2008.

Zhao, B., Wang, S., Donahue, N. M., Jathar, S. H., & Robinson, A. L. : Quantifying the effect of organic aerosol aging and intermediate-volatility emissions on regional-scale aerosol pollution in china. Scientific Reports, 6, doi: 10.1038/srep28815, 2016.

Zheng, B., Zhang, Q., Zhang, Y., He, K. B., Wang, K., & Zheng, G. J., et al. : Heterogeneous chemistry: a mechanism missing in current models to explain secondary inorganic aerosol formation during the January 2013 haze episode in North China, Atmospheric Chemistry & Physics, 14(15), 2031-2049, doi:10.5194/acp-15-2031-2015, 2015.

Zheng, B., Tong, D., Li, M., Liu, F., Hong, C. P., Geng, G. N., et al. : Trends in China's

anthropogenic emissions since 2010 as the consequence of clean air actions, Atmospheric Chemistry & Physics, 18(19), 14095-14111. https://doi.org/10.5194/acp-18-14095-2018, 2018.

Zhu, J., Zeng, X., Zhang, M., Dai, Y., Ji, D., & Li, F., et al. : Evaluation of the new dynamic global vegetation model in CAS-ESM, Advances in Atmospheric Sciences, 35(6), 659-670, 2018.

Figures

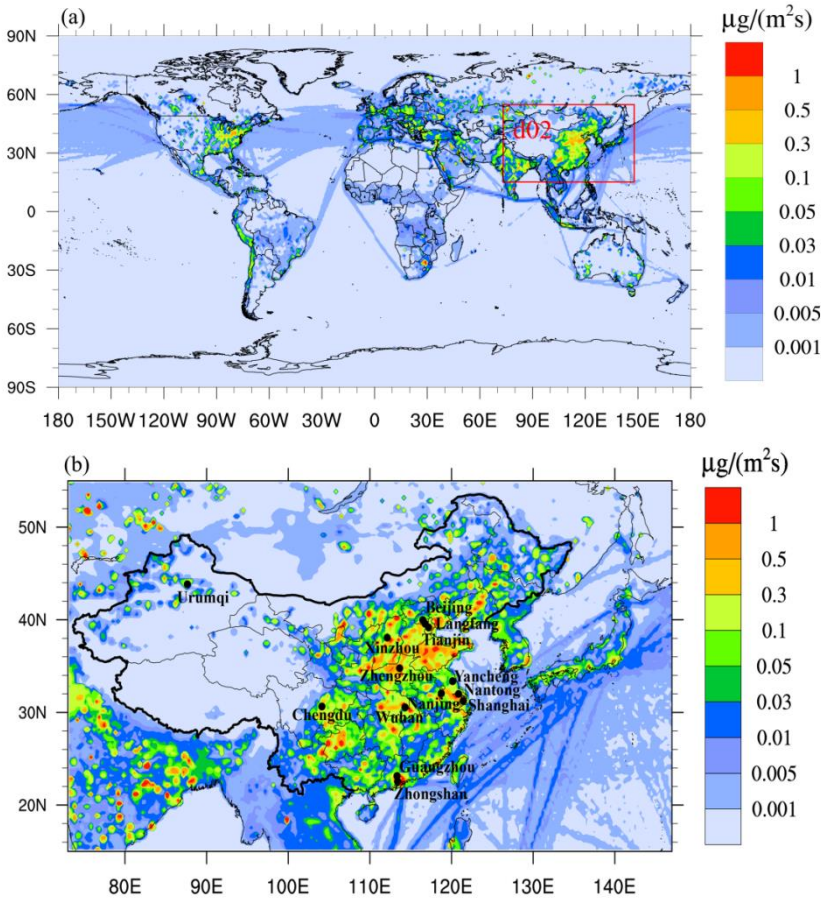

1160 Fig. 1. The simulation domain with total SO_2 emission (μg m^{-2} s^{-1}). (a) domain 1; (b) domain 2, black circles are locations of the city sites in China.

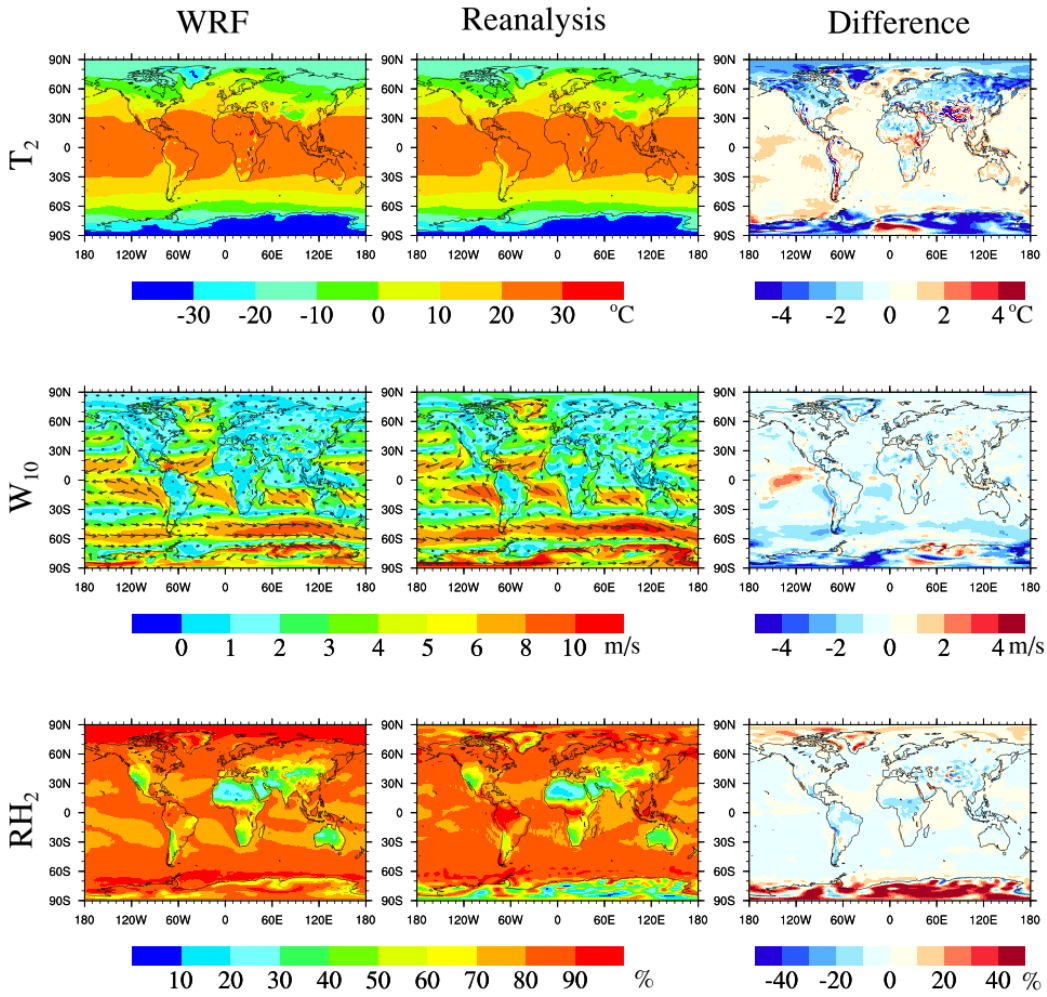

Fig. 2. Comparison of annual meteorological fields. The left column is WRF simulation, the middle column is reanalysis data, and the right column is the
1165 difference between simulation and reanalysis (WRF-Reanalysis). The reanalysis data is NCEP Reanalysis1.

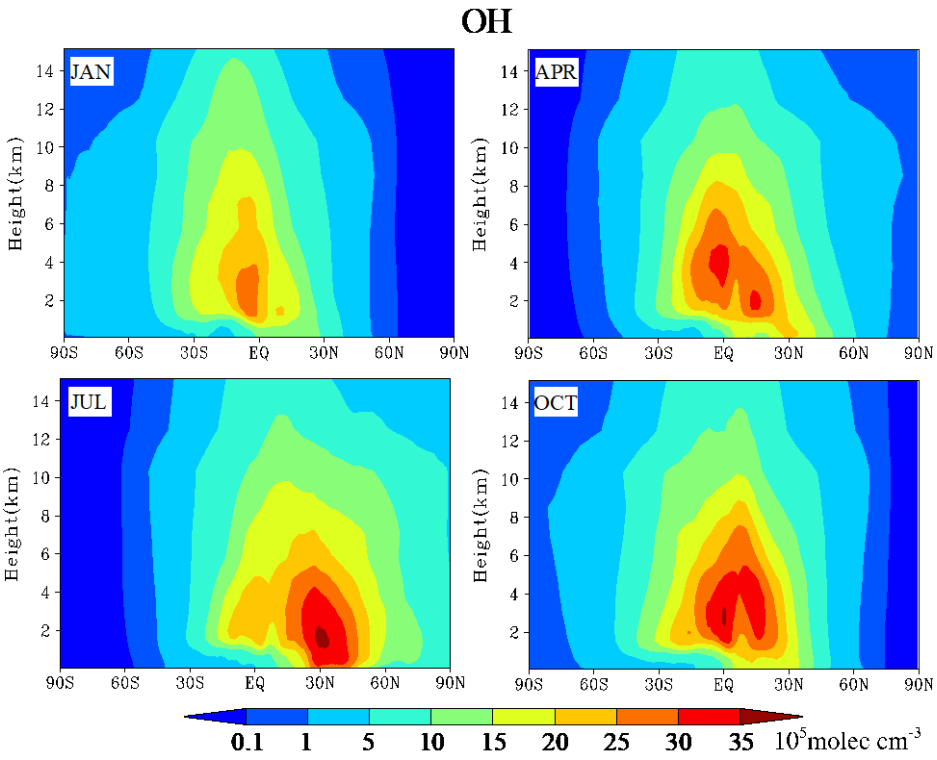

Fig. 3 Zonal monthly mean concentration of OH in the troposphere for January, April, July and October by the IAP-AACM. The unit is 10^5 molecule cm^{-3}.

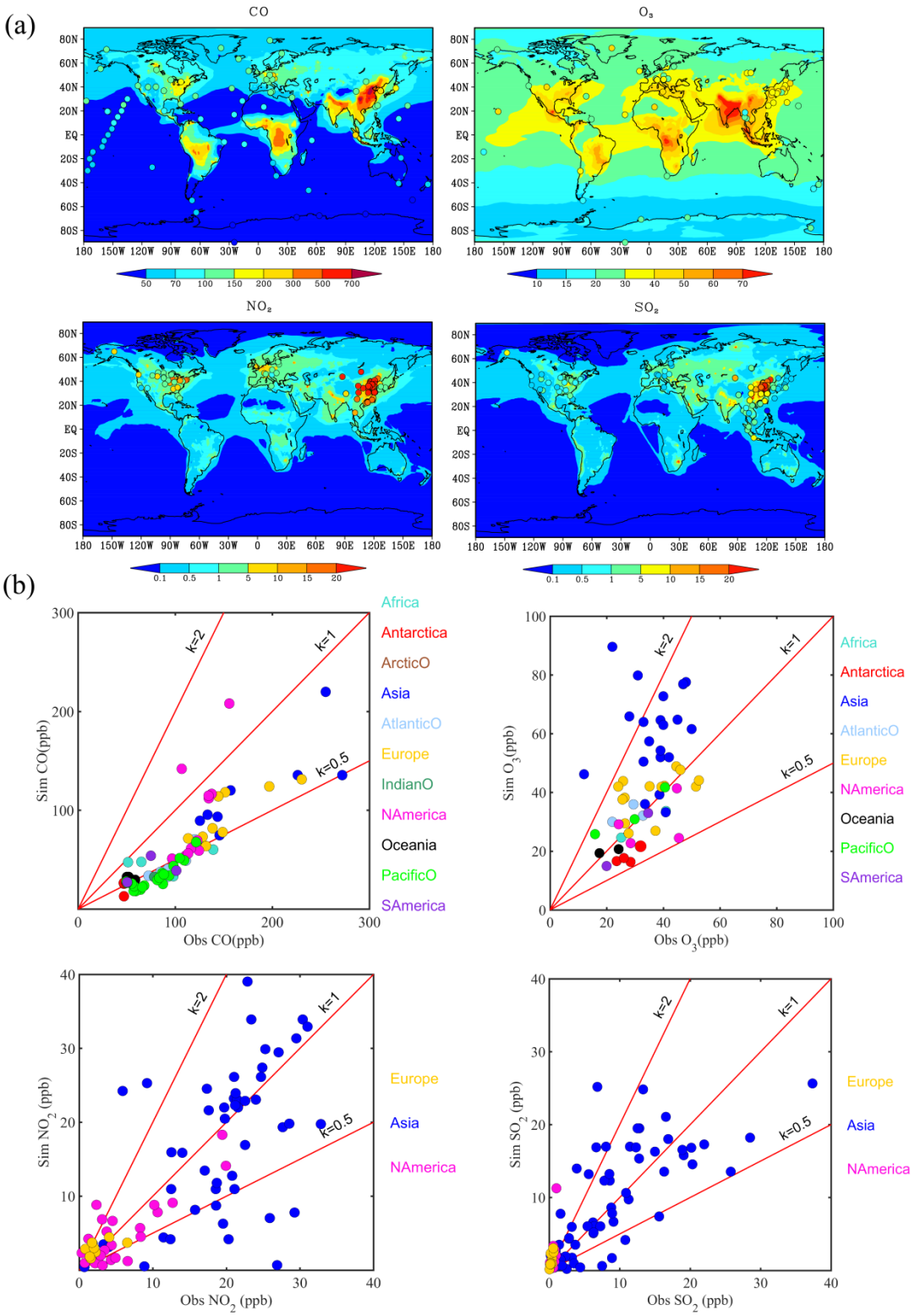

Fig. 4. Annual mean concentration (ppb) of the surface layer in IAP-AACM compared with observations. (a) The circles represent site observations. The first row is CO and
1175 O_3, the bottom row is NO_2 and SO_2. (b) Scatter plots in Africa, Antarctica, Arctic Ocean (ArcticO), Asia, Atlantic Ocean (AtlanticO), Europe, Indian Ocean (IndianO), North America (NAmerica), South America (SAmerica), Oceania and Pacific Ocean

(PacificO). The abscissa shows the observation and the ordinate shows the simulation. The color of the points represents different regions.

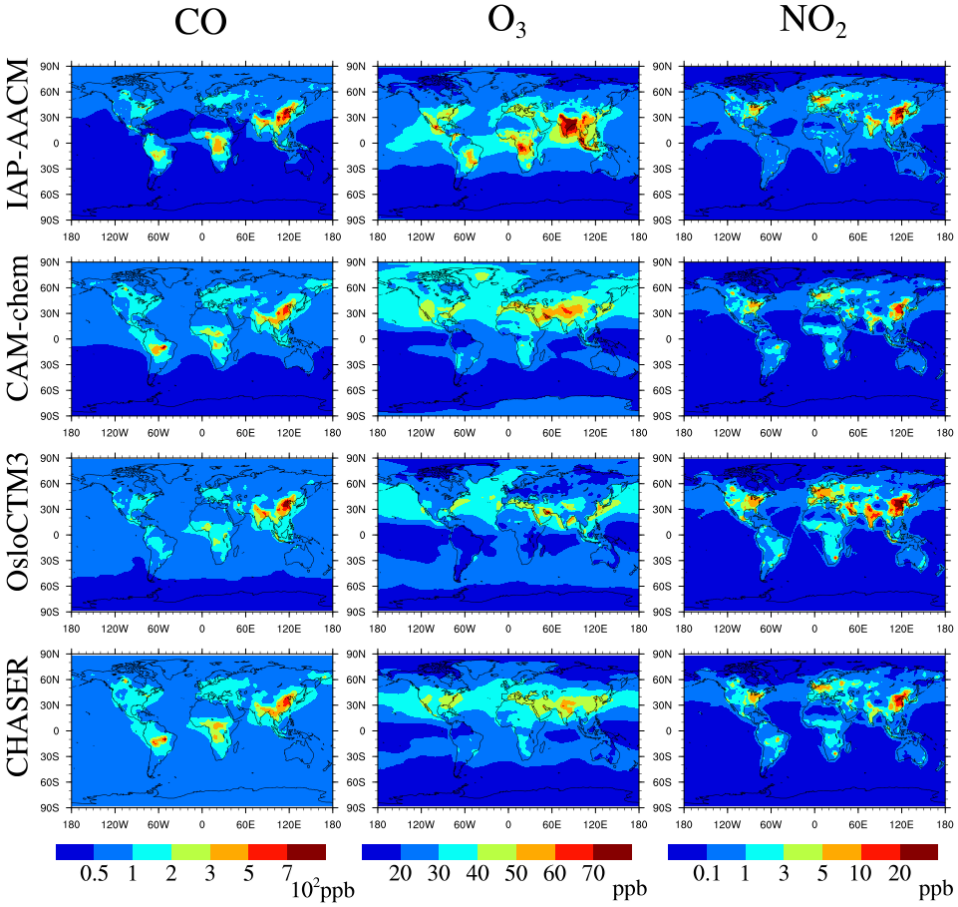

Fig. 5. Annual mean surface distributions (ppb) from IAP-AACM compared with HTAP models. Rows from top to bottom represent IAP-AACM, CAM-Chem, OsloCTM3 and CHASER respectively. The left column displays CO, the middle column displays O_3 and the right column is NO_2.

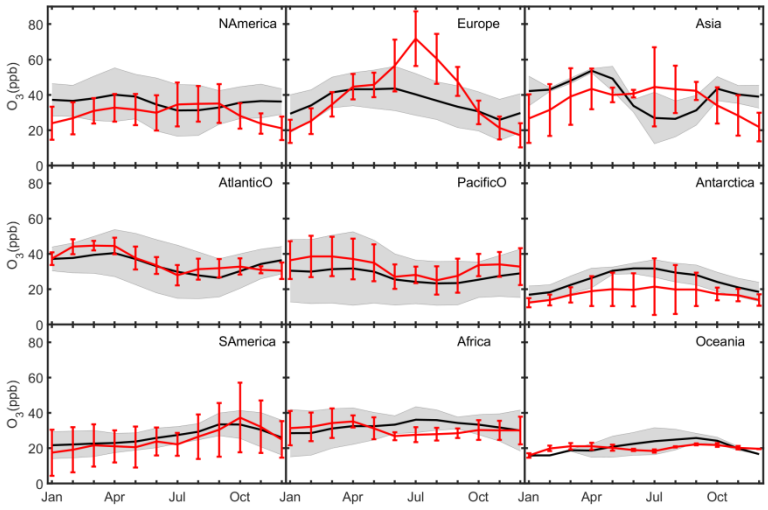

Fig. 6. Mean seasonal variation of O_3 (ppb) over NAmerica, Europe, Asia, AtlanticO, PacificO, Antarctica, SAmerica, Africa and Oceania sites. Black lines and red lines represent the average of observations and simulations respectively. Gray shaded areas

and red vertical bars show 1 standard deviation over the sites for observations and for model results respectively.

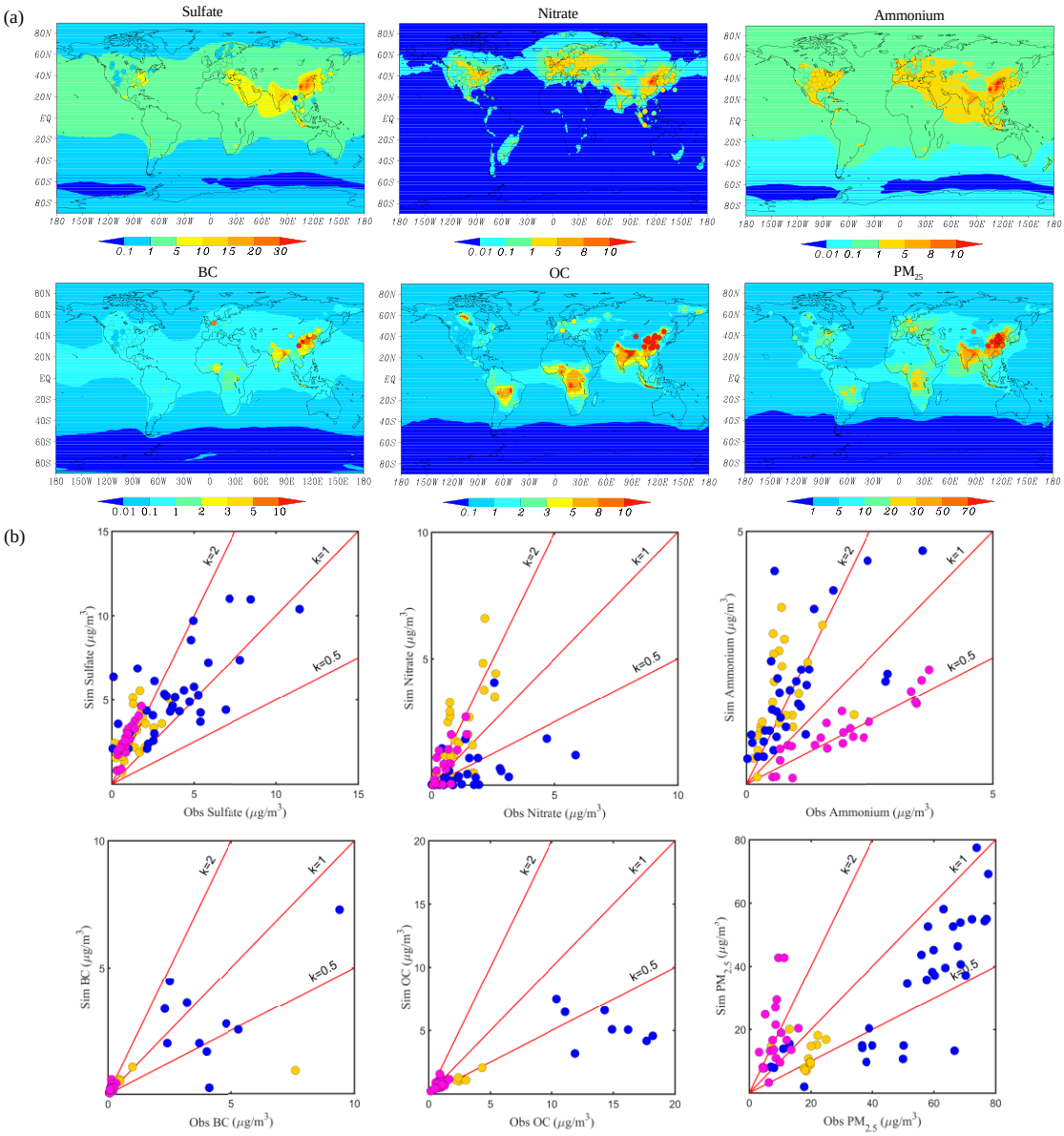

Fig. 7. (a) The same as Fig. 4, except the species are sulfate, nitrate, ammonium, BC, OC, and $PM_{2.5}$ and the unit is μg m^{-3}. The top row is sulfate, nitrate and ammonium, the bottom row is BC, OC and $PM_{2.5}$. (b) Scatter plot of annual mean concentration. The order of the subplot is in accordance with Fig. 7(a). Solid circles in blue, yellow and magenta represent Asia, Europe and NAmerica, respectively.

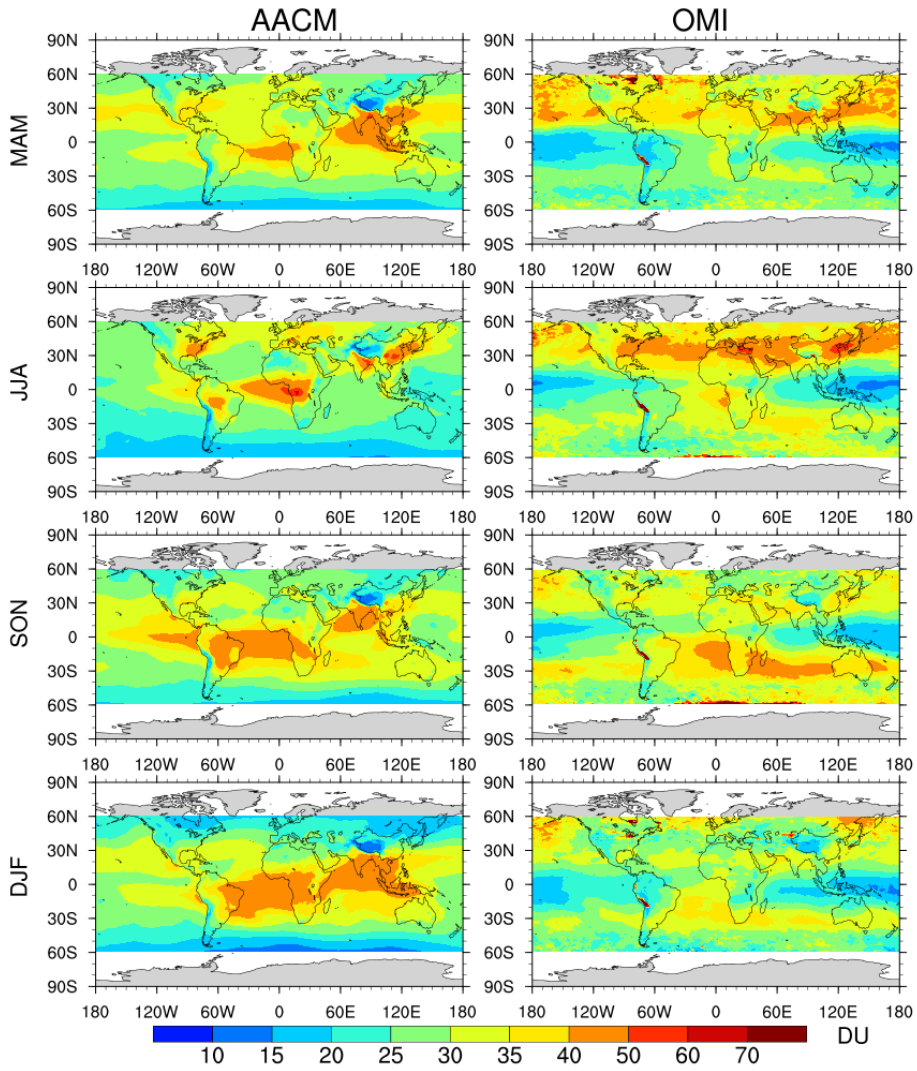

Fig. 8. Seasonal mean column concentration of O_3 from IAP-AACM (left column) and OMI (right column). Seasons are defined as March-April-May (MAM), June-July-August (JJA), and September-October-November (SON), and December-January-February (DJF). The unit is DU.

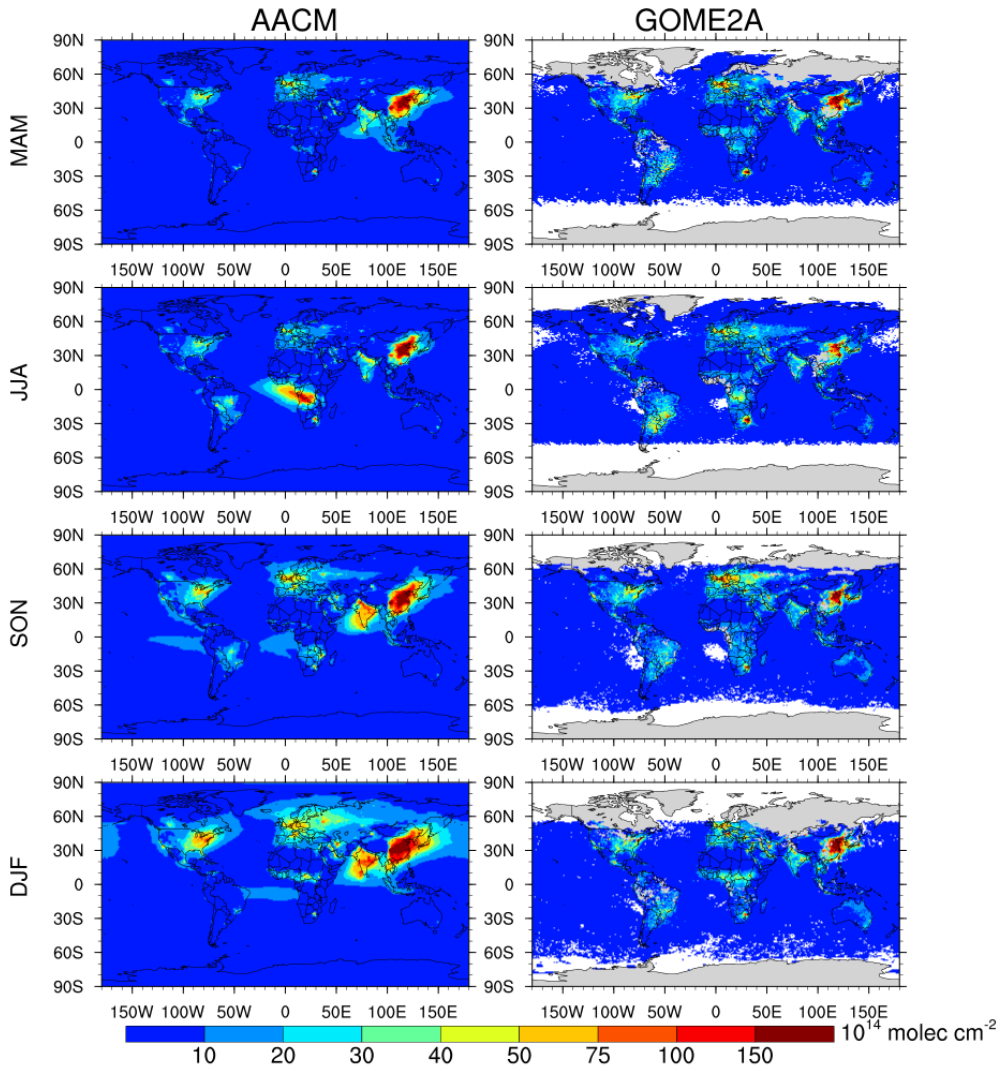

1205 Fig. 9. Seasonal mean column concentration of NO_2 from IAP-AACM (left column) and GOME-2A (right column). The unit is 10^{14} molecule cm^{-2}.

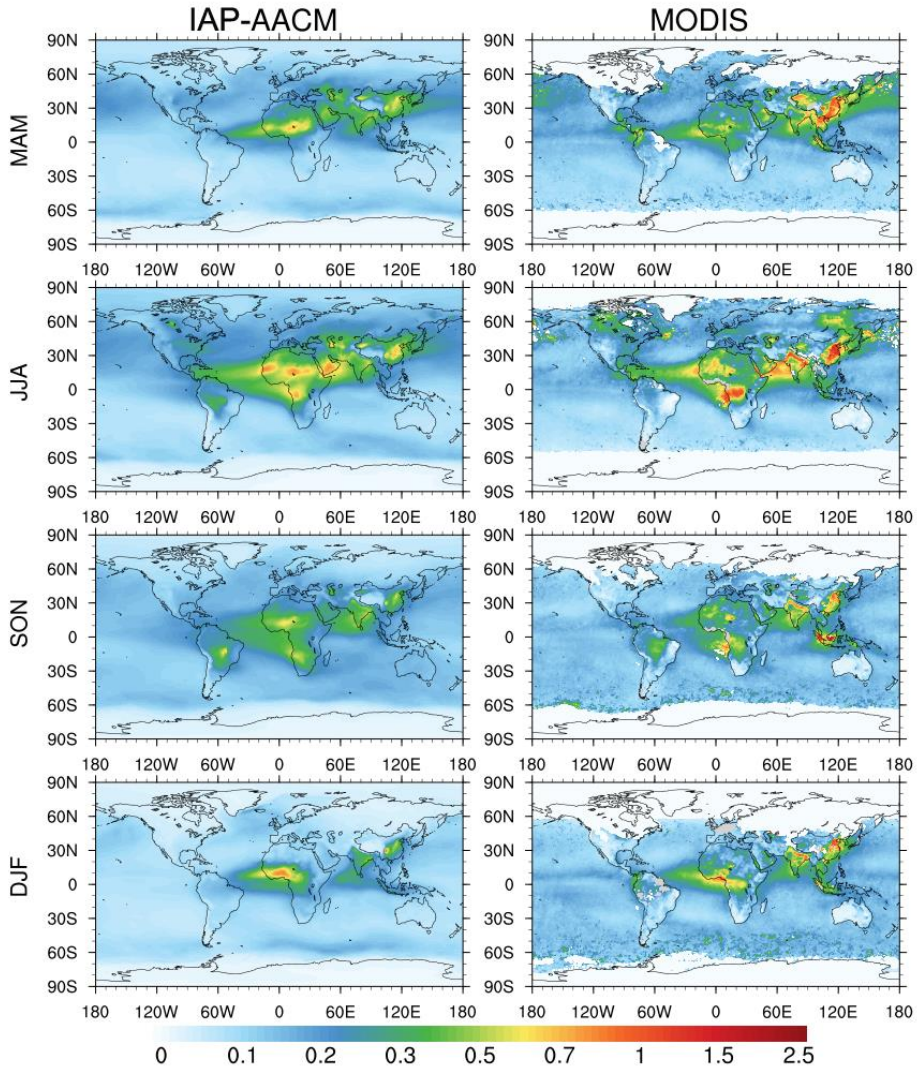

Fig. 10. Seasonal mean AOD from IAP-AACM (left column) and MODIS (right column).

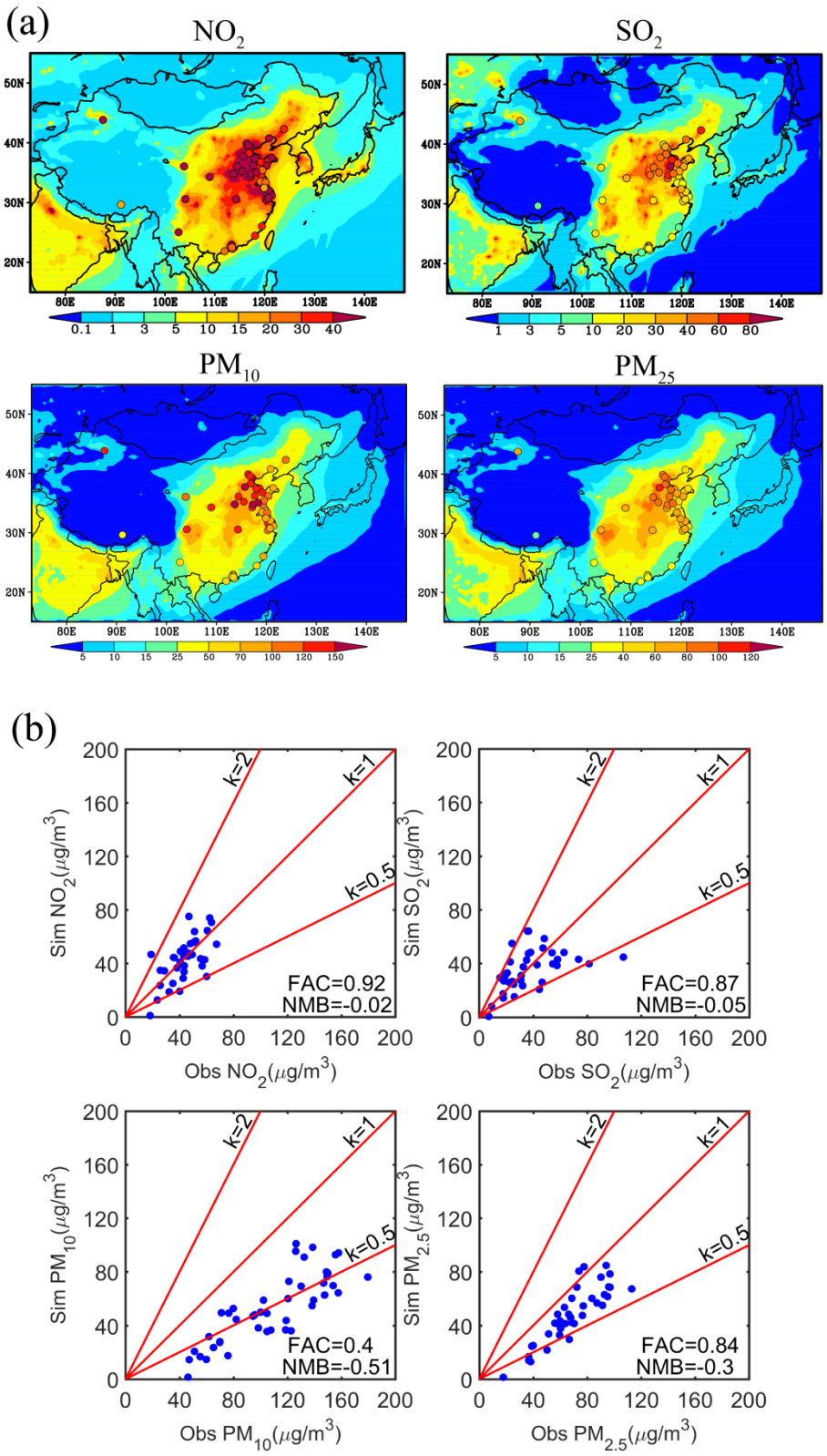

Fig. 11. (a) Surface annual mean concentration (μg m^{-3}) of the nested domain. The circles represent sites observations. The top row is NO_2 and SO_2, the bottom row is PM_{10} and $PM_{2.5}$. (b) Scatter plots of annual mean concentrations (μg m^{-3}) in nested domain. The order of the subplot is in accordance with Fig. 11(a). The abscissa shows the observation and the ordinate shows the simulation.

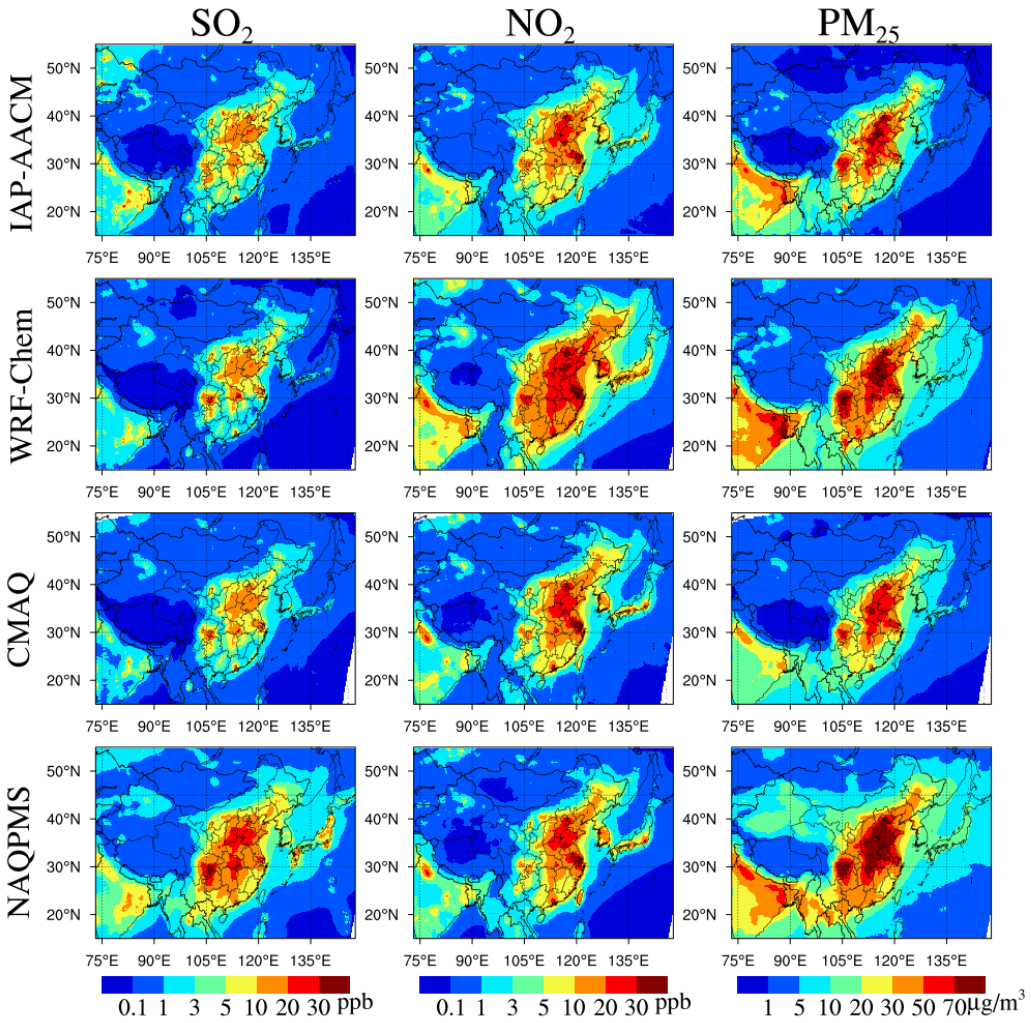

Fig. 12. Annual surface distributions from nested IAP-AACM compared with regional models from MICS-Asia. Each row from top to bottom represents IAP-AACM, WRF-Chem, CMAQ and NAQPMS respectively. The left column is SO_2 (ppb), the middle column is NO_2 (ppb) and the right column is $PM_{2.5}$ (μg m^{-3}).

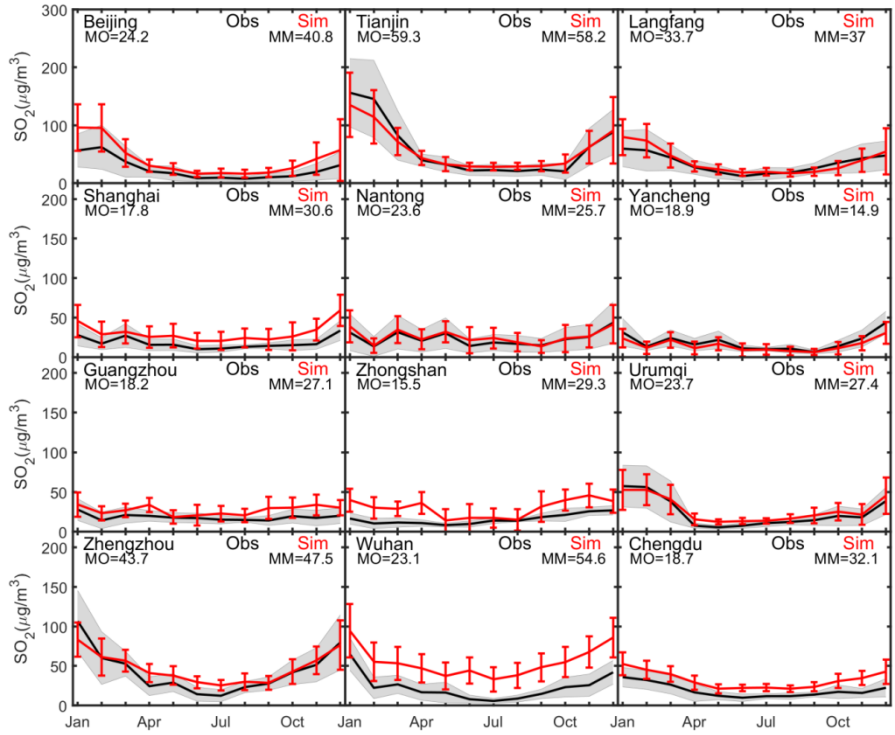

Fig. 13. Mean seasonal variation of SO_2 (μg m^{-3}) over China. The black line and red line represent monthly mean concentration of city-averaged observation and
1225 simulation respectively. Gray shaded areas and red vertical bars show 1 standard deviation over the sites for observations and for model results, respectively. MO and MM stand for annual mean concentration of observation and simulation respectively.

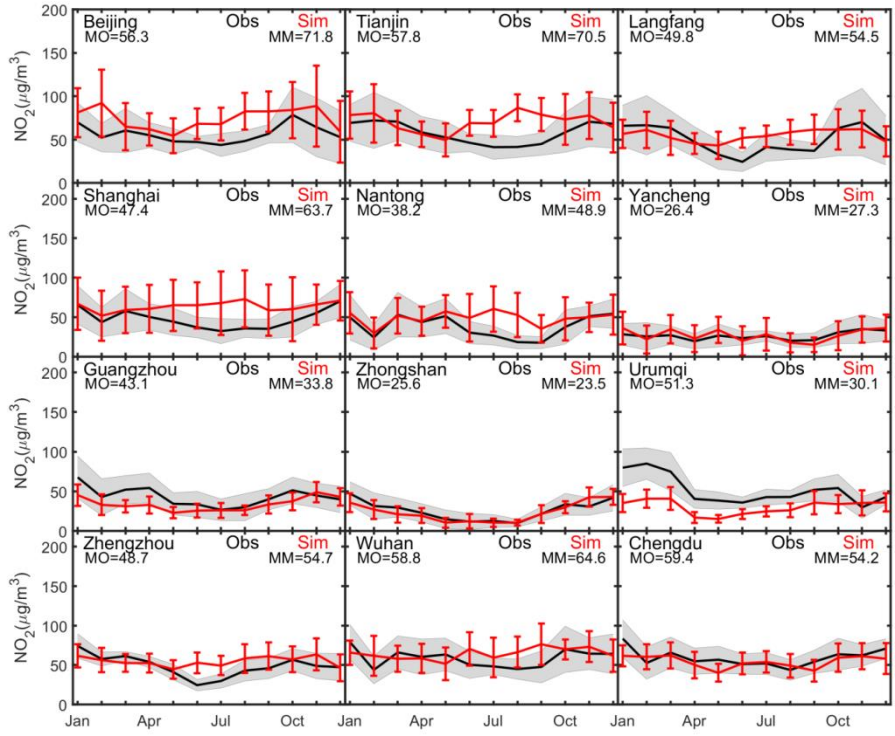

Fig. 14. The same as Fig. 15, except the pollutant is NO_2.

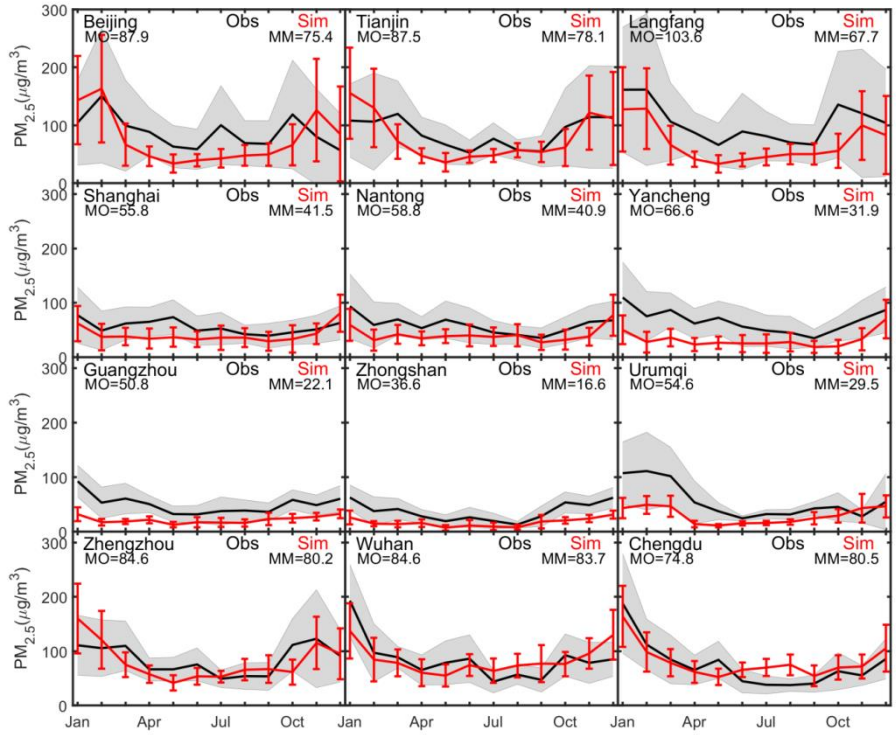

1230

Fig. 15. The same as Fig. 15, except the pollutant is $PM_{2.5}$. The components of $PM_{2.5}$ includes primary $PM_{2.5}$, BC, POA, SOA and SNA.

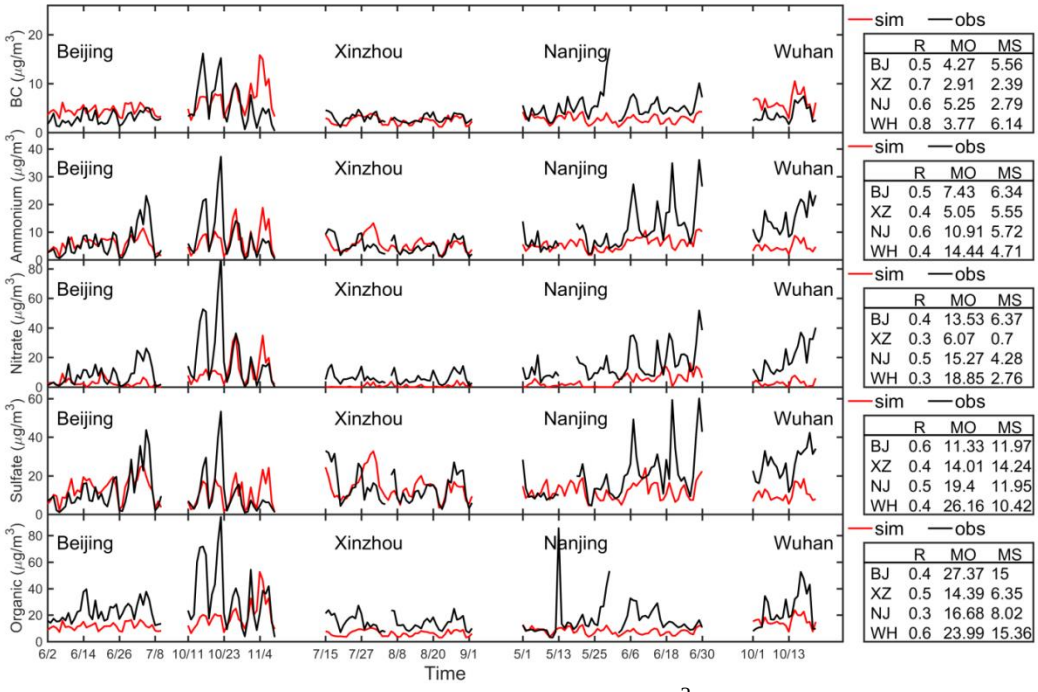

Fig. 16. Daily variation of aerosol components (μg m^{-3}) over China. The black line and red line represent daily mean concentration of city-averaged observation and simulation respectively. BJ, XZ, NJ and WH mean Beijing, Xinzhou, Nanjing and Wuhan respectively. R, MO and MM stand for correlation coefficient, mean concentration of observation and model respectively.

1235

Tables

Table 1. Emissions used in IAP-AACM

Database	Abbreviation	Base year	Source type	Reference
Hemispheric Transport of Air Pollution version2	HTAP-v2	2010	Anthropogenic	Janssens-maenhout et al., 2015
Global Fire Emissions Database version4	GFED-v4	2010	Biomass burning	Randerson et al., 2015
Model of Emissions of Gases and Aerosols from Nature–Monitoring Atmospheric Composition and Climate	MEGAN-MACC	2010	Biogenic	Sindelarova et al., 2014
Regional Emission inventory in Asia	REAS	2001	Soil (NOx)	Yan et al., 2005
Precursors of Ozone and their Effects in the Troposphere	POET	2000	Ocean (VOCs)	Granier et al., 2005
Global Emission InitiAtive	GEIA	Average of 1983 ~ 1990	Lightning (NOx)	Price et al., 1997

Table 2. Summary of statistical of annual and seasonal meteorology in the nested domain compared with NCDC sites. Seasons are defined as spring (March–May), summer (June–August), fall (September–November), and winter (December–February). MO, MM, RMSE and R represents mean value of observation, mean value of model, root mean square error and correlation coefficients respectively. T_2, W_{10} and RH_2 represent temperature at 2m (℃), wind speed at 10 m (m/s) and relative humidity at 2m (%) respectively.

	Period	MO	MM	MB	RMSE	R
T_2	2014	17.6	17.5	-0.1	1.8	0.98
	Spring	16.3	16.2	-0.1	1.9	0.97
	Summer	24.3	24.0	-0.3	2.0	0.93
	Autumn	17.2	17.0	-0.2	1.7	0.97
	Winter	9.5	9.5	0.0	1.7	0.96
W_{10}	2014	3.1	2.5	-0.6	1.5	0.53
	Spring	3.2	2.7	-0.5	1.8	0.61
	Summer	2.9	2.1	-0.8	1.9	0.48
	Autumn	3.0	2.3	-0.7	1.7	0.53
	Winter	3.1	2.4	-0.7	1.8	0.56
RH_2	2014	64.8	61.7	-3.1	12.3	0.84
	Spring	58.5	56.2	-2.3	12.6	0.86
	Summer	71.2	68.0	-3.2	11.7	0.86
	Autumn	68.1	64.0	-4.1	11.7	0.83
	Winter	61.4	58.6	-2.8	13.2	0.76

Table 3. Summary of the site observation datasets

Dataset	Site number	Year	Region of sites located	Observed species
WDCGG	131	2014	Global	CO, O_3, SO_2, NO_2
EANET	41	2014	East Asia	SO_2, NO_2, O_3, $PM_{2.5}$, sulfate, nitrate, ammonium
EMEP	46	2014	Europe	$PM_{2.5}$, BC, OC, sulfate, nitrate, ammonium
IMPROVE	23	2014	America	$PM_{2.5}$, BC, OC, sulfate, nitrate, ammonium
EPA	93	2014	America	SO_2, NO_2, $PM_{2.5}$
CAWNET	13	2006	China	BC, OC
CNEMC	89	2014	China	CO, O_3, SO_2, NO_2, PM_{10}, $PM_{2.5}$
Others	4	2014	China	BC, OM, sulfate, nitrate, ammonium

1250 Table 4. Global budgets for DMS, SO_2 and sulfate

Species		IAP-AACM	Other models[a]
DMS	Sources (Tg S yr^{-1})	22.8	
	Emission	22.8	10.7~23.7
	Sinks (Tg S yr^{-1})	22.8	
	Dry deposition	0.0	
	Oxidation	22.8	
	Burden (Tg S)	0.19 ↑[b]	0.02~0.15
	Lifetime (days)	3	0.5~3.0
SO_2	Sources (Tg S yr^{-1})	77.1	
	Emission	54.3 ↓[b]	63.4~94.9
	DMS oxidation	22.8	10.0~25.6
	Sinks (Tg S yr^{-1})	77.1	
	Dry deposition	28.0	16.0~55.0
	Wet deposition	0.0	0~19.9
	Gas-phase oxidation	19.3	6.1~22.0
	Aqueous-phase oxidation	29.8	24.5~57.8
	Burden (Tg S)	0.63	0.2~0.69
	Lifetime (days)	3.0 ↑[b]	0.6~2.6
Sulfate	Sources (Tg S yr^{-1})	50.5	
	Emission	1.4	0~3.5
	Gas-phase oxidation	19.3	6.1~22.0
	Aqueous-phase oxidation	29.8	24.5~57.8
	Sinks (Tg S yr^{-1})	50.5	
	Dry deposition	2.9	0.8~18.0
	Wet deposition	47.6	34.7~61.1
	Burden (Tg S)	0.82	0.38~1.07
	Lifetime (days)	5.9	3.0~7.9

[a] including Liu et al. (2005), Lee et al. (2015), and those listed in Liu et al. (2005), the range of sulfate is also refer to the GISS-TOMAS (Lee et al., 2010), ACCMIP (Lee et al., 2013) and the AeroCom (Textor et al., 2006) results.

[b] outside the range of other models

Table 5. Global budgets for carbonaceous aerosol

Species		IAP-AACM	Other models[a]
BC	Sources (Tg yr^{-1})	7.42	
	Emission	7.42	7.4~19.0
	Sinks (Tg yr^{-1})	7.42	
	Dry deposition	1.01	0.3~4.6
	Wet deposition	6.41	3.8~13.7
	Burden (Tg)	0.13	0.08~0.59
	Lifetime (days)	6.4	3.3~9.4
OM[b]	Sources (Tg yr^{-1})	56.7	50~216
	Emission	48.7	34~144
	Chemical production	8.0	7.8~120
	Sinks (Tg yr^{-1})	56.7	
	Dry deposition	6.79	2~36
	Wet deposition	49.9	28~209
	Burden (Tg)	1.16	0.7~3.8
	Lifetime (days)	7.4	3.5~9.2

[a] including Liu et al. (2005), Lee et al. (2010), Lee et al. (2013), Lee et al. (2015), Textor et al. (2006), and those listed in Liu et al. (2005).

[b] the convert factor from OC to OM is 1.7 in IAP-AACM.

Table 6. Summary of statistics for global and nested domains. D1 and D2 represent results of domain 1 and domain 2, respectively. City Ave means average over all the cities.

Species	City	R		RMSE (μg m^{-3})		MB (μg m^{-3})		NMB	
		D1	D2	D1	D2	D1	D2	D1	D2
$PM_{2.5}$	Beijing	0.69	0.70	54.28	55.65	-12.33	-16.89	-0.14	-0.19
	Tianjin	0.67	0.72	46.63	46.51	-11.00	-13.27	-0.13	-0.15
	Langfang	0.72	0.79	66.02	65.22	-28.58	-38.34	-0.28	-0.37
	Shanghai	0.71	0.71	29.51	27.99	-18.23	-16.00	-0.33	-0.29
	Nantong	0.69	0.75	31.46	29.70	-18.32	-17.84	-0.31	-0.30
	Yancheng	0.74	0.80	45.52	43.30	-35.60	-33.99	-0.53	-0.51
	Guangzhou	0.43	0.63	38.75	36.91	-29.91	-29.39	-0.59	-0.58
	Zhongshan	0.51	0.76	26.16	26.77	-16.08	-20.38	-0.44	-0.56
	Urumqi	0.31	0.50	59.32	48.10	-38.40	-25.88	-0.70	-0.47
	Zhengzhou	0.59	0.63	41.98	43.05	0.70	-7.30	0.01	-0.09
	Wuhan	0.57	0.64	44.49	42.28	-11.32	-12.09	-0.13	-0.14
	Chengdu	0.76	0.77	37.18	36.14	5.23	-0.19	0.07	0.00

	City Ave	0.68	0.70	49.86	51.07	-10.01	-10.95	-0.11	-0.12
SO_2	Beijing	0.87	0.89	26.99	25.00	21.32	16.58	0.88	0.68
	Tianjin	0.85	0.85	35.45	29.51	-10.96	-1.10	-0.18	-0.02
	Langfang	0.74	0.76	24.65	18.90	11.49	3.38	0.34	0.10
	Shanghai	0.50	0.75	38.48	18.10	30.43	12.76	1.71	0.72
	Nantong	0.69	0.78	13.55	12.08	-0.23	2.17	-0.01	0.09
	Yancheng	0.78	0.83	9.75	8.79	-4.29	-4.02	-0.23	-0.21
	Guangzhou	0.26	0.40	10.42	14.96	-0.96	8.86	-0.05	0.49
	Zhongshan	0.59	0.33	7.33	21.65	1.65	13.74	0.11	0.88
	Urumqi	0.63	0.60	23.04	20.01	-11.88	3.68	-0.50	0.16
	Zhengzhou	0.79	0.82	24.51	20.06	12.34	3.84	0.28	0.09
	Wuhan	0.70	0.48	18.72	40.28	12.03	31.47	0.52	1.36
	Chengdu	0.52	0.60	48.52	17.61	44.44	13.33	2.37	0.71
	City Ave	0.76	0.83	31.50	27.35	5.18	7.74	0.12	0.19
NO_2	Beijing	0.48	0.68	26.00	26.82	11.98	15.68	0.21	0.28
	Tianjin	0.41	0.51	26.24	27.39	9.88	13.02	0.17	0.23
	Langfang	0.39	0.53	33.84	23.83	19.60	4.91	0.39	0.10
	Shanghai	0.57	0.56	29.28	32.17	8.79	16.79	0.19	0.35
	Nantong	0.60	0.59	21.86	24.11	3.63	10.69	0.10	0.28
	Yancheng	0.44	0.49	18.33	16.53	-1.55	1.78	-0.06	0.07
	Guangzhou	0.40	0.51	28.34	20.28	-20.41	-9.19	-0.47	-0.21
	Zhongshan	0.63	0.70	13.47	12.51	-3.01	-2.06	-0.12	-0.08
	Urumqi	0.24	0.41	41.73	30.31	-35.18	-21.39	-0.69	-0.42
	Zhengzhou	0.32	0.44	23.68	18.75	13.65	5.97	0.28	0.12
	Wuhan	0.25	0.22	25.36	28.39	5.77	6.16	0.10	0.10
	Chengdu	0.31	0.43	27.26	20.77	-18.88	-5.84	-0.32	-0.10
	City Ave	0.44	0.60	26.05	26.92	10.82	13.99	0.19	0.25

Supplement

Figures

Table S1. The list of observation sites information

Number	Site name (ID)	Longitude	Latitude
WDCGG Dataset			
1	asc107s00.noa	-14.42	-7.92
2	ask123n00.noa	5.63	23.27
3	azr638n00.noa	-27.37	38.77
4	bhd541s00.noa	174.87	-41.4
5	bkt500s00.bmg	100.32	-0.2
6	bmw432n00.noa	-64.87	32.27
7	brw471n00.noa	-156.6	71.32
8	cba455n00.noa	-162.72	55.2
9	cfa519s00.csi	147.05	-19.3
10	cgo540s00.csi	144.68	-40.7
11	cmn644n00.isa	10.7	44.18
12	cpt134s00.saw	18.48	-34.4
13	crz146s00.noa	51.85	-46.5
14	cvo116n00.uyr	-24.87	16.85
15	cya766s00.csi	110.53	-66.3
16	egb444n01.ec.	-79.78	44.23
17	eic327s00.noa	-109.45	-27.1
18	etl454n00.ec.	-104.98	54.35
19	glh636n00.uml	14.22	36.07
20	gmi513n00.noa	144.78	13.43
21	hba775s00.noa	-26.5	-75.6
22	hpb647n00.noa	11.02	47.8
23	hun646n00.noa	16.65	46.95
24	ice663n00.noa	-20.28	63.4
25	izo128n00.aem	-16.5	28.3
26	key425n00.noa	-80.2	25.67
27	kos649n00.chm	15.08	49.58
28	kum519n00.noa	-154.82	19.52
29	kvv646n00.ars	14.53	46.3
30	lef445n00.noa	-90.27	45.92
31	lln223n00.noa	120.87	23.47
32	lmp635n00.noa	12.63	35.52
33	maa767s00.csi	62.87	-67.6
34	mex419n00.noa	-97.17	19.98
35	mhd653n00.noa	-9.9	53.33
36	mid528n00.noa	-177.37	28.2

Number	Site name (ID)	Longitude	Latitude
37	mlo519n00.csi	-155.58	19.54
38	mnm224n00.jma	153.98	24.28
39	mqa554s00.csi	158.97	-54.5
40	nat306s00.noa	-35.2	-6
41	nmb123s00.noa	15.02	-23.6
42	nwr440n01.noa	-105.59	40.05
43	oxk650n00.noa	11.8	50.03
44	pal667n00.noa	24.12	67.97
45	poc900n00.noa	-155	0
46	poc905n00.noa	-151	5
47	poc905s00.noa	-159	-5
48	poc910n00.noa	-149	10
49	poc910s00.noa	-161	-10
50	poc915n00.noa	-145	15
51	poc915s00.noa	-171	-15
52	poc920n00.noa	-141	20
53	poc920s00.noa	-174	-20
54	poc925n00.noa	-139	25
55	poc925s00.noa	-171	-25
56	poc930n00.noa	-135	30
57	poc930s00.noa	-176	-30
58	psa764s00.noa	-64	-64.9
59	rig646n00.emp	8.45	46.07
60	rpb413n00.noa	-59.43	13.17
61	ryo239n00.jma	141.82	39.03
62	sey104s00.noa	55.17	-4.67
63	sgp436n00.noa	-97.5	36.78
64	smo514s00.noa	-170.57	-14.2
65	spo789s00.csi	-24.8	-90
66	sum672n00.noa	-38.48	72.58
67	syo769s00.noa	39.58	-69
68	tap236n00.noa	126.12	36.72
69	thd441n00.noa	-124.15	41.05
70	ush354s00.noa	-68.31	-54.9
71	uta439n00.noa	-113.72	39.88
72	uum244n00.noa	111.08	44.45
73	wis631n00.noa	34.87	31.12
74	wlg236n00.cma	100.9	36.28
75	yon224n00.jma	123.02	24.47
76	zep678n00.noa	11.88	78.9
77	dig654n00.ioe	22.07	54.15
78	glh636n00.uml	14.22	36.07
79	irb645n00.ars	14.87	45.57

Number	Site name (ID)	Longitude	Latitude
80	kos649n00.chm	15.08	49.58
81	kps646n00.hms	19.55	46.97
82	pay646n00.emp	6.95	46.82
83	rcv656n00.lhm	21.17	56.16
84	rig646n00.emp	8.45	46.07
85	amy236n00.kma	126.32	36.53
86	arh777s00.noa	166.67	-77.8
87	ask123n00.onm	5.63	23.27
88	bhd541s00.niw	174.87	-41.4
89	bmw432n00.noa	-64.87	32.27
90	brw471n00.noa	-156.6	71.32
91	cpt134s00.saw	18.48	-34.4
92	cvo116n00.uyr	-24.87	16.85
93	glh636n00.uml	14.22	36.07
94	irb645n00.ars	14.87	45.57
95	jfj646n00.emp	7.99	46.55
96	kos649n00.chm	15.08	49.58
97	kps646n00.hms	19.55	46.97
98	kvk646n00.ars	15.1	46.12
99	kvv646n00.ars	14.53	46.3
100	lau545s00.noa	169.67	-45
101	mhd653n00.nui	-9.9	53.33
102	mlo519n00.noa	-155.58	19.54
103	mnm224n00.jma	153.98	24.28
104	nmy770s00.awi	-8.25	-70.7
105	nwr440n00.noa	-105.54	40.04
106	pay646n00.emp	6.95	46.82
107	prs645n00.rse	7.7	45.93
108	rig646n00.emp	8.45	46.07
109	rpb413n00.noa	-59.43	13.17
110	ryo239n00.jma	141.82	39.03
111	smo514s00.noa	-170.57	-14.2
112	spo789s00.noa	-24.8	-90
113	sum672n00.noa	-38.48	72.58
114	syo769s00.jma	39.58	-69
115	thd441n00.noa	-124.15	41.05
116	tkb236n10.jma	140.13	36.05
117	tll330s00.dmc	-70.8	-30.2
118	ush354s00.smn	-68.31	-54.9
119	vdl664n00.ivl	19.77	64.25
120	yon224n00.jma	123.02	24.47
121	zrn646n00.ars	15	46.43
122	zsn657n00.lhm	25.54	57.08

Number	Site name (ID)	Longitude	Latitude
123	dig654n00.ioe	22.07	54.15
124	glh636n00.uml	14.22	36.07
125	irb645n00.ars	14.87	45.57
126	jfj646n00.emp	7.99	46.55
127	kos649n00.chm	15.08	49.58
128	kps646n00.hms	19.55	46.97
129	pay646n00.emp	6.95	46.82
130	rcv656n00.lhm	21.17	56.16
131	rig646n00.emp	8.45	46.07

EANET

num	staid	lon	lat
1	PhnomPenh	104.83	11.55
2	Jakarta	106.83	-6.18
3	Serpong	106.57	6.25
4	Bandung	107.58	6.9
5	Rishiri	141.2	45.12
6	Ochishi	145.5	43.15
7	Tappi	140.35	41.25
8	Sado-seki	138.4	38.23
9	Ijira	136.68	35.57
10	Oki	133.18	36.28
11	Banryu	131.8	34.68
12	Hedo	128.25	26.87
13	Ogasawara	142.22	27.08
14	PetalingJaya	101.65	3.1
15	DanumValley	117.85	4.98
16	Yangon	96.12	16.5
17	Kanghwa	126.28	37.7
18	Cheju	126.17	33.3
19	Imsil	127.18	35.6
20	Listvyanka	104.9	51.85
21	Irkutsk	104.25	52.23
22	Primorskaya	132.12	43.7
23	Bangkok	100.53	13.77
24	Khanchanaburi	98.58	14.77
25	ChiangMai	98.93	18.77
26	NakhonRatchasima	101.88	14.45
27	Hanoi	105.85	21.02
28	HoaBinh	105.33	20.82
29	Tokyo	139.75	35.68
30	NakhonRatchasima	101.88	14.45
31	Mt.Sto.Tomas 1	120.6	6.42
32	Hongwen	118.13	24.47

Number	Site name (ID)	Longitude	Latitude
33	XiangZhou	113.57	22.27
34	Kototabang	100.32	0.2
35	Ulaanbaatar	106.82	47.9
36	Samutprakarn	100.57	13.73
37	Mondy	101	51.67
38	Happo	137.8	36.7
39	MtStoTomas	120.6	16.42
40	Khanchanaburi	98.58	14.77
	EMEP		
1	Waldhof	10.76	52.8
2	Schauinsland	7.91	47.91
3	Neuglobsow	13.03	53.17
4	Lahemaa	25.9	59.5
5	Uto	21.38	59.78
6	Virolahti	27.69	60.53
7	Pallas	24.24	68
8	K-puszta	19.58	46.97
9	Oak	-6.92	52.87
10	Malin	-7.34	55.38
11	Carnsore	-6.36	52.18
12	Rucava	21.17	56.16
13	Birkenes	8.25	58.39
14	Karvatn	8.88	62.78
15	Zeppelin	11.89	78.91
16	Hurdal	11.08	60.37
17	Jarczew	21.97	51.81
18	Sniezka	15.74	50.74
19	Leba	17.53	54.75
20	Diabla	22.07	54.15
21	Danki	37.8	54.9
22	Iskrba	14.87	45.57
23	Starina	22.27	49.05
24	Melpitz_l	12.93	51.53
25	Ispra	8.63	45.8
26	Cabauw	4.92	51.97
27	Illmitz	16.77	47.77
28	Vorhegg	12.97	46.68
29	Zoebelboden	14.44	47.84
30	Payerne	6.94	46.81
31	Tanikon	8.9	47.48
32	Chaumont	6.98	47.05
33	Rigi	8.46	47.07
34	Churanov	13.6	49.07

Number	Site name (ID)	Longitude	Latitude
35	Westerland	8.31	54.93
36	Zingst	12.73	54.43
37	Harwell	-1.32	51.57
38	Auchencorth	-3.24	55.79
39	Kamenicki	21.95	43.4
40	Schmucke	10.77	50.65
41	San	-4.35	39.55
42	Cabo	3.32	42.32
43	Zarra	-1.1	39.09
44	Penausende	-5.87	41.28
45	Els	0.72	41.4
46	Rao	11.91	57.39
	IMPROVE		
1	ACAD1	-68.261	44.377
2	BLMO1	-96.191	43.716
3	BRMA1	-70.729	44.107
4	CEBL1	-99.763	38.77
5	DENA1	-148.968	63.723
6	EVER1	-80.681	25.391
7	GAAR1	-151.517	66.903
8	GRRI1	-91.405	43.937
9	HEGL1	-92.922	36.614
10	KALM1	-124.059	42.552
11	LOST1	-102.402	48.642
12	MING1	-90.143	36.972
13	NEBR1	-100.339	41.889
14	OWVL1	-118.331	37.361
15	PMRF1	-72.869	44.528
16	RAFA1	-120.007	34.734
17	SAGO1	-116.913	34.194
18	SENE1	-85.95	46.289
19	SIME1	-160.506	55.325
20	TALL1	-96.56	38.434
21	TRIN1	-122.805	40.786
22	WHIT1	-105.535	33.469
23	ZICA1	-113.151	37.198
	EPA		
1	10730023	-86.82	33.55
2	40128000	-113.56	34.24
3	60530002	-121.64	36.7
4	60831008	-120.05	34.49
5	90090027	-72.9	41.3
6	120573002	-82.54	27.89

7	120860033	-80.16	25.73
8	170310022	-87.64	41.88
9	171190024	-90.16	38.61
10	180570007	-85.77	39.29
11	191770006	-92.01	40.7
12	201330003	-95.48	37.68
13	360610079	-73.9	40.82
14	380171004	-96.86	46.93
15	380250003	-102.53	47.31
16	410510080	-122.6	45.5
17	420010001	-77.31	39.92
18	420031008	-79.73	40.61
19	450450015	-82.41	34.84
20	460990006	-96.7	43.55
21	461030020	-103.27	44.09
22	461270001	-96.71	42.75
23	550870009	-88.81	45.56
24	560030003	-108.39	44.84
25	20200018	-149.82	61.21
26	21100004	-134.57	58.39
27	21221006	-151.69	59.46
28	21700008	-149.03	61.53
29	40131003	-111.87	33.41
30	40133010	-112.12	33.46
31	40278011	-114.61	32.69
32	51190007	-92.28	34.76
33	60070008	-121.84	39.76
34	60090001	-120.68	38.2
35	60510005	-119.12	37.96
36	60970001	-123.02	38.8
37	60990005	-120.99	37.64
38	120570083	-82.38	27.86
39	150030010	-158.09	21.32
40	300290009	-114.34	48.4
41	300710010	-107.86	48.32
42	410390059	-123.14	44.07
43	420030003	-79.77	40.45
44	530330080	-122.31	47.57
45	530630021	-117.36	47.67
46	560350100	-110.06	42.79
47	560370007	-109.22	41.59
48	560370300	-109.79	41.75
49	560370866	-109.79	41.63
50	560370867	-108.67	41.75

51	10030010	-87.88	30.5
52	21220008	-151.07	60.49
53	40011235	-109.44	35.88
54	50010011	-91.56	34.52
55	60010007	-121.78	37.69
56	60410001	-122.52	37.97
57	60670006	-121.37	38.61
58	60710306	-117.33	34.51
59	60730003	-116.94	32.79
60	60731006	-116.77	32.84
61	60750005	-122.4	37.77
62	60771002	-121.27	37.95
63	61111004	-119.23	34.45
64	100010002	-75.56	38.99
65	131210039	-84.44	33.8
66	131350002	-84.07	33.96
67	150011006	-155.11	19.72
68	160410001	-111.81	42.01
69	330115001	-71.88	42.86
70	380070002	-103.38	46.89
71	471570047	-90.02	35.17
72	550090005	-87.99	44.51
73	560290001	-109.07	44.53
74	20900034	-147.73	64.85
75	40070009	-110.86	33.4
76	60010011	-122.28	37.81
77	80013001	-104.95	39.84
78	90010012	-73.16	41.2
79	120110010	-80.17	26.13
80	120170006	-82.64	28.96
81	160050004	-112.52	42.92
82	170191001	-88.37	40.05
83	220150008	-93.75	32.54
84	230090103	-68.26	44.38
85	230112005	-69.79	44.23
86	230310009	-70.77	43.11
87	240053001	-76.47	39.31
88	271095008	-92.45	44
89	300490004	-111.99	46.85
90	390350038	-81.68	41.48
91	390810017	-80.62	40.37
92	390850003	-81.42	41.67
93	401430235	-96	36.13

CAWNET

1	Chengdu	104.3	30.6
2	Dalian	121.6	38.9
3	Dunhuang	94.67	40.1
4	Gaolanshan	105.8	36
5	Gucheng	115.8	39.1
6	Jinsha	114.2	29.6
7	LinAn	119.7	30.3
8	Longfengshan	127.5	44.7
9	Shangdianzi	117.1	40.7
10	Taiyangshan	111.7	29.2
11	Xian	109	34.5
12	Zhenbeitai	109.2	38.5
13	Zhengzhou	113.7	34.8
	CNEMC		
1	110000041	116.17	40.29
2	110000244	116.43	39.95
3	110000245	116.43	39.87
4	110000246	116.4	39.98
5	110000247	116.47	39.97
6	110000249	116.22	39.93
7	110000250	116.36	39.94
8	110000251	116.32	39.99
9	110000252	116.37	39.87
10	110000253	116.72	40.14
11	110000254	116.64	40.39
12	110000255	116.23	40.2
13	440100051	113.24	23.14
14	440100057	113.26	23.13
15	440100063	113.28	23.16
16	440100064	113.26	23.1
17	440100073	113.32	23.14
18	440100088	113.35	23.09
19	440100089	113.43	23.1
20	440100090	113.35	22.95
21	440100091	113.21	23.39
22	440100092	113.57	23.28
23	442000051	113.38	22.52
24	442000052	113.39	22.55
25	442000053	113.41	22.51
26	131000402	116.68	39.52
27	131000403	116.77	39.57
28	131000407	116.71	39.56
29	131000408	116.75	39.53
30	410100051	113.64	34.75

31	410100052	113.6	34.75
32	410100053	113.68	34.75
33	410100054	113.64	34.77
34	410100062	113.68	34.8
35	410100063	113.56	34.8
36	410100064	113.73	34.72
37	410100065	113.73	34.72
38	420100051	114.28	30.62
39	420100052	114.15	30.48
40	420100053	114.25	30.55
41	420100054	114.3	30.55
42	420100055	114.37	30.57
43	420100056	114.43	30.61
44	420100057	114.3	30.59
45	420100075	114.39	30.48
46	420100076	114.21	30.64
47	320600073	120.86	32
48	320600074	120.87	32.02
49	320600077	120.94	31.93
50	320600078	120.81	32.04
51	320900401	120.12	33.4
52	320900402	120.16	33.39
53	320900403	120.13	33.37
54	320900406	120.22	33.39
55	310000051	121.4	31.24
56	310000052	121.54	31.27
57	310000053	121.48	31.2
58	310000055	121.47	31.3
59	310000056	121.43	31.23
60	310000057	121.41	31.17
61	310000058	121.53	31.23
62	310000059	121.58	31.21
63	310000251	121.7	31.19
64	510100051	104.05	30.66
65	510100052	104.03	30.65
66	510100054	104.12	30.64
67	510100064	104.07	30.68
68	510100073	104.08	30.57
69	510100074	104.18	30.69
70	510100075	103.97	30.71
71	120000051	117.15	39.1
72	120000062	117.14	39.17
73	120000072	117.18	39.12
74	120000081	117.19	39.17

75	120000095	117.24	39.11
76	120000100	117.27	39.13
77	120000104	117.2	39.09
78	120000137	117.46	38.84
79	120000143	117.71	39.03
80	120000168	117.31	39.09
81	120000186	117.18	39.23
82	120000301	117.4	39.12
83	120000302	117.76	39.16
84	650100051	87.6	43.77
85	650100055	87.58	43.83
86	650100056	87.55	43.87
87	650100071	87.64	43.83
88	650100072	87.42	43.87
89	650100091	87.64	43.96
Aerosol sites in China			
1	Beijing	116.371	39.974
2	Xinzhou	112.12	38.07
3	Nanjing	118.749	32.057
4	Wuhan	114.284	30.62

Table S2. The budget of O_3 and CO compared with the other models.

Species	Process		IAP-AACM
CO	Emission ($Tg\ yr^{-1}$) Total 994	Anthrop.	546.4
		Bio. burning	336.2
		Biogenic	92.7
		Others	18.3
	Top condition inflow ($Tg\ yr^{-1}$)		28
	Chem pro ($Tg\ yr^{-1}$)		1270
	Chem lss ($Tg\ yr^{-1}$)		2292
	Dry dep ($Tg\ yr^{-1}$)		0
	Burden (Tg)		327
	Lifetime (days)		52
O_3	Top condition inflow ($Tg\ yr^{-1}$)		398
	Chemical production ($Tg\ yr^{-1}$)		4526
	Chemical loss ($Tg\ yr^{-1}$)		3875
	Dry dep. ($Tg\ yr^{-1}$)		1049
	Burden (Tg)		370
	Lifetime (days)		27.4

Table S3. NMB of global domain in different regions. The NMB is calculated with annual average concentration. ASO_4, ANO_3 and ANH_4 represents sulfate, nitrate and ammonium, respectively.

	CO	O_3	NO_2	SO_2	ASO_4	ANO_3	ANH_4	BC	OC	$PM_{2.5}$
Africa	-0.47	-0.09								
Antarctica	-0.50	-0.34								
ArcticO	-0.45									
Asia	-0.34	0.94	-0.14	0.05	0.36	-0.61	0.85	-0.4	-0.67	-0.36
AtlanticO	-0.54	0.16								
Europe	-0.39	0.10	0.16	3.79	1.1	0.74	1.49	-0.62	-0.55	-0.35
IndianO	-0.53									
NAmerica	-0.23	-0.18	-0.14	3.51	1.94	0.50	-0.46	0.64	-0.12	1.16
Oceania	-0.45	-0.04								
PacificO	-0.59	0.14								
SAmerica	-0.47	-0.12								

Figures

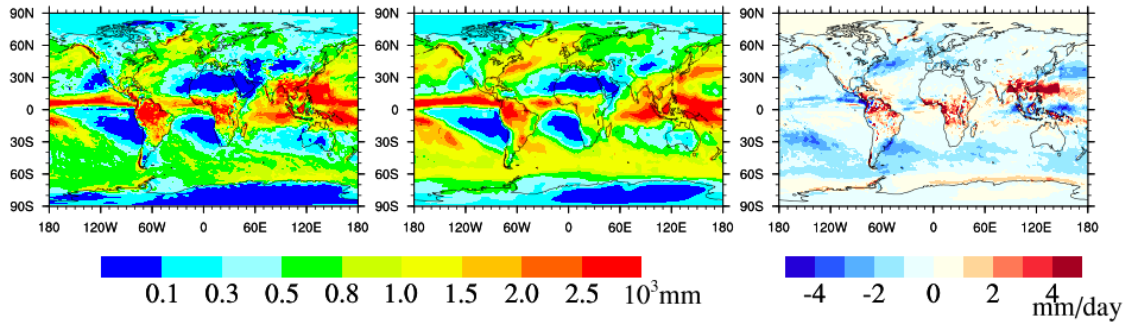

Fig. S1. Annual mean precipitation of WRF compared with GPCP data. The left column is WRF simulation (unit: mm), the middle column is GPCP reanalysis data (unit: mm), the right column is the difference between simulation and reanalysis (WRF-GPCP) (unit: mm day^{-1}).

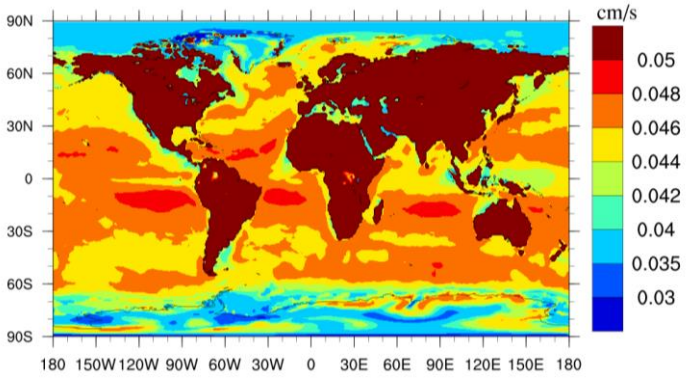

Fig. S2. Annual mean dry deposition velocity of ozone in IAP-AACM. The unit is cm s^{-1}.

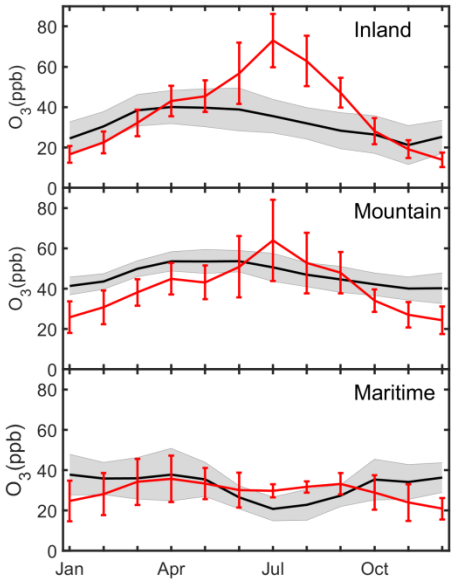

Fig. S3. Mean seasonal variation of O_3 (ppb) over inland, mountain and maritime area

in Northern Hemisphere compared with site records. Black lines and red lines represent the average of observations and simulations respectively. Gray shaded areas and red vertical bars show 1 standard deviation over the sites for observations and for model results respectively.

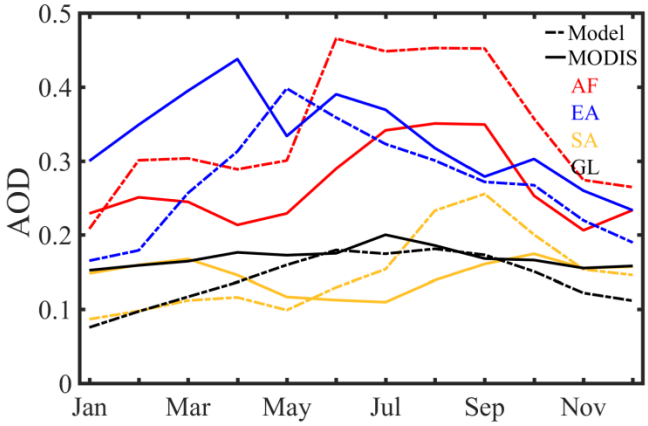

Fig. S4. Gridded mean value of monthly averaged AOD for 2014, AF, EA, SA and GL represents Africa, East Asia, South America and global. Dash line and solid line represents model results and observation derived from MODIS, respectively.

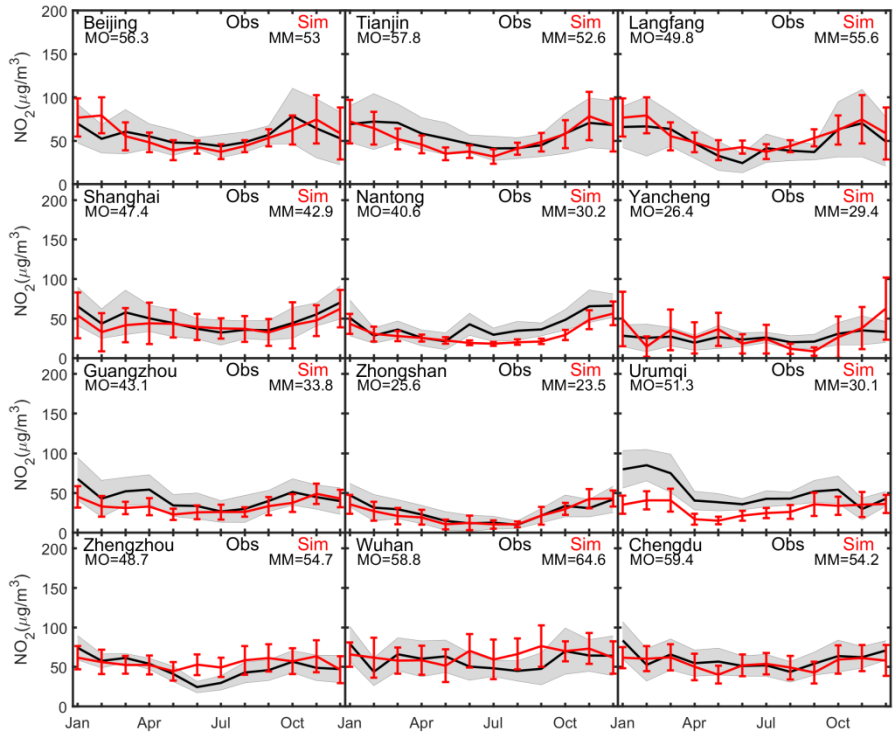

Fig. S5. Seasonal cycle of NO_2 (μg m^{-3}) simulated without heterogeneous chemical process over China. The black line and red line represent monthly mean concentration of city-averaged observation and simulation respectively. Gray shaded areas and red

vertical bars show 1 standard deviation over the sites for observations and for model results, respectively. MO and MM stand for annual mean concentration of observation and simulation respectively.

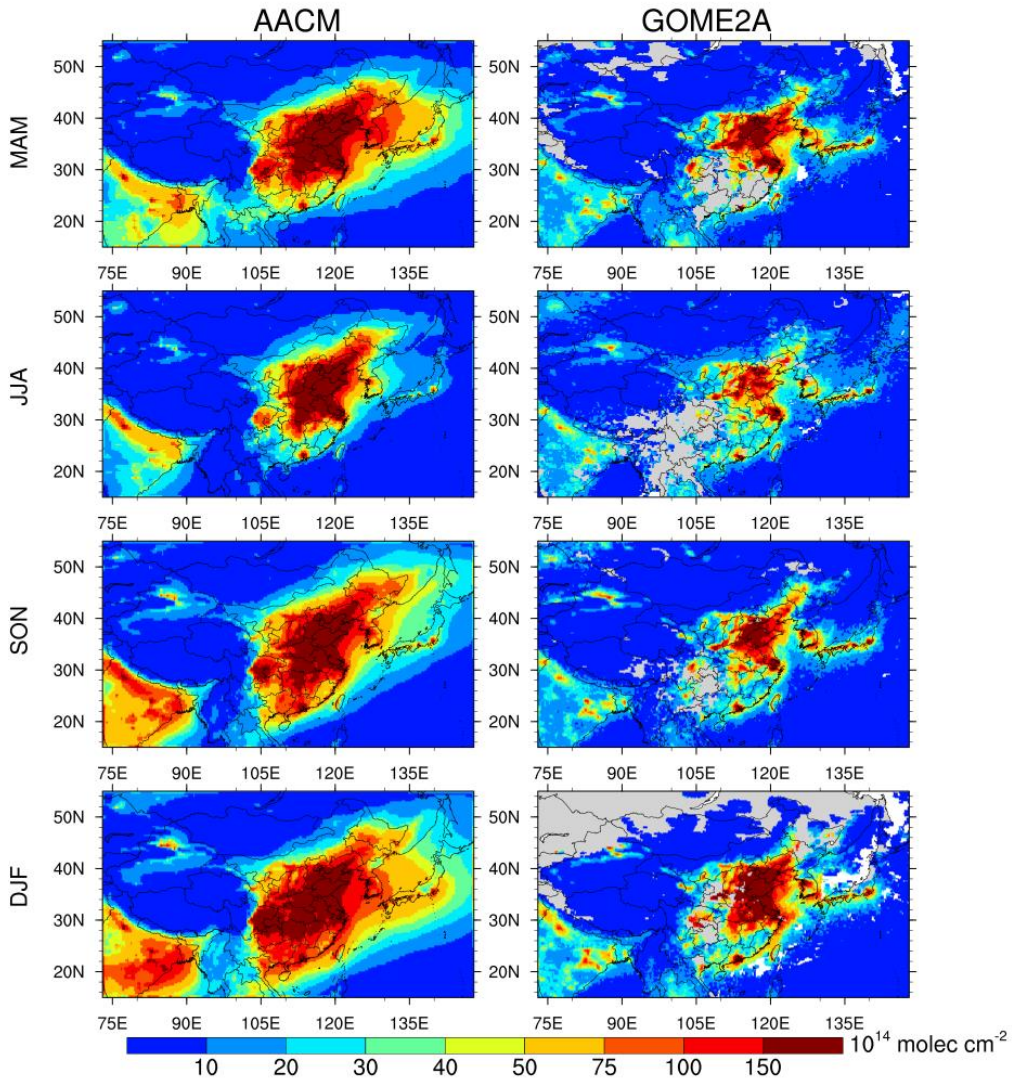

Fig. S6. Seasonal mean column concentration (10^{14} molecule cm^{-2}) of NO_2 in IAP-AACM and GOME-2A over China.